

AD-A064 394 AIR FORCE INST OF TECH WRIGHT-PATTERSON AFB OHIO SCH--ETC F/G 20/5  
PHOTON STATISTICS IN TWO-MODE LASERS. (U)  
DEC 78 B R ANDERSON

UNCLASSIFIED

AFIT/GEP/PH/78-1

NL

1 of 2  
AD-A064394



ASSIF

1 OF 2

AD

A064394



AFIT/GEP/PH/78-1

1

ADA064394

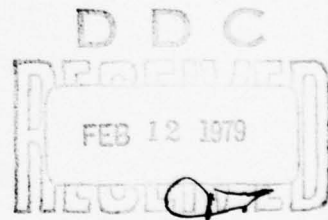
DDC FILE COPY

PHOTON STATISTICS IN  
TWO-MODE LASERS

THESIS

AFIT/GEP/PH/78-1

Bruce R. Anderson  
Capt USAF



Approved for public release; distribution unlimited

79 01 30 099

⑥ PHOTON STATISTICS IN  
TWO-MODE LASERS

⑨ Master's thesis  
THESIS

Presented to the Faculty of the School of Engineering  
of the Air Force Institute of Technology  
Air University  
in Partial Fulfillment of the  
Requirements for the Degree of

Master of Science

⑫ 97 P

⑭ AFIT/GEP/PH/78-1

⑩ by  
Bruce R. Anderson, B.S.

Capt USAF

Graduate Engineering Physics

⑪ December 1978

Approved for public release; distribution unlimited

7

ADDRESS	8112	Brilliant
100	8112	Brilliant
200	8112	Brilliant
300	8112	Brilliant
400	8112	Brilliant
500	8112	Brilliant
600	8112	Brilliant
700	8112	Brilliant
800	8112	Brilliant
900	8112	Brilliant
1000	8112	Brilliant
1100	8112	Brilliant
1200	8112	Brilliant
1300	8112	Brilliant
1400	8112	Brilliant
1500	8112	Brilliant
1600	8112	Brilliant
1700	8112	Brilliant
1800	8112	Brilliant
1900	8112	Brilliant
2000	8112	Brilliant
2100	8112	Brilliant
2200	8112	Brilliant
2300	8112	Brilliant
2400	8112	Brilliant
2500	8112	Brilliant
2600	8112	Brilliant
2700	8112	Brilliant
2800	8112	Brilliant
2900	8112	Brilliant
3000	8112	Brilliant
3100	8112	Brilliant
3200	8112	Brilliant
3300	8112	Brilliant
3400	8112	Brilliant
3500	8112	Brilliant
3600	8112	Brilliant
3700	8112	Brilliant
3800	8112	Brilliant
3900	8112	Brilliant
4000	8112	Brilliant
4100	8112	Brilliant
4200	8112	Brilliant
4300	8112	Brilliant
4400	8112	Brilliant
4500	8112	Brilliant
4600	8112	Brilliant
4700	8112	Brilliant
4800	8112	Brilliant
4900	8112	Brilliant
5000	8112	Brilliant
5100	8112	Brilliant
5200	8112	Brilliant
5300	8112	Brilliant
5400	8112	Brilliant
5500	8112	Brilliant
5600	8112	Brilliant
5700	8112	Brilliant
5800	8112	Brilliant
5900	8112	Brilliant
6000	8112	Brilliant
6100	8112	Brilliant
6200	8112	Brilliant
6300	8112	Brilliant
6400	8112	Brilliant
6500	8112	Brilliant
6600	8112	Brilliant
6700	8112	Brilliant
6800	8112	Brilliant
6900	8112	Brilliant
7000	8112	Brilliant
7100	8112	Brilliant
7200	8112	Brilliant
7300	8112	Brilliant
7400	8112	Brilliant
7500	8112	Brilliant
7600	8112	Brilliant
7700	8112	Brilliant
7800	8112	Brilliant
7900	8112	Brilliant
8000	8112	Brilliant
8100	8112	Brilliant
8200	8112	Brilliant
8300	8112	Brilliant
8400	8112	Brilliant
8500	8112	Brilliant
8600	8112	Brilliant
8700	8112	Brilliant
8800	8112	Brilliant
8900	8112	Brilliant
9000	8112	Brilliant
9100	8112	Brilliant
9200	8112	Brilliant
9300	8112	Brilliant
9400	8112	Brilliant
9500	8112	Brilliant
9600	8112	Brilliant
9700	8112	Brilliant
9800	8112	Brilliant
9900	8112	Brilliant
10000	8112	Brilliant
10100	8112	Brilliant
10200	8112	Brilliant
10300	8112	Brilliant
10400	8112	Brilliant
10500	8112	Brilliant
10600	8112	Brilliant
10700	8112	Brilliant
10800	8112	Brilliant
10900	8112	Brilliant
11000	8112	Brilliant
11100	8112	Brilliant
11200	8112	Brilliant
11300	8112	Brilliant
11400	8112	Brilliant
11500	8112	Brilliant
11600	8112	Brilliant
11700	8112	Brilliant
11800	8112	Brilliant
11900	8112	Brilliant
12000	8112	Brilliant
12100	8112	Brilliant
12200	8112	Brilliant
12300	8112	Brilliant
12400	8112	Brilliant
12500	8112	Brilliant
12600	8112	Brilliant
12700	8112	Brilliant
12800	8112	Brilliant
12900	8112	Brilliant
13000	8112	Brilliant
13100	8112	Brilliant
13200	8112	Brilliant
13300	8112	Brilliant
13400	8112	Brilliant
13500	8112	Brilliant
13600	8112	Brilliant
13700	8112	Brilliant
13800	8112	Brilliant
13900	8112	Brilliant
14000	8112	Brilliant
14100	8112	Brilliant
14200	8112	Brilliant
14300	8112	Brilliant
14400	8112	Brilliant
14500	8112	Brilliant
14600	8112	Brilliant
14700	8112	Brilliant
14800	8112	Brilliant
14900	8112	Brilliant
15000	8112	Brilliant
15100	8112	Brilliant
15200	8112	Brilliant
15300	8112	Brilliant
15400	8112	Brilliant
15500	8112	Brilliant
15600	8112	Brilliant
15700	8112	Brilliant
15800	8112	Brilliant
15900	8112	Brilliant
16000	8112	Brilliant
16100	8112	Brilliant
16200	8112	Brilliant
16300	8112	Brilliant
16400	8112	Brilliant
16500	8112	Brilliant
16600	8112	Brilliant
16700	8112	Brilliant
16800	8112	Brilliant
16900	8112	Brilliant
17000	8112	Brilliant
17100	8112	Brilliant
17200	8112	Brilliant
17300	8112	Brilliant
17400	8112	Brilliant
17500	8112	Brilliant
17600	8112	Brilliant
17700	8112	Brilliant
17800	8112	Brilliant
17900	8112	Brilliant
18000	8112	Brilliant
18100	8112	Brilliant
18200	8112	Brilliant
18300	8112	Brilliant
18400	8112	Brilliant
18500	8112	Brilliant
18600	8112	Brilliant
18700	8112	Brilliant
18800	8112	Brilliant
18900	8112	Brilliant
19000	8112	Brilliant
19100	8112	Brilliant
19200	8112	Brilliant
19300	8112	Brilliant
19400	8112	Brilliant
19500	8112	Brilliant
19600	8112	Brilliant
19700	8112	Brilliant
19800	8112	Brilliant
19900	8112	Brilliant
20000	8112	Brilliant
20100	8112	Brilliant
20200	8112	Brilliant
20300	8112	Brilliant
20400	8112	Brilliant
20500	8112	Brilliant
20600	8112	Brilliant
20700	8112	Brilliant
20800	8112	Brilliant
20900	8112	Brilliant
21000	8112	Brilliant
21100	8112	Brilliant
21200	8112	Brilliant
21300	8112	Brilliant
21400	8112	Brilliant
21500	8112	Brilliant
21600	8112	Brilliant
21700	8112	Brilliant
21800	8112	Brilliant
21900	8112	Brilliant
22000	8112	Brilliant
22100	8112	Brilliant
22200	8112	Brilliant
22300	8112	Brilliant
22400	8112	Brilliant
22500	8112	Brilliant
22600	8112	Brilliant
22700	8112	Brilliant
22800	8112	Brilliant
22900	8112	Brilliant
23000	8112	Brilliant
23100	8112	Brilliant
23200	8112	Brilliant
23300	8112	Brilliant
23400	8112	Brilliant
23500	8112	Brilliant
23600	8112	Brilliant
23700	8112	Brilliant
23800	8112	Brilliant
23900	8112	Brilliant
24000	8112	Brilliant
24100	8112	Brilliant
24200	8112	Brilliant
24300	8112	Brilliant
24400	8112	Brilliant
24500	8112	Brilliant
24600	8112	Brilliant
24700	8112	Brilliant
24800	8112	Brilliant
24900	8112	Brilliant
25000	8112	Brilliant
25100	8112	Brilliant
25200	8112	Brilliant
25300	8112	Brilliant
25400	8112	Brilliant
25500	8112	Brilliant
25600	8112	Brilliant
25700	8112	Brilliant
25800	8112	Brilliant
25900	8112	Brilliant
26000	8112	Brilliant
26100	8112	Brilliant
26200	8112	Brilliant
26300	8112	Brilliant
26400	8112	Brilliant
26500	8112	Brilliant
26600	8112	Brilliant
26700	8112	Brilliant
26800	8112	Brilliant
26900	8112	Brilliant
27000	8112	Brilliant
27100	8112	Brilliant
27200	8112	Brilliant
27300	8112	Brilliant
27400	8112	Brilliant
27500	8112	Brilliant
27600	8112	Brilliant
27700	8112	Brilliant
27800	8112	Brilliant
27900	8112	Brilliant
28000	8112	Brilliant
28100	8112	Brilliant
28200	8112	Brilliant
28300	8112	Brilliant
28400	8112	Brilliant
28500	8112	Brilliant
28600	8112	Brilliant
28700	8112	Brilliant
28800	8112	Brilliant
28900	8112	Brilliant
29000	8112	Brilliant
29100	8112	Brilliant
29200	8112	Brilliant
29300	8112	Brilliant
29400	8112	Brilliant
29500	8112	Brilliant
29600	8112	Brilliant
29700	8112	Brilliant
29800	8112	Brilliant
29900	8112	Brilliant
30000	8112	Brilliant

A

Approved for public release; distribution unlimited

012 225

elt

Acknowledgements

I would like to thank my advisor Dr. Donn Shankland for his assistance and inspiration throughout this study, especially in the suggested approach and development of equations. I would also like to thank Dr. Hugo Weichel for his helpful suggestions in the development of the background theory. Finally, I would like to thank my wife and family for their support and understanding.

Bruce R. Anderson

## Contents

	Page
Acknowledgements .....	ii
List of Figures .....	v
List of Tables .....	vii
List of Symbols .....	viii
Abstract .....	x
I. Introduction .....	1
Background .....	1
Purpose .....	1
Approach .....	2
II. Theory .....	3
Background .....	3
Single-Mode Theory .....	3
Two-Mode Theory .....	5
Derivation of Moment Rate Equations .....	9
General Evolution Equations .....	9
Transition Rates .....	11
Laser Rate Equations .....	14
Equilibrium Analysis of Moment Equations .....	17
First-Moment Equations .....	17
Characterization of Singular Points .....	21
Second-Moment Equations .....	24
III. Approach .....	26
Computational Scheme .....	26
Selection of Values for Laser Parameters .....	26
Selection of Initial Conditions .....	29
IV. Results and Discussion .....	33
Equilibrium Analysis .....	33
Photon Densities .....	33
Second Moments .....	37
Dynamic Analysis .....	40
General .....	40
Below Threshold .....	41
At Threshold .....	41
Above Threshold .....	44
Mode Buildup From Vacuum .....	54
V. Conclusions and Recommendations .....	58
Conclusions .....	58

Contents

	Page
Recommendations for Further Study .....	59
Bibliography .....	60
Appendix A: Derivation of the Evolution Equations .....	62
Appendix B: Linearization of the Photon Rate Equations .....	70
Appendix C: Additional Evolution Curves .....	73
Vita .....	83

List of Figures

<u>Figure</u>	<u>Page</u>
1 Phase Curves Showing the Transient Behavior for Weakly-Coupled Modes Experiencing Equal Pumping (as predicted by Lamb) .....	7
2 Phase Curves Showing the Ransient Behavior for Weakly-Coupled Modes With One Mode Inhibited .....	7
3 Phase Curves Showing the Transient Behavior for Strongly-Coupled Modes Experiencing Equal Pumping .....	8
4 Transition Rates Associated With a Laser System in the Internal State $\underline{x} = (n_1, n_2)$ .....	12
5 Types of Singular Points .....	22
6 Evolution Curves for Case A41 .....	42
7 Evolution Curves for Case A42 .....	43
8 Evolution Curves for Case A35 .....	45
9 Evolution Curves for Case A21 .....	46
10 Evolution Curves for Case A22 .....	48
11 Evolution Curves for Case A23 .....	50
12 Evolution Curves for Case A24 .....	52
13 Evolution Curves for Case A25 .....	53
14 Time Evolution of Moments During Buildup of Photon Densities .....	55
15 Evolution Curves for Case A11 .....	74
16 Evolution Curves for Case A12 .....	75
17 Evolution Curves for Case A13 .....	76
18 Evolution Curves for Case A14 .....	77
19 Evolution Curves for Case A15 .....	78
20 Evolution Curves for Case A31 .....	79

List of Figures (cont.)

<u>Figure</u>		<u>Page</u>
21	Evolution Curves for Case A33 .....	80
22	Evolution Curves for Case A51 .....	81
23	Evolution Curves for Case A52 .....	82

List of Tables

<u>Table</u>	<u>Page</u>
I Laser Parameter Values .....	30
II Classification of Photon Density Singular Points .....	34
III Stable Equilibrium Values for the First and Second Moments of the Photon Density Distribution .....	38

### List of Symbols

#### Symbol

$a, b, c, d$	coefficients of linearized rate equations
$a_1, a_2$	gain coefficients ( $a_1 = g_{21} - h_1$ )
$a'_1, a'_2$	effective gain coefficients
$a_{n_1}$	upward transition rate for $n_1$
$B$	general covariance tensor
$\equiv$	
BLCKDQ	subroutine used to solve the system of rate equations numerically
$b_{n_1}$	downward transition rate for $n_1$
$c$	coupling constant
$c_{n_2}$	upward transition rate for $n_2$
$c_1$	first moment of the transition rate $w(y, z)$
$c_2$	second moment of the transition rate $w(y, z)$
$d_{n_2}$	downward transition rate for $n_2$
$E$	identity tensor
$\equiv$	
FCN	subroutine containing the rate equations
$g_{11}, g_{22}$	spontaneous emission terms
$g_{21}, g_{12}$	stimulated emission terms
$h_1, h_2$	cavity loss coefficients
$I_1, I_2$	dimensionless intensities of the electric fields in modes 1 and 2
$K_1, K_2$	coupling coefficients between the lasing mode and the lasing medium
$l_1, l_2$	equilibrium lines for modes 1 and 2
$N_1$	population density of lower lasing level
$N_u$	population density of upper lasing level
NMAX	plotting area dimension in $(n_1, n_2)$ space
$n_1, n_2$	photon number densities for modes 1 and 2
$n_1^0, n_2^0$	photon number densities at equilibrium
$n'_1, n'_2$	small density disturbance around equilibrium
$n^k$	kth moment of the photon distribution
$P(\underline{X}, t)$	probability distribution of $\underline{X}$
$P(\underline{x}, t)$	probability distribution of $\underline{x}$

List of Symbols (cont.)

Symbol

$\underline{r}$	transition vector (always in terms of the extensive variable)
$s_1, s_2$	standard deviations
$W(\underline{x}, \underline{r})$	transition rate for a jump from $\underline{x}$ by an amount $\underline{r}$
$w(\underline{x}, \underline{r})$	transition rate for a jump from $\underline{x}$ by an amount $\underline{r}$ /
$\underline{x}$	extensive macrovariable
$X_{IN}$	time at which BLCKDQ begins
$X_{OUT}$	time at which BLCKDQ provides solutions to the rate equations
$\underline{x}$	intensive macrovariable
$\Delta x$	small change in $x$
$\underline{Y}$	expected value of $\underline{x}$
$\underline{z}$	fluctuation of $\underline{x}$ about $\underline{Y}$
$\alpha_{11}, \alpha_{22}$	saturation coefficients used in rate equations
$\alpha_{12}, \alpha_{21}$	coupling coefficients used in rate equations
$\alpha$	linear gain coefficient
$\beta$	saturation coefficient
$\beta_1, \beta_2$	saturation coefficients
$\Theta_{12}, \Theta_{21}$	coupling coefficients
$\underline{\underline{\Delta}}$	general inverse covariance tensor
$\underline{\underline{\lambda}}$	covariance tensor for $\underline{x}$
$\underline{\underline{\Upsilon}}$	loss coefficient
$\rho_{12}$	correlation coefficient
$\rho_{nn}$	diagonal elements of the field density matrix
$\underline{\underline{\Sigma}}$	covariance tensor for $\underline{x}$
$\tau_c$	photon cavity lifetime
$\Omega$	size of the system
$\sim$	denotes transpose of a vector or tensor quantity

Abstract

The evolution of the first and second moments of the photon density distribution for a two-mode laser system was studied by proposing appropriate transition rate expressions and using the Kubo equations developed for a Chapman-Kolmogorov system. A numerical analysis technique was used in solving the rate equations and computer plots were generated for various combinations of laser parameter values. Anomalously large fluctuations, similar to those occurring in single-mode lasers, were observed during photon buildup of the modes. When only one mode was oscillating, a photon buildup in the non-lasing mode was seen to cause similar fluctuations in the lasing mode. In all cases, these fluctuations were accompanied by a strong linear relationship between the modes.

## PHOTON STATISTICS IN TWO-MODE LASERS

### I Introduction

#### Background

Since the development of the laser in 1960, the statistics for single-mode lasers have been studied extensively using both the semiclassical approach and the fully quantum-mechanical theory. Calculations have been made of the single-mode photon distributions below, at, and above threshold. Calculations have also been made of the time-behavior of the moments of the photon distribution as the laser operates away from equilibrium. These calculations have subsequently been verified by experiment.

The statistics for multimode lasers are not as well developed. Only the two-mode laser has been studied in any detail; and then, using only the semiclassical approach which neglects the particle or quantized nature of the light field in favor of a classical electric field. The fully quantum-mechanical treatment has just recently begun to be analyzed.

#### Purpose

The purpose of this work was to extend the study of two-mode lasers by investigating the photon distributions in equilibrium and the time behavior of the first and second moments of the distributions away from equilibrium for a two-mode laser. Of particular interest was the behavior of the system (for several pump levels and degrees of mode interaction) during buildup of photons from a photon vacuum and during transition from unstable to stable equilibrium. Transition from various

non-equilibrium points was also considered.

#### Approach

To study the behavior of the laser system, it was assumed that the system could be described by the Chapman-Kolmogorov master equation. Therefore, the resultant general evolution equations developed by Kubo were applicable. Transition rates which included terms to account for spontaneous and stimulated emission, as well as mode interaction and self-saturation, were proposed for the laser. These were then inserted into the general evolution equations, and rate equations for the first and second moments of the photon density distributions were obtained.

Appropriate values corresponding to various combinations of pump levels and degrees of mode coupling were chosen for the laser parameters. For each combination, the pump was considered constant while the coupling was assumed to take place through the mode population densities. The equilibrium points for each set of laser parameters were then obtained analytically from the rate equations and were classified using linear vibration theory to predict the behavior of the photon densities around each point.

To solve the moment rate equations dynamically and observe the laser system through transition, a computational scheme was developed which included a time-incremented numerical solution of the equations. Finally, using a series of initial photon densities with associated variances, this program was run for each combination of parameter values and several plots were obtained.

## II Theory

### Background

Just as there are two basic approaches to quantum mechanics, there are two main methods for deriving laser fluctuations fully quantum-mechanically. One method (associated more with the Schroedinger picture) utilizes a density operator to derive a "master equation". The other method (associated more with the Heisenberg picture) consists of "adding Langevin operators to the Heisenberg equation of the field operator and of the atomic operators" (Ref 9:273). The two methods are equivalent in that they solve the problem equally well. However, the master equation approach is more appropriate in that the resulting non-linear equations can be reduced to a form solvable by numerical methods, whereas the Langevin method requires analytical solutions which restrict its use to linear or linearized equations (Ref 9:273). Details of both methods can be found in the work of Sargent, Scully, and Lamb (Ref 11).

Single-Mode Theory. Using the master equation approach for single-mode lasers, the probabilities of  $n$  photons existing are determined by the diagonal elements  $\rho_{nn}$  of the associated field density matrix (Ref 11:284). Therefore, the equations of motion for these elements determine the flow of probability into and out of each  $n$  state:

$$\dot{\rho}_{nn}(t) = -[\alpha - \beta(n+1)](n+1)\rho_{nn}(t) + (\alpha - \beta n)n\rho_{n-1,n-1}(t) - \gamma n\rho_{nn}(t) + \gamma(n+1)\rho_{n+1,n+1}(t) \quad (1)$$

where  $\alpha$  is the linear gain coefficient,  $\gamma$  is the loss coefficient,

$\beta$  is the saturation coefficient, and the sign (positive or negative) of each term on the right-hand side indicates probability gains or losses, respectively, for the state  $n$  (Ref 10:2424). The photon distribution is then determined by solving these equations (Eqs (1)). It is important to note that the diagonal elements  $\rho_{nn}$  are coupled only to other diagonal elements. Therefore, to determine the photon statistics, the off-diagonal elements of the density matrix can be ignored.

In studying the behavior of any system, it is often of interest to consider the behavior of the moments of the distribution defined by

$$\langle n^k \rangle = \sum_{n=0}^{\infty} n^k p_n \quad (2)$$

where  $p_n$  is synonymous with  $\rho_{nn}$  above. When Eq (1) is substituted into the time derivative of Eq (2), the result is a set of equations of motion for the moments of the photon distribution which can then be solved numerically to observe the behavior of the moments at as well as away from equilibrium. Of particular interest are the first and second moments ( $k=1$  and  $k=2$ , respectively) since they can often be determined experimentally for comparison, whereas the distribution function cannot.

The behavior of these moments has been calculated from the initial condition that no photons exist to equilibrium conditions (Ref 10:2426-2427). The results for the expected value of the photon number (first moment) show an initial slow rise dominated by spontaneous emission, followed quickly by a rapid, almost linear, increase as the spontaneous emission is amplified by stimulated emission. However, as equilibrium is approached, the saturation effects of the laser begin to modify the system gain and the rate of increase of the average photon number approaches zero. The root mean square deviation is determined by

combining the first and second moments:

$$S = \sqrt{\langle n^2 \rangle - \langle n \rangle^2} \quad (3)$$

This deviation initially tends to follow an exponential rise as for thermal (incoherent) light and exceeds the equilibrium value as not only the photon numbers, but also the fluctuations in photon numbers, are amplified. Then, as the system moves into the saturation region, amplification of already stimulated photons becomes predominant and the deviations diminish to their relatively small equilibrium values. It is important to note that when this problem was solved semiclassically, using Langevin forces to account for noise, similar results were obtained (Ref 9:262-263).

Two-Mode Theory. Unlike single-mode lasers, the fully quantum-mechanical treatment of multimode lasers has only very recently begun to be analyzed (Ref 8). Therefore, for these lasers the theory remains centered primarily around Lamb's paper (Ref 7) which gave the first comprehensive treatment of laser action. Following this semiclassical theory, the equations of motion for a two-mode laser system are

$$\dot{I}_1 = 2I_1(a_1 - \beta_1 I_1 - \theta_{12} I_2) \quad (4)$$

and

$$\dot{I}_2 = 2I_2(a_2 - \beta_2 I_2 - \theta_{21} I_1) \quad (5)$$

where  $I_1$  and  $I_2$  are the dimensionless intensities of the electric fields for the two modes,  $a_1$  and  $a_2$  are the gain coefficients,  $\beta_1$  and  $\beta_2$  are the self-saturation coefficients, and  $\theta_{12}$  and  $\theta_{21}$  are the cross-coupling coefficients. When these equations are integrated simultaneously for a range of initial intensities, the result is a set of phase

curves in the  $I_1$ - $I_2$  plane (Refs 7:A1441-A1442; and 11:125-127).

The possible equilibrium points are determined by setting  $\dot{I}_1 = \dot{I}_2 = 0$  and solving (4) and (5) together.  $I_1$  and/or  $I_2$  equal to zero are obvious solutions, with single frequency solutions of

$$(I_1, I_2) = (0, \alpha_z/\beta_z) \quad (6)$$

and

$$(I_1, I_2) = (\alpha_1/\beta_1, 0) \quad (7)$$

For both modes to oscillate at equilibrium, the parenthesized expressions in (4) and (5) must be zero. Therefore,

$$\beta_1 I_1 + \theta_{1z} I_2 = \alpha_1 \quad (8)$$

and

$$\beta_2 I_2 + \theta_{2z} I_1 = \alpha_z \quad (9)$$

which are linear expressions in  $I_1$  and  $I_2$  and have the solutions

$$I_1 = \frac{[\alpha_1 - (\theta_{2z}/\beta_2)\alpha_z]}{1 - C} \quad (10)$$

$$I_2 = \frac{[\alpha_z - (\theta_{1z}/\beta_1)\alpha_1]}{1 - C} \quad (11)$$

where the coupling constant is defined as

$$C \equiv \frac{\theta_{1z} \theta_{2z}}{\beta_1 \beta_2} \quad (12)$$

For this solution to be a physically realizeable point, both  $I_1$  and  $I_2$

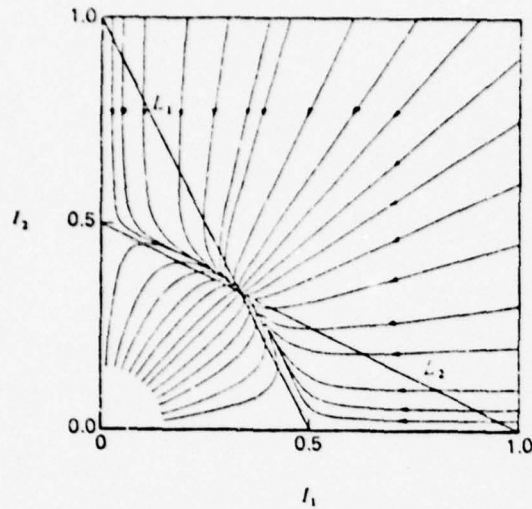


Figure 1. Phase curves showing the transient behavior of two mode oscillation. Lines  $L_1$  and  $L_2$  represent Eqs (8) and (9) with coefficients  $a_1 = 1$ ,  $a_2 = 1$ ,  $\beta_1 = \beta_2 = 2$ , and  $\theta_{1z} = \theta_{2z} = 1$ . (Ref 11:126)

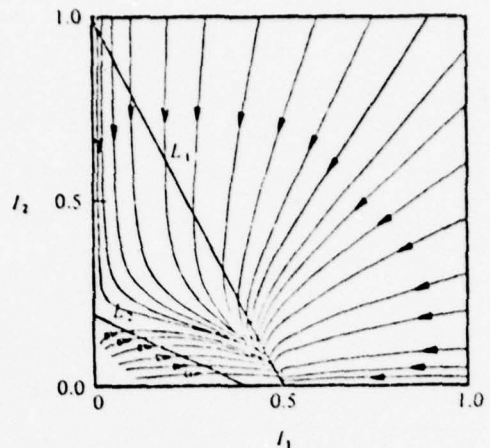


Figure 2. Diagram similar to Fig. 1, except the gain parameter for the second mode is now  $a_2 = 0.4$ , and mode 1 inhibits mode 2 at equilibrium. (Ref 11:125)

must be non-negative values. When  $C < 1$ , this occurs when both

$$a'_1 = a_1 - (\theta_{2z}/\beta_2) a_2 \quad (13)$$

and

$$a'_2 = a_2 - (\theta_{1z}/\beta_1) a_1 \quad (14)$$

are non-negative. See Fig. 1 (Ref 11:126).  $a'_1$  and  $a'_2$  are called the effective gains of their respective modes. If either effective gain is negative, then the associated mode will not oscillate and the laser will lapse into single-mode operation as shown in Fig. 2 (Ref 11:125) with mode intensities as defined by either (6) or (7), as appropriate. In this case, assuming both  $a_1$  and  $a_2$  are positive, the oscillating mode is said to inhibit oscillation in the other mode.

When  $C > 1$ , the intersection of the two lines (8) and (9) is a physical point only when both  $a'_1$  and  $a'_2$  are non-positive; that is, when each mode tends to inhibit the other. In this case, the intersection point is an unstable equilibrium and, as with the inhibition of one mode, the system relaxes into single-mode operation. Now, however, both single-mode solutions defined by (6) and (7) are stable solutions and the point to which the system evolves depends on the initial conditions.

See Fig. 3 (Ref 11:127).

When  $C = 1$ , lines (8) and (9) are parallel and Eqs (10) and (11) are indeterminate. In this instance, any combination of intensities on either mode equilibrium line (as defined by Eqs (8) and (9)) will be stable. Along these lines, the stability will be neutral with any deviations neither damped nor magnified. Deviations away from these lines, however, will decay in time, bringing the system back to the line.

As can be seen, the degree of coupling between modes, as expressed by the coupling constant  $C$ , is an important factor in determining the behavior of the system. The critical point is when  $C = 1$ . Therefore, three regions of coupling strength are defined:

$$C < 1 \quad \text{weak coupling} \quad (15a)$$

$$C = 1 \quad \text{neutral coupling} \quad (15b)$$

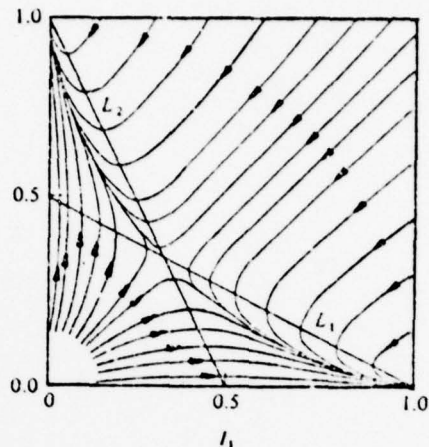


Figure 3. Phase curves showing the transient behavior of two-mode oscillation with coefficients  $a_1 = a_2 = 1$ ,  $\beta_1 = \beta_2 = 1$ , and  $\Theta_{11} = \Theta_{22} = 2$ . (Ref 11:127)

$C > 1$ 

strong coupling

(15c)

where the degree of coupling applied to each region was determined by considering Eq (12) and the relationship of  $\theta_{12}\theta_{21}$  to  $\beta_1\beta_2$ . Weak coupling implies that the cross-coupling coefficients, while they exist and affect the system, are not the dominant terms. Instead, the self-saturation coefficients are primarily responsible for limiting the growth of the system. Qualitatively, this is expressed as  $\theta_{12}\theta_{21} < \beta_1\beta_2$  or  $C < 1$ . Conversely, strong coupling indicates that cross-coupling is the dominant effect, and is expressed as  $\theta_{12}\theta_{21} > \beta_1\beta_2$ . Neutral coupling, then, corresponds to neither effect dominant, or  $\theta_{12}\theta_{21} = \beta_1\beta_2$ .

#### Derivation of Moment-Rate Equations

General Evolution Equations. The two-mode laser (or more correctly, the two laser modes) can be considered as a system composed of many elementary units which interact with themselves and with the environment. As such, a set of macrovariables is defined:

$$\underline{X} = (X_1, X_2) \quad (16)$$

where  $X_1$  and  $X_2$  represent the photon numbers present in modes 1 and 2, respectively. It is assumed that  $\underline{X}$  is a stochastic variable which follows a Markovian process as it evolves in time. Therefore, the master equation of the system is the Chapman-Kolmogorov equation, which may be written as

$$\frac{\partial}{\partial t} P(\underline{X}, t) = - \int W(\underline{X}, \underline{c}) P(\underline{X}, t) d\underline{c} + \int W(\underline{X} - \underline{c}, \underline{c}) P(\underline{X} - \underline{c}, t) d\underline{c} \quad (17)$$

where  $P(\underline{X}, t)$  is the probability distribution of  $\underline{X}$  (i.e., the probability that there exist  $X_1$  photons in mode 1 and  $X_2$  photons in mode 2) at time

$t$ , and  $W(\underline{X}, \underline{x})$  is the transition rate for a jump from  $\underline{X}$  by an amount  $\underline{x}$ .

The evolution of variables governed by this equation has been studied extensively, beginning with the work of van Kampen (Ref 16) and continued by Kubo (Refs 4; 5; and 6) and Haken (Ref 3). Therefore, the resulting evolution equations for the system are just listed here:

$$\dot{\underline{y}}(t) = \underline{c}_1(\underline{y}, t) \quad (18)$$

and

$$\begin{aligned} \dot{\underline{\sigma}}(t) = & \frac{1}{\Omega} \underline{c}_2(\underline{y}, t) + \underline{\sigma} \nabla_{\underline{y}} \tilde{\underline{c}}_1(\underline{y}, t) \\ & + \widetilde{(\nabla_{\underline{y}} \tilde{\underline{c}}_1(\underline{y}, t))} \underline{\sigma} \end{aligned} \quad (19)$$

where  $\Omega$  is the size of the system,  $\underline{y}(t)$  is the expected value of the normalized intensive macrovariable (representing the photon densities) of the system,  $\underline{x}(t) = \underline{X}/\Omega$ , and  $\underline{\sigma}(t)$  is the covariance tensor for  $\underline{x}$ . The variables  $\underline{c}_1$  and  $\underline{c}_2$ , as defined by

$$\underline{c}_1(\underline{y}, t) = \int d\underline{\sigma} \omega(\underline{y}, \underline{\sigma}) \tilde{\underline{\sigma}} \quad (20)$$

$$\underline{c}_2(\underline{y}, t) = \int d\underline{\sigma} \omega(\underline{y}, \underline{\sigma}) \underline{\sigma} \tilde{\underline{\sigma}} \quad (21)$$

are the first and second moments of  $w(\underline{y}, \underline{x})$ , the transition rate for the intensive variable  $\underline{x}$ :

$$\omega(\underline{y}, \underline{\sigma}) = \omega(\underline{x}, \underline{\sigma}) = W(\underline{X}, \underline{\sigma})/\Omega \quad (22)$$

A derivation of Eqs (18) and (19), starting from (17) and parallelling the single variable derivation of Kubo (Ref 5), is included in Appendix A.

A general analysis of Eqs (18) and (19) predicts some interesting behavior on the part of the laser system. First, the expected values of the photon number densities follow deterministic paths. For a given set of laser operating conditions, the path to equilibrium is determined solely by the initial photon densities. For a non-linear relaxation, the fluctuations generally exhibit unusual behavior as the system moves toward equilibrium. This effect becomes very pronounced when the system moves from the vicinity of an unstable equilibrium toward a stable equilibrium. Around each point, both the photon number densities and their fluctuations grow or decay exponentially, depending on the stability of the point. In between, the fluctuations grow anomalously large, peaking about half-way to the final equilibrium. (Refs 6:78-79; and 4:6-8) This enhanced fluctuation is predicted for and has been observed in single-mode lasers (Ref 2). It has also been predicted for two-mode lasers by Arecchi and Ricca in a paper which used a generalized version of the Volterra-Wiener functional technique to study multimode laser action (Ref 1).

Transition Rates. To make the evolution equations (18) and (19) specific to the two-mode laser problem requires the proper specification of the transition rates  $w(y, \underline{x})$ . It is important to note that the size of the transition,  $\underline{x}$ , is in terms of the extensive variable  $\underline{X}$  or the total number of photons, whereas the dependence on the state of the system is in terms of the intensive variable  $\underline{x}$  or the photon density.

The basic problem is depicted in Fig. 4 for a system in the state  $\underline{x} = (n_1, n_2)$ .  $a_{n_1}$  and  $b_{n_1}$  are the upward and downward transition rates,

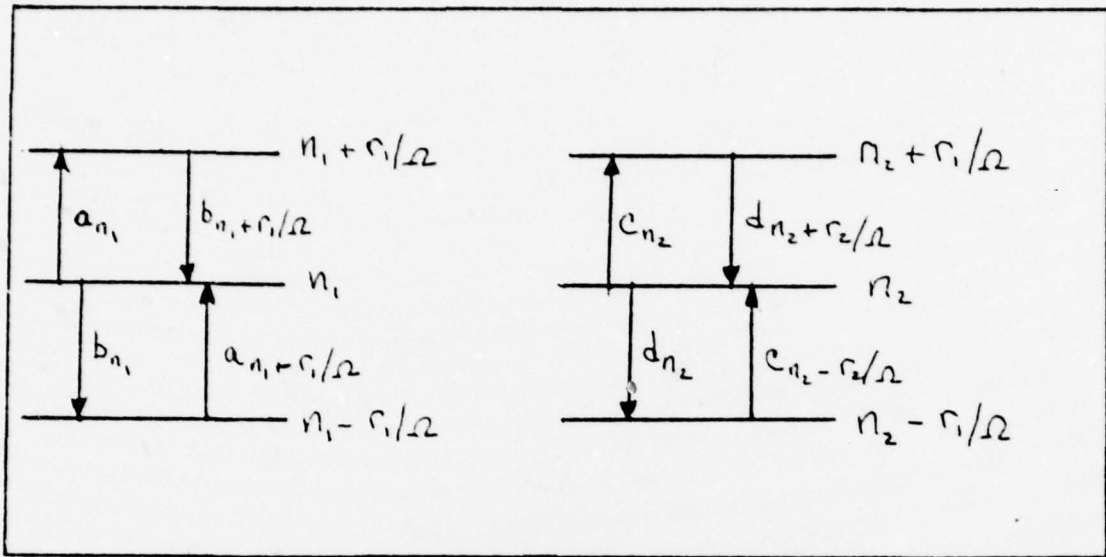


Figure 4. Transition rates associated with a laser system in the internal state  $\underline{x} = (n_1, n_2)$ . Upward transitions ( $\uparrow$ ) correspond to photon emissions while downward transitions ( $\downarrow$ ) signify photon losses.

respectively, for  $x_1$  to make a jump  $r_1/\Omega$ , and  $c_{n_2}$  and  $d_{n_2}$  are corresponding terms for  $x_2$ . It is assumed that photons are added to or deleted from the system one at a time. Therefore, the only non-zero values for  $r_1$  and  $r_2$  with associated non-zero rates are 1 and -1.

Furthermore, even for these values, the associated rates for one mode will be non-zero only if  $r_1 = 0$  for the other mode. Therefore, there are only four events with non-zero associated transition rates:  $x_1$  increases by one,  $\underline{r} = (1, 0)$ ;  $x_1$  decreases by one,  $\underline{r} = (-1, 0)$ ;  $x_2$  increases by one,  $\underline{r} = (0, 1)$ ; and  $x_2$  decreases by one,  $\underline{r} = (0, -1)$ . Based on this and on Fig. 4, the transition rates for  $\underline{x} = (n_1, n_2)$  can be written as

$$\omega(\underline{x}, \underline{r}) = \begin{cases} a_{n_1}, & \underline{r} = (1, 0) \\ b_{n_1}, & \underline{r} = (-1, 0) \\ c_{n_2}, & \underline{r} = (0, 1) \\ d_{n_2}, & \underline{r} = (0, -1) \end{cases} \quad (23)$$

These rates are also valid for  $w(y, \underline{x})$  since  $y(t)$  is just the expected value of  $\underline{x}$ .

How, then, should  $a_{n_1}$ ,  $b_{n_1}$ ,  $c_{n_2}$ , and  $d_{n_2}$  be characterized?  $b_{n_1}$  and  $d_{n_2}$  essentially are the loss terms of the system, including internal cavity losses as well as the amount coupled out of the system. Therefore, they can be expressed as

$$b_{n_1} = h_1 n_1 \quad (24)$$

and

$$d_{n_2} = h_2 n_2 \quad (25)$$

where  $h_1$  and  $h_2$  are determined by the cavity lifetime for a photon in modes 1 and 2, respectively (Ref 12:413).  $a_{n_1}$  and  $c_{n_2}$ , representing the gain of each mode of the system, are somewhat more complicated. Each gain expression must include terms to account for both stimulated and spontaneous emission as well as for self-saturation and cross-coupling. The self-saturation occurs because there is only a finite pump which excites a finite number of atoms or molecules which may then be stimulated to contribute to the system of photons. Cross-coupling occurs when both modes have to compete for some of the same atoms or molecules.

The expression chosen which meets these requirements for  $a_{n_1}$  is

$$a_{n_1} = \frac{g_{11} + g_{21} n_1}{1 + \alpha_{11} n_1 + \alpha_{12} n_2} \quad (26)$$

where  $g_{11}$  and  $g_{21}$  are factors accounting for spontaneous and stimulated emission, respectively, and  $\alpha_{11}$  and  $\alpha_{12}$  account for self-saturation and cross-coupling, respectively. A similar expression for  $c_{n_2}$  is

$$C_{n_2} = \frac{g_{12} + g_{22} n_2}{1 + \alpha_{11} n_1 + \alpha_{22} n_2} \quad (27)$$

with  $g_{12}$ ,  $g_{22}$ ,  $\alpha_{11}$ , and  $\alpha_{22}$  having the same meaning for mode 2 as  $g_{11}$ ,  $g_{21}$ ,  $\alpha_{12}$  and  $\alpha_{21}$  do for mode 1. It is important to note that with these expressions the transition rates will always be non-negative. The validity of these choices will be demonstrated in a later section.

Laser Rate Equations. When the transition rates (Eqs (24)-(27)) are inserted into the evolution equations (18) and (19), the resultant equations are the desired laser rate equations for the first and second moments of the photon density distributions. For ease of manipulation, the evolution equations will be handled in their component form. Therefore, Eq (18) becomes

$$\dot{y}_j(t) = c_{1j}(y) \quad (28)$$

and Eq (19) is written as

$$\dot{\sigma}_{jk}(t) = \frac{1}{\pi} c_{2jk} + \sum_l \left( \sigma_{jl} \frac{\partial c_{1k}}{\partial y_l} + \frac{\partial c_{1j}}{\partial y_l} \sigma_{lk} \right) \quad (29)$$

where now  $c_1(y)$  and  $c_2(y)$  are expressed as

$$c_{1j}(y) = \int dr r_j \omega(y, \xi) \quad (30)$$

and

$$c_{2jk}(y) = \int dr r_j r_k \omega(y, \xi) \quad (31)$$

Dealing first with Eq (30), Eqs (24)-(27) are appropriately inserted

into Eq (30) as determined by Eqs (23). The resulting components of  $\underline{c}_1(\underline{y})$  are

$$\begin{aligned}
 c_{11}(\underline{y}) &= \int dr r_1 \omega(\underline{y}, \underline{r}) \\
 &= a_{n_1} + (-1) b_{n_1} \\
 &= \frac{g_{11} + g_{21} n_1}{1 + \alpha_{11} n_1 + \alpha_{12} n_2} - h_1 n_1, \tag{32}
 \end{aligned}$$

and

$$\begin{aligned}
 c_{12}(\underline{y}) &= \int dr r_2 \omega(\underline{y}, \underline{r}) \\
 &= c_{n_2} + (-1) d_{n_2} \\
 &= \frac{g_{12} + g_{22} n_2}{1 + \alpha_{21} n_1 + \alpha_{22} n_2} - h_2 n_2 \tag{33}
 \end{aligned}$$

Similarly, the diagonal elements of  $\underline{c}_2(\underline{y})$  are found from Eq (31) to be

$$c_{211} = \frac{g_{11} + g_{21} n_1}{1 + \alpha_{11} n_1 + \alpha_{12} n_2} + h_1 n_1, \tag{34}$$

and

$$c_{222} = \frac{g_{12} + g_{22} n_2}{1 + \alpha_{21} n_1 + \alpha_{22} n_2} + h_2 n_2 \tag{35}$$

Since mutually exclusive events were assumed,  $r_j$  or  $r_k$  must equal zero whenever  $j \neq k$ . Therefore, the off-diagonal elements of  $\underline{c}_2$  are both zero.

To complete the development of the rate equations, the partial derivatives of (32) and (33) with respect to  $y_1$  and  $y_2$  must be determined. In doing this, as throughout this development, it should be pointed out that  $n_1$  and  $n_2$  are defined as synonymous with  $y_1$  and  $y_2$ , respectively. When this is done and Eqs (32)-(35) are inserted into Eqs (28) and (29) as appropriate, the rate equations for the first and second moments of the photon density distributions become

$$\dot{n}_1 = \frac{g_{11} + g_{21}n_1}{1 + \alpha_{11}n_1 + \alpha_{12}n_2} - h_1 n_1 \quad (36)$$

$$\dot{n}_2 = \frac{g_{12} + g_{22}n_2}{1 + \alpha_{21}n_1 + \alpha_{22}n_2} - h_2 n_2 \quad (37)$$

$$\begin{aligned} \dot{\sigma}_{11} = 2\sigma_{11} & \left[ \frac{g_{21} - g_{11}\alpha_{11} + g_{21}\alpha_{12}n_2}{(1 + \alpha_{11}n_1 + \alpha_{12}n_2)^2} - h_1 \right] - 2\sigma_{12} \left[ \frac{\alpha_{12}(g_{11} + g_{21}n_1)}{(1 + \alpha_{11}n_1 + \alpha_{12}n_2)^2} \right] \\ & + \frac{1}{\sqrt{2}} \left( \frac{g_{11} + g_{21}n_1}{1 + \alpha_{11}n_1 + \alpha_{12}n_2} + h_1 n_1 \right) \end{aligned} \quad (38)$$

$$\begin{aligned} \dot{\sigma}_{22} = 2\sigma_{22} & \left[ \frac{g_{12} - g_{12}\alpha_{22} + g_{22}\alpha_{21}n_1}{(1 + \alpha_{21}n_1 + \alpha_{22}n_2)^2} - h_2 \right] - 2\sigma_{12} \left[ \frac{\alpha_{21}(g_{12} + g_{22}n_2)}{(1 + \alpha_{21}n_1 + \alpha_{22}n_2)^2} \right] \\ & + \frac{1}{\sqrt{2}} \left( \frac{g_{12} + g_{22}n_2}{1 + \alpha_{21}n_1 + \alpha_{22}n_2} + h_2 n_2 \right) \end{aligned} \quad (39)$$

and

$$\begin{aligned}\dot{\sigma}_{12} = & -\sigma_{11} \left[ \frac{\alpha_{21} (g_{12} + g_{22} n_2)}{(1 + \alpha_{11} n_1 + \alpha_{22} n_2)^2} \right] - \sigma_{22} \left[ \frac{\alpha_{12} (g_{11} + g_{21} n_1)}{(1 + \alpha_{11} n_1 + \alpha_{22} n_2)^2} \right] \\ & + \sigma_{12} \left[ \frac{g_{21} - g_{11} \alpha_{11} + g_{21} \alpha_{12} n_2}{(1 + \alpha_{11} n_1 + \alpha_{22} n_2)^2} + \frac{g_{12} - g_{12} \alpha_{22} + g_{12} \alpha_{11} n_1}{(1 + \alpha_{11} n_1 + \alpha_{22} n_2)^2} - h_1 - h_2 \right] \quad (40)\end{aligned}$$

There is actually a sixth rate equation, for  $\sigma_{21}$ , but it is identical in form to (40). Also, the equality of  $\sigma_{11}$  and  $\sigma_{22}$  due to the symmetry of the covariance matrix is used to combine terms in Eqs (38), (39), and (40). Therefore, only the five equations (36)-(40) need be solved simultaneously to determine the behavior of the laser system.

#### Equilibrium Analysis of Moment Equations

As stated previously, the purpose of this study was to determine the behavior of a two-mode laser system as it transitioned from non-equilibria to equilibrium. This was the reason for developing the laser rate equations and solving them dynamically. However, before applying numerical methods to these equations to follow the system through its transition, a basic understanding of the system can be gained by determining analytically the positions of all equilibria, both stable and unstable, and the behavior of the system around each of these points. Of particular interest is the first-moment equilibria, since these values for  $n_1$  and  $n_2$  are necessary to do any equilibrium analysis on the variances. Therefore, the photon rate equations (36) and (37) are considered first, followed by a brief discussion of the variance rate equations (38), (39), and (40) in equilibrium.

First-Moment Equations. Recalling the first-moment or photon

density rate equations (36) and (37), equilibria will occur when both  $\dot{n}_1$  and  $\dot{n}_2$  are zero. These are also referred to as singular points of the system. The point  $n_1 = n_2 = 0$  can only be a solution if  $g_{11} = g_{22} = 0$ ; but this corresponds to zero noise or spontaneous emission in the system, which is an unrealizable situation. In fact, neither  $n_1$  nor  $n_2$  equal to zero can be a solution for finite values of  $n$ . Therefore, there is some combination of non-zero  $(n_1, n_2)$  for which equilibrium will exist.

As a first approximation, assume  $n_1$  and  $n_2 \gg 1$ ,  $g_{11} = g_{21}$ , and  $g_{12} = g_{22}$ . Then Eqs (36) and (37), set to equilibrium, become

$$\dot{n}_1 = 0 = \left[ g_{z1} / (1 + \alpha_{11} n_1 + \alpha_{12} n_2) - h_1 \right] n_1 \quad (41)$$

and

$$\dot{n}_2 = 0 = \left[ g_{zz} / (1 + \alpha_{z1} n_1 + \alpha_{z2} n_2) - h_2 \right] n_2 \quad (42)$$

Since only non-zero values of  $n_1$  and  $n_2$  are of interest, the bracketed quantities in (41) and (42) are set to zero and examined. After rearranging, the resultant equations are

$$\alpha_{11} n_1 + \alpha_{12} n_2 = \frac{g_{z1}}{h_1} - 1 \quad (43)$$

and

$$\alpha_{z1} n_1 + \alpha_{z2} n_2 = \frac{g_{zz}}{h_2} - 1 \quad (44)$$

These are just two straight lines (call them  $l_1$  and  $l_2$ , respectively) in  $(n_1, n_2)$  space with  $n_1$ - and  $n_2$ -intercepts of

$$\frac{1}{\alpha_{11}} \left( \frac{g_{z1}}{h_1} - 1 \right) \quad \text{and} \quad \frac{1}{\alpha_{12}} \left( \frac{g_{z1}}{h_1} - 1 \right) \quad (45)$$

for  $l_1$ , and

$$\frac{1}{\alpha_{21}} \left( \frac{g_{z2}}{h_2} - 1 \right) \quad \text{and} \quad \frac{1}{\alpha_{22}} \left( \frac{g_{z2}}{h_2} - 1 \right) \quad (46)$$

for  $l_2$ .

Within the limits of the original assumption ( $n_1, n_2 \gg 1$ ), the point of intersection of these two lines is the location of one equilibrium or singular point. To find this point of intersection, equations (43) and (44) are solved simultaneously. This results in

$$n_1 = \frac{\frac{1}{h_1 \alpha_{11}} (g_{z1} - h_1) - \frac{\alpha_{12}}{\alpha_{11}} \frac{1}{h_2 \alpha_{22}} (g_{z2} - h_2)}{1 - \frac{\alpha_{21} \alpha_{12}}{\alpha_{11} \alpha_{22}}} \quad (47)$$

and

$$n_2 = \frac{\frac{1}{h_2 \alpha_{22}} (g_{z2} - h_2) - \frac{\alpha_{21}}{\alpha_{22}} \frac{1}{h_1 \alpha_{11}} (g_{z1} - h_1)}{1 - \frac{\alpha_{21} \alpha_{12}}{\alpha_{11} \alpha_{22}}} \quad (48)$$

Now, if the following substitutions are made,

$$g_{z1} - h_1 = \alpha_1 \quad g_{z2} - h_2 = \alpha_2 \quad (49a)$$

$$h_1 \alpha_{11} = \beta_1 \quad h_2 \alpha_{22} = \beta_2 \quad (49b)$$

$$h_1 \alpha_{12} = \theta_{12} \quad h_2 \alpha_{21} = \theta_{21} \quad (49c)$$

equations (47) and (48) become

$$n_1 = \frac{(a_1 - (\theta_{12}/\beta_2) a_2)/\beta_1}{1 - C} \quad (50)$$

and

$$n_2 = \frac{(a_2 - (\theta_{21}/\beta_1) a_1)/\beta_2}{1 - C} \quad (51)$$

where

$$C = \frac{\alpha_{12} \alpha_{21}}{\alpha_{11} \alpha_{22}} = \frac{\theta_{12} \theta_{21}}{\beta_1 \beta_2} \quad (52)$$

is a measure of the degree of coupling, as previously discussed. Comparing this to the semiclassical development of Lamb presented earlier, it is seen that Eqs (50) and (51) are essentially identical to Eqs (10) and (11) with the normalized intensities  $I_1$  and  $I_2$  replaced by their quantum equivalent, the photon number densities. Furthermore, when Eqs (41) and (42) are expressed as single fractions (with non-zero denominators), they can be reduced to

$$\dot{n}_1 = 0 = n_1 [(g_{21} - h_1) - h_1 \alpha_{11} n_1 - h_1 \alpha_{12} n_2] \quad (53)$$

and

$$\dot{n}_2 = 0 = n_2 [(g_{12} - h_2) - h_2 \alpha_{22} n_2 - h_2 \alpha_{21} n_1] \quad (54)$$

which are equivalent to Lamb's equations of motion for  $I_1$  and  $I_2$ , Eqs (4) and (5), at equilibrium. Therefore, in the limits of equilibrium and of large  $n$  (or zero noise), the chosen transition rates  $a_{n_1}$ ,  $b_{n_1}$ ,  $c_{n_2}$ , and  $d_{n_2}$  are valid, and the semiclassical equilibrium analysis done by Lamb can be applied.

When the spontaneous emission terms  $g_{11}$  and  $g_{12}$  are not assumed away, the singularities for the system are determined by setting Eqs (36) and (37) to zero and solving simultaneously. Solving Eq (36) for  $n_2$  and substituting the obtained expression into (37), the result is the fourth order equation

$$\begin{aligned}
 & h_1^2 h_2 \alpha_{11} (\alpha_{12} \alpha_{21} - \alpha_{11} \alpha_{22}) n_1^4 + h_1 [h_2 (g_{11} - h_1) (2\alpha_{11} \alpha_{22} - \alpha_{12} \alpha_{21}) \\
 & - h_1 \alpha_{11} \alpha_{12} (g_{22} - h_2)] n_1^3 + [h_1 \alpha_{12} (g_{12} h_1 \alpha_{12} + (g_{22} - h_2) (g_{21} - h_1) \\
 & - h_2 \alpha_{21} g_{11}) + h_2 \alpha_{22} (2g_{11} h_1 \alpha_{11} - (g_{21} - h_1)^2)] n_1^2 + [h_1 g_{11} \alpha_{12} (g_{22} - h_2) \\
 & - 2g_{11} h_2 \alpha_{22} (g_{21} - h_1)] n_1 - h_2 \alpha_{22} g_{11}^2 = 0 \quad (55)
 \end{aligned}$$

This is then solved using basic algebraic techniques (Ref 14:107) and, depending on the coefficients, generally results in four singular points for the system.

Characterization of Singular Points. The behavior of the system around a given singularity is determined by considering a small disturbance around that point. Based on this behavior, the singularity can then be classified into one of six basic types, as shown in Fig. 5.

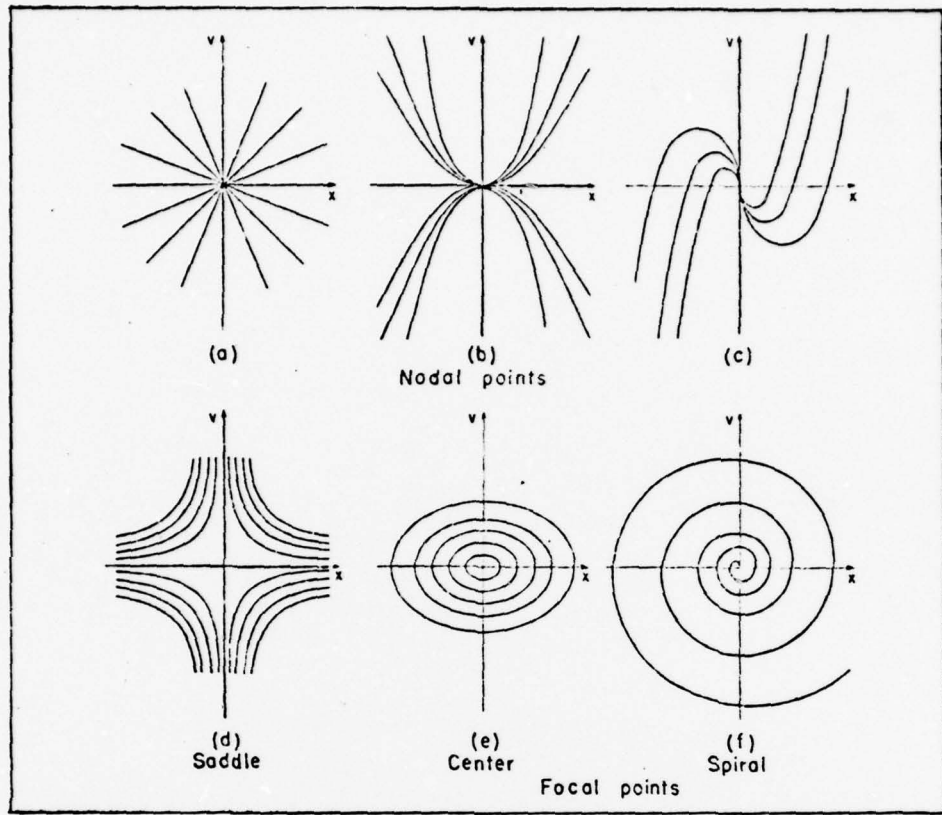


Figure 5. Types of Singular Points (Ref 15:39)

Letting  $n_1 = n_1^0 + n_1'$  and  $n_2 = n_2^0 + n_2'$  (where  $n_1^0$  and  $n_2^0$  are the singular point values) and inserting these into Eqs (36) and (37), the resulting linearized forms of the photon rate equations are

$$\dot{n}_1 = \frac{-h_1\alpha_{11}n_1^0n_2' + (g_u - h_1 - 2h_1\alpha_{11}n_1^0 - h_1\alpha_{12}n_2^0)n_1'}{1 + \alpha_{11}n_1^0 + \alpha_{12}n_2^0} \quad (56)$$

and

$$\dot{n}_2 = \frac{(g_u - h_2 - 2h_2\alpha_{22}n_2^0 - h_2\alpha_{21}n_1^0)n_2' - h_2\alpha_{21}n_1^0n_2'}{1 + \alpha_{21}n_1^0 + \alpha_{22}n_2^0} \quad (57)$$

For a complete development of Eqs (56) and (57) see Appendix B. These

equations can be combined in the form

$$\frac{dn'_1}{dn'_2} = \frac{an'_2 + bn'_1}{cn'_2 + dn'_1} \quad (58)$$

where

$$a = -h_1 \alpha_{12} n_1^\circ / (1 + \alpha_{11} n_1^\circ + \alpha_{12} n_2^\circ) \quad (59a)$$

$$b = (g_{21} - h_1 - 2h_1 \alpha_{11} n_1^\circ - h_1 \alpha_{12} n_2^\circ) / (1 + \alpha_{11} n_1^\circ + \alpha_{12} n_2^\circ) \quad (59b)$$

$$c = (g_{22} - h_2 - 2h_2 \alpha_{22} n_2^\circ - h_2 \alpha_{21} n_1^\circ) / (1 + \alpha_{21} n_1^\circ + \alpha_{22} n_2^\circ) \quad (59c)$$

and

$$d = -h_2 \alpha_{21} n_1^\circ / (1 + \alpha_{21} n_1^\circ + \alpha_{22} n_2^\circ) \quad (59d)$$

The type of singularity can then be determined by a series of expressions involving these coefficients. These expressions, and their relationships to the types of singular points as shown in Fig. 5, are as follows (Ref 15:44) :

$$\text{I. } (b-c)^2 + 4ad > 0 \quad \begin{cases} ad - bc < 0 & \text{Node (Fig. 5a, 5b)} \\ ad - bc > 0 & \text{Saddle (Fig. 5d)} \end{cases}$$

$$\text{II. } (b-c)^2 + 4ad < 0 \quad \begin{cases} b + c = 0 & \text{Center (Fig. 5e)} \\ b + c \neq 0 & \text{Spiral (Fig. 5f)} \end{cases}$$

$$\text{III. } (b-c)^2 + 4ad = 0 \quad \text{Node (Fig. 5c)}$$

Also, a node or spiral is unstable or stable depending on whether  $b + c$  is positive or negative, respectively.

Second-Moment Equations. Knowing the equilibrium values for the photon densities, the variance rate equations (38), (39), and (40) can be set to equilibrium and solved simultaneously. The zero of  $\dot{\sigma}_{11}$  in Eq (38) represents a plane parallel to the  $\sigma_{22}$  axis in  $(\sigma_{11}, \sigma_{22}, \sigma_{12})$  space. Similarly, Eq (39) represents a plane parallel to the  $\sigma_{11}$  axis, whereas Eq (40) is the equation for a straight line. Therefore, for a given singular point  $(n_1, n_2)$ , there will be at most a single equilibrium point for the variances. Eqs (38) and (39) are solved for  $\sigma_{11}$  and  $\sigma_{22}$ , respectively, to get

$$\sigma_{11} = \frac{-(2B\sigma_{12} + C)}{2A} \quad (60)$$

and

$$\sigma_{22} = \frac{-(2E\sigma_{12} + C)}{2D} \quad (61)$$

where

$$A = (g_{21} - g_{11}\alpha_{11} + g_{21}\alpha_{12}n_2)(1 + \alpha_{11}n_1 + \alpha_{12}n_2)^{-2} - h_1 \quad (62a)$$

$$B = -\alpha_{12}(g_{11} + g_{21}n_1)(1 + \alpha_{11}n_1 + \alpha_{12}n_2)^{-2} \quad (62b)$$

$$C = \frac{1}{2} \left[ (g_{11} + g_{21}n_1)(1 + \alpha_{11}n_1 + \alpha_{12}n_2)^{-1} + h_1 n_1 \right] \quad (62c)$$

$$D = (g_{22} - g_{12}\alpha_{22} + g_{22}\alpha_{21}n_1)(1 + \alpha_{21}n_1 + \alpha_{22}n_2)^{-2} - h_2 \quad (62d)$$

$$E = -\alpha_{21}(g_{12} + g_{22}n_2)(1 + \alpha_{21}n_1 + \alpha_{22}n_2)^{-2} \quad (62e)$$

and

$$F = \frac{1}{\Omega} \left[ (g_{12} + g_{22}n_2) \left( 1 + \alpha_{11}n_1 + \alpha_{22}n_2 \right)^{-1} + h_2n_2 \right] \quad (62f)$$

Eqs (60) and (61) are then inserted into Eq (40) and the resulting expression for  $\sigma_{12}$  is

$$\sigma_{12} = \frac{CED + ABF}{2 \left[ (A+D)(AD-EB) \right]} \quad (63)$$

This value is then used in Eqs (60) and (61) to obtain corresponding values of  $\sigma_{11}$  and  $\sigma_{22}$ , respectively.

### III Approach

#### Computational Scheme

In studying the behavior of the laser system using the laser rate equations (36)-(40), several steps were accomplished. The first of these was the development of a computer program which included the selection of a numerical analysis scheme capable of solving the system of rate equations (36)-(40) in arbitrary time increments. The routine chosen for this most important procedure is a FORTRAN IV subroutine called BLCKDQ (Ref 13). It uses a predictor-corrector formula of 8th order with user specified tolerances, which were set to  $10^{-15}$  because of initial rapid changes in the moments. Time-incremented solutions are possible because BLCKDQ solves the system of equations at a user specified time (XOUT), given appropriate initial values at some prior user specified time (XIN). Therefore, the system is incremented to equilibrium by calling BLCKDQ within a loop where the "initial" values are set equal to the solutions from the previous time step, XIN is set equal to the previous XOUT, and XOUT is incremented by some predetermined amount. Built around this loop, the remainder of the program was then developed to solve the rate equations to equilibrium for a series of initial value points and to store for plotting all sets of solutions belonging to a given set of laser parameters. The laser rate equations are contained in a user supplied subroutine FCN which is called by BLCKDQ.

#### Selection of Values for Laser Parameters

The second step in making the rate equations solvable was to determine appropriate values for the various laser parameters ( $g_{ij}$ ,  $\alpha_{ij}$ ,  $h_i$ ) for the desired combinations of pump levels and degrees of coupling.

To do this, several assumptions were made. First, it was assumed that the cavity losses, the self-saturation, and the cross-coupling were the same for both modes. That is

$$h_1 = h_2 \quad (64a)$$

$$\alpha_{11} = \alpha_{22} \quad (64b)$$

$$\alpha_{12} = \alpha_{21} \quad (64c)$$

Comparing Siegman's photon rate equation (Ref 12:418) to Eqs (36) and (37), and noting that Siegman has no saturation or coupling terms, the following equivalences can be made:

$$g_{11} = K_1 (N_u - N_l) \quad (65a)$$

$$g_{22} = K_2 (N_u - N_l) \quad (65b)$$

$$g_{11} = K_1 N_u \quad (65c)$$

$$g_{12} = K_2 N_u \quad (65d)$$

where  $N_u$  and  $N_l$  are population densities of the upper and lower lasing levels and  $K_1$  and  $K_2$  are coupling coefficients between the lasing modes and the lasing medium. It is assumed that the lower lasing level depopulates essentially instantaneously ( $N_l \approx 0$ ) and the upper lasing level is maintained constant. Therefore,  $g_{11} = g_{21} = \text{constant}$  and  $g_{12} = g_{22} = \text{constant}$ .

To select a value for  $h$ , the following relationship is noted (Ref 12:418):

$$h = 1/\gamma_c \quad (66)$$

where  $\tau_c$  is the photon cavity lifetime. A representative value for  $\tau_c$  is  $10^{-8}$  sec. Therefore

$$h = h_1 = h_2 = 10^8 \quad (67)$$

is used for all combinations of  $g_{ij}$  and  $\alpha_{ij}$ . The saturation and coupling coefficients are somewhat more elusive. To get an idea of at least an order of magnitude, the expressions (49) were recalled and compared with values for  $\beta_i$  and  $\Theta_i$  used by Lamb (Ref 11:121). Therefore, for each type of coupling (as determined by (6) and (52)), the following values were chosen:

$$\text{weak coupling } (c < 1): \quad \alpha_{11} = \alpha_{22} = 2 \times 10^{-10} \quad (68)$$

$$\alpha_{12} = \alpha_{21} = 10^{-10}$$

$$\text{neutral coupling } (c = 1): \quad \alpha_{ij} = 10^{-10} \quad (69)$$

$$\text{strong coupling } (c > 1): \quad \alpha_{11} = \alpha_{22} = 10^{-10} \quad (70)$$

$$\alpha_{12} = \alpha_{21} = 2 \times 10^{-10}$$

In selecting appropriate pump parameters  $g_{ij}$ , five different pump levels were defined:

well above threshold:	$g_{21} > 2h_1$	$g_{22} > 2h_2$
slightly above threshold:	$h_1 < g_{21} < 1.1h_1$	$h_2 < g_{22} < 1.1h_2$
threshold:	$g_{21} = h_1$	$g_{22} = h_2$
slightly below threshold:	$0.9h_1 < g_{21} < h_1$	$0.9h_2 < g_{22} < h_2$
well below threshold:	$g_{21} < 0.5h_1$	$g_{22} < 0.5h_2$

For each pump level, both  $g_{21} = g_{22}$  and  $g_{21} > g_{22}$  were considered.

For the case of  $g_{21} > g_{22}$ , the values were chosen so that mode 2 was

totally inhibited by mode 1. This corresponds to  $n_2$  being negative at the equilibrium defined by (48). The values chosen for the pump parameters are found in Table I, as well as the other laser parameter values previously mentioned.

The only other variable in the laser rate equations which must be specified is the size of the system,  $\Omega$ . The only restriction on  $\Omega$  is that it be some finite, positive value. Therefore, for convenience, a size of  $\Omega = 1$  was chosen.

#### Selection of Initial Conditions

For each set of laser parameters the final step before running the program and plotting the results was to determine a series of initial value points in  $(n_1, n_2)$  and their associated variances. The general goal was to select between 20 and 25 starting points per set of parameters spread around the  $n_1$  vs.  $n_2$  plot area. To do this required the determination of a maximum photon number NMAX which then became the dimension (in  $(n_1, n_2)$  space) for the square plotting area. For cases with pump levels above threshold, NMAX was taken to be the maximum intercept value of  $l_1$  and  $l_2$  as defined by (45) and (46). For threshold and below threshold cases, NMAX was determined by identifying the stable equilibrium for the particular case and multiplying the larger n- coordinate by an arbitrary factor between approximately three and ten. This ensured that the stable equilibrium was within the plotting area, but was not obscured by the axes. The values chosen for NMAX, as shown in Table I, were constant for each pump level, regardless of the degree of coupling. Initial points were then selected evenly around the edge of the plotting area in addition to several points around the origin and points close to any pre-determined unstable equilibria.

Table I. Laser Parameter Values

Pump Level	Weak Coupling			Strong Coupling			Neutral Coupling		
	matched	unmatched	matched	unmatched	matched	unmatched	unmatched	unmatched	unmatched
well above NMAX = $4 \times 10^{10}$	A11 $E_{ij} = 5.0 \times 10^8$	A12 $E_{21} = 5.0 \times 10^8$	A13 $E_{ij} = 5.0 \times 10^8$	A14 $E_{21} = 5.0 \times 10^8$	A15 $E_{22} = 2.5 \times 10^8$	A16 $E_{22} = 2.5 \times 10^8$	A17 $E_{21} = 5.0 \times 10^8$	A18 $E_{21} = 5.0 \times 10^8$	A19 $E_{22} = 2.5 \times 10^8$
slightly above NMAX = $8 \times 10^8$	A21 $E_{ij} = 1.08 \times 10^8$	A22 $E_{21} = 1.08 \times 10^8$	A23 $E_{ij} = 1.08 \times 10^8$	A24 $E_{21} = 1.08 \times 10^8$	A25 $E_{21} = 1.08 \times 10^8$	A26 $E_{22} = 1.02 \times 10^8$	A27 $E_{21} = 1.08 \times 10^8$	A28 $E_{21} = 1.08 \times 10^8$	A29 $E_{22} = 1.02 \times 10^8$
threshold NMAX = $1.8 \times 10^5$	A31 $E_{ij} = 10^8$		A33 $E_{ij} = 10^8$				A35 **		
slightly below NMAX = 250	A41 $E_{ij} = 0.98 \times 10^8$	A42 $E_{21} = 0.98 \times 10^8$	A43 $E_{ij} = 0.98 \times 10^8$	A44 $E_{21} = 0.98 \times 10^8$	A45 $E_{21} = 0.98 \times 10^8$	A46 $E_{22} = 0.92 \times 10^8$	A47 $E_{21} = 0.98 \times 10^8$	A48 $E_{21} = 0.98 \times 10^8$	A49 $E_{22} = 0.92 \times 10^8$
well below NMAX = 16	A51 $E_{ij} = 0.5 \times 10^8$	A52 $E_{21} = 0.6 \times 10^8$	A53 $E_{ij} = 0.5 \times 10^8$	A54 $E_{21} = 0.6 \times 10^8$	A55 $E_{22} = 0.1 \times 10^8$	A56 $E_{22} = 0.1 \times 10^8$	A57 $E_{22} = 0.1 \times 10^8$	A58 $E_{21} = 0.6 \times 10^8$	A59 $E_{22} = 0.1 \times 10^8$
	$\alpha_{11} = \alpha_{22} = 2.0 \times 10^{-10}$		$\alpha_{11} = \alpha_{22} = 1.0 \times 10^{-10}$				$\alpha_{11} = \alpha_{22} = \alpha_{12}$		
	$\alpha_{12} = \alpha_{21} = 1.0 \times 10^{-10}$		$\alpha_{11} = \alpha_{22} = 2.0 \times 10^{-10}$				$= \alpha_{21} = 10^{-10}$		
	$h_1 = h_2 = 10^8$		$h_1 = h_2 = 10^8$				$h_1 = h_2 = 10^8$		

\*\* matched modes  
 A\_— identification by which each set of conditions will referred in the plots

Having selected the initial  $(n_1, n_2)$ , the question is how to determine, or choose, appropriate initial variances for each point. To do this, another question was asked. How would each initial point be attained physically so that the system could then make a transition to the desired stable equilibrium? One possibility is to first change some of the laser parameters such that the initial point becomes a stable equilibrium point. The system is then returned "instantaneously" to the original configuration and the behavior of the system in transition is observed. This scheme was used, varying the cavity loss terms  $h_1$  and  $h_2$ , as in a Q-switched laser. The necessary "new" loss terms were determined by solving Eqs (36) and (37) at equilibrium for  $h_1$  and  $h_2$ , respectively, given  $n_1$  and  $n_2$ . Then, using these "new" values and the initial  $n_1$  and  $n_2$ , the associated variances were obtained by solving Eqs (63), (60), and (61). In several cases (above threshold, strongly-coupled), some of the initial points could not be changed into stable equilibria by merely changing the cavity losses. In these instances, the initial values for the variances were arbitrarily set as follows:

$$\sigma_{11} = n_1^2 \quad (71a)$$

$$\sigma_{22} = n_2^2 \quad (71b)$$

$$\sigma_{12} = -n_1 n_2 \quad (71c)$$

In running the computer program to determine the behavior of the laser system, it was decided that the standard deviations  $s_1$  and  $s_2$  and the correlation coefficient defined by

$$s_1 = \sqrt{\sigma_{11}} \quad , \quad s_2 = \sqrt{\sigma_{22}} \quad (72)$$

and

$$\rho_{12} = \frac{\sigma_{12}}{\sqrt{\sigma_{11} \sigma_{22}}} \quad (73)$$

would be of more interest than the actual variances. Therefore, these values were calculated and printed out along with the photon densities, the variances, and XOUT each time the program cycled through the BLCKDQ loop. In addition, besides the  $n_1$  vs.  $n_2$  plots similar to Lamb's results, three-dimensional plots involving  $s_1$ ,  $s_2$ , and  $\rho_{12}$  were produced.

#### IV Results and Discussion

##### Equilibrium Analysis

Photon Densities. The photon density equilibrium points for each combination of laser parameter values (as defined in Table I) are listed in Table II. Included is the classification of each point. As expected, there are generally four such points for each set. The only exception is when the modes are neutrally coupled (i.e., when the cross-coupling terms equal the self-saturation terms). In this case, there are either two or three singular points, depending on whether the pump parameters are equal or unequal, respectively. For all but the threshold cases, these points are very close to the equilibria of the noiseless approximation (as defined by Eqs (41) and (42)). The difference, though small, is important because it indicates that a photon vacuum is never an equilibrium, stable or unstable, for either mode. Therefore, even when there is no net gain for the system, there is some positive average-photon-density to which the system will relax.

For each set of parameters, there is at least one stable and one unstable node. The type of the other singularities depends on both the degree of coupling and the level of pump. For all weak and neutral coupled cases, these other equilibria are all saddle points, each of which has one negative coordinate thus ensuring that the system can move toward stability from any physically realizeable point. When the laser modes are strongly coupled, the type of these other singularities is determined by the level of pumping. At threshold, these two equilibria are both complex-valued. Below threshold, both singularities are unstable, one being a saddle point and the other an unstable node.

Table II. Classification of Photon Density Singular Points

Data Set ID	$n_1$	$n_2$	Type
A11	$1.333 \times 10^{10}$	$1.333 \times 10^{10}$	stable node
	$2.000 \times 10^{10}$	-2.500	saddle
	-2.500	$2.000 \times 10^{10}$	saddle
	-1.250	-1.250	unstable node
A12	$2.000 \times 10^{10}$	5.000	stable node
	-1.538	$7.500 \times 10^9$	saddle
	$2.167 \times 10^{10}$	$-3.333 \times 10^9$	saddle
	-1.250	-1.667	unstable node
A13	$4.000 \times 10^{10}$	1.250	stable node
	$1.333 \times 10^{10}$	$1.333 \times 10^{10}$	saddle
	1.250	$4.000 \times 10^{10}$	stable node
	-1.250	-1.250	unstable node
A14	$4.000 \times 10^{10}$	0.3846	stable node
	-5.000	$1.500 \times 10^{10}$	saddle
	$-3.333 \times 10^9$	$2.167 \times 10^{10}$	stable spiral
	-1.250	-1.667	unstable node
A15	$4.000 \times 10^{10}$	1.000	stable node
	-2.003	$1.500 \times 10^{10}$	saddle
	-1.250	-1.667	unstable node
A21	$4.000 \times 10^8$	-27.000	saddle
	-27.000	$4.000 \times 10^8$	saddle
	$2.667 \times 10^8$	$2.667 \times 10^8$	stable node
	-13.500	-13.500	unstable node
A22	$4.000 \times 10^8$	51.000	stable node
	-15.429	$1.000 \times 10^8$	saddle
	$4.667 \times 10^8$	$-1.333 \times 10^8$	saddle
	-13.500	-51.000	unstable node

Table II. Classification of Photon Density Singular Points (cont)

Data Set ID	$n_1$	$n_2$	Type
A23	$8.000 \times 10^8$	13.500	stable node
	13.500	$8.000 \times 10^8$	stable node
	$2.667 \times 10^8$	$2.667 \times 10^8$	saddle
	-13.500	-13.500	unstable node
A24	$8.000 \times 10^8$	7.286	stable node
	-27.000	$2.000 \times 10^8$	saddle
	$-1.333 \times 10^8$	$4.667 \times 10^8$	stable spiral
	-13.500	-51.000	unstable node
A25	$8.000 \times 10^8$	17.000	stable node
	-18.000	$2.000 \times 10^8$	saddle
	-13.5000	-51.000	unstable node
A31	$1.000 \times 10^5$	$-1.000 \times 10^5$	saddle
	$-1.000 \times 10^5$	$1.000 \times 10^5$	saddle
	$5.7735 \times 10^4$	$5.7735 \times 10^4$	stable node
	$-5.7735 \times 10^4$	$5.7735 \times 10^4$	unstable node
A33	$5.7735 \times 10^4$	$5.7735 \times 10^4$	stable node
	$-5.7735 \times 10^4$	$-5.7735 \times 10^4$	unstable node
	$1.000 \times 10^5 i$	$-1.000 \times 10^5 i$	complex
	$-1.000 \times 10^5 i$	$1.000 \times 10^5 i$	complex
A35	$7.0711 \times 10^4$	$7.0711 \times 10^4$	stable node
	$-7.0711 \times 10^4$	$7.0711 \times 10^4$	unstable node
A41	49.000	49.000	stable node
	$-6.667 \times 10^7$	$-6.667 \times 10^7$	unstable node
	$-1.000 \times 10^8$	98.000	saddle
	98.000	$-1.000 \times 10^8$	saddle
A42	49.000	11.500	stable node
	-49.000	$-4.000 \times 10^8$	unstable node
	$-1.000 \times 10^8$	13.143	saddle
	$1.333 \times 10^8$	$-4.667 \times 10^8$	saddle

Table II. Classification of Photon Density Singular Points (cont)

Data Set ID	$n_1$	$n_2$	Type
A43	49.000	49.000	stable node
	$-6.667 \times 10^7$	$-6.667 \times 10^7$	saddle
	$-2.000 \times 10^8$	-49.000	unstable node
	-49.000	$-2.000 \times 10^8$	unstable node
A44	49.000	11.500	stable node
	$-2.000 \times 10^8$	23.000	saddle
	-7.000	$-8.000 \times 10^8$	unstable node
	$-4.667 \times 10^8$	$1.333 \times 10^8$	unstable spiral
A45	49.000	11.5000	stable node
	$-2.000 \times 10^8$	15.333	saddle
	-16.333	$-8.000 \times 10^8$	unstable node
A51	1.000	1.000	stable node
	$-1.667 \times 10^9$	$-1.667 \times 10^9$	unstable node
	$-2.500 \times 10^9$	2.000	saddle
	2.000	$-2.500 \times 10^9$	saddle
A52	1.500	0.1111	stable node
	-11.994	$-4.500 \times 10^9$	unstable node
	$-2.000 \times 10^9$	0.1429	saddle
	$3.333 \times 10^8$	$-4.667 \times 10^9$	saddle
A53	1.000	1.000	stable node
	$-1.667 \times 10^9$	$-1.667 \times 10^9$	saddle
	$-5.000 \times 10^9$	-1.000	unstable node
	$-1.000 \times 10^9$	$-5.000 \times 10^9$	unstable node
A54	1.500	0.1111	stable node
	$-4.000 \times 10^9$	1.000	saddle
	$-4.667 \times 10^9$	$3.333 \times 10^8$	unstable spiral
	-0.4286	$-9.000 \times 10^9$	unstable node
A55	1.500	0.1111	stable node
	$-4.000 \times 10^9$	0.2000	saddle
	-1.200	$-9.000 \times 10^9$	unstable node

or an unstable spiral. Above threshold, when the two modes are pumped equally, there is a second stable node which is physically realizeable. The fourth singularity is a saddle point lying essentially at the intersection of lines  $l_1$  and  $l_2$  (Eqs (43) and (44)). Given the initial conditions, it determines to which stable node the system will relax. When only one mode is inhibited, the second stable equilibrium point moves to a non-physical point and becomes a stable spiral. The saddle moves to a point just outside the physical region and maintains its relative position between the two stable points to prevent physical points from relaxing towards the non-physical stable point.

Second Moments. For each photon density singularity, there is one set of equilibrium values for the second moments (as determined by Eqs (60), (61), and (63)). For the unstable photon-density-equilibria, the associated second-moment equilibria are non-physical; at least one of the variances,  $\rho_{11}$  or  $\rho_{22}$ , is negative. However, since the points are unstable in the photon densities, the uncertainties and thus the second moments will grow or diverge in time, and the system will move away from instead of towards these non-physical variances.

For the stable photon singularities, the associated second-moment equilibria are real, physically meaningful points. As such, they are listed in Table III along with the associated relative standard deviations and correlation coefficients. At and below threshold the system experiences large uncertainties as the standard deviations are of the same order as the photon number densities. These large uncertainties are also experienced by modes above threshold which are inhibited by the other mode from lasing. Once a mode begins lasing, the relative standard deviation at equilibrium drops sharply, decreasing as the

Table III. Stable Equilibrium Values for the First and Second Moments  
of the Photon Density Distribution

Data Set ID	$\frac{n_1}{n_2}$	$\frac{\sigma_{11}}{n_2}$	$\frac{\sigma_{22}}{n_2}$	$\frac{\sigma_{12}}{n_2}$	$\frac{s_1}{n_2}$	$\frac{s_2}{n_2}$	$\frac{p_{12}}{n_2}$
A11	1.33x10 <sup>10</sup>	1.33x10 <sup>10</sup>	3.33x10 <sup>10</sup>	3.33x10 <sup>10</sup>	-1.67x10 <sup>10</sup>	1.37x10 <sup>-5</sup>	1.37x10 <sup>-5</sup>
A12	2.00x10 <sup>10</sup>	5.000	2.50x10 <sup>10</sup>	30.00	-16.72	7.91x10 <sup>-6</sup>	1.931x10 <sup>-5</sup>
A13	4.00x10 <sup>10</sup>	1.250	5.00x10 <sup>10</sup>	2.813	-4.732	5.59x10 <sup>-6</sup>	1.26x10 <sup>-5</sup>
A14	4.00x10 <sup>10</sup>	0.3846	5.00x10 <sup>10</sup>	0.5325	-0.8405	5.59x10 <sup>-6</sup>	5.15x10 <sup>-6</sup>
A15	4.00x10 <sup>10</sup>	1.000	5.00x10 <sup>10</sup>	2.000	-2.000	5.59x10 <sup>-6</sup>	6.325x10 <sup>-6</sup>
A21	2.67x10 <sup>8</sup>	2.67x10 <sup>8</sup>	7.20x10 <sup>9</sup>	7.20x10 <sup>9</sup>	-3.60x10 <sup>9</sup>	3.18x10 <sup>-4</sup>	3.18x10 <sup>-4</sup>
A22	4.00x10 <sup>8</sup>	51.00	5.40x10 <sup>9</sup>	2.65x10 <sup>3</sup>	-1.33x10 <sup>3</sup>	1.84x10 <sup>-4</sup>	1.010
A23	8.00x10 <sup>8</sup>	13.50	1.08x10 <sup>10</sup>	195.8	-378.5	1.30x10 <sup>-4</sup>	1.037
A24	8.00x10 <sup>8</sup>	7.286	1.08x10 <sup>10</sup>	60.37	-115.6	1.30x10 <sup>-4</sup>	1.066
A25	8.00x10 <sup>8</sup>	17.00	1.08x10 <sup>10</sup>	306.0	-306.0	1.30x10 <sup>-4</sup>	1.029
A31	5.77x10 <sup>4</sup>	5.77x10 <sup>4</sup>	2.08x10 <sup>9</sup>	2.08x10 <sup>9</sup>	-4.17x10 <sup>8</sup>	.7905	.7905
A33	5.77x10 <sup>4</sup>	5.77x10 <sup>4</sup>	3.33x10 <sup>9</sup>	3.33x10 <sup>9</sup>	-1.67x10 <sup>9</sup>	1.000	1.000
A35	7.07x10 <sup>4</sup>	7.07x10 <sup>4</sup>	3.75x10 <sup>9</sup>	3.75x10 <sup>9</sup>	-1.25x10 <sup>9</sup>	.8660	.8660

Table III. Stable Equilibrium Values for the First and Second Moments  
of the Photon Density Distribution (cont.)

Data Set ID	$n_1$	$n_2$	$\sigma_{11}$	$\sigma_{22}$	$\sigma_{12}$	Relative $s_1$	Relative $s_2$	$\rho_{12}$
A41	49.00	49.00	2450	2450	$-6.00 \times 10^{-4}$	1.010	1.010	$-2.45 \times 10^{-7}$
A42	49.00	11.50	2450	143.7	$-3.52 \times 10^{-5}$	1.010	1.042	$-5.935 \times 10^{-8}$
A43	49.00	49.00	2450	2450	$-1.20 \times 10^{-3}$	1.010	1.010	$-4.900 \times 10^{-7}$
A44	49.00	11.50	2450	143.7	$-7.04 \times 10^{-5}$	1.010	1.042	$-1.19 \times 10^{-7}$
A45	49.00	11.50	2450	143.7	$-3.52 \times 10^{-5}$	1.010	1.042	$-5.935 \times 10^{-8}$
A51	1.000	1.000	2.000	2.000	$-4.00 \times 10^{-10}$	1.414	1.414	$-2.00 \times 10^{-10}$
A52	1.500	0.1111	3.750	0.1235	$-4.63 \times 10^{-11}$	1.291	3.163	$-6.80 \times 10^{-11}$
A53	1.000	1.000	2.000	2.000	$-8.00 \times 10^{-10}$	1.414	1.414	$-4.00 \times 10^{-10}$
A54	1.500	0.1111	3.750	0.1235	$-9.26 \times 10^{-11}$	1.291	3.163	$-1.36 \times 10^{-10}$
A55	1.500	0.1111	3.750	0.1235	$-4.63 \times 10^{-11}$	1.291	3.163	$-6.80 \times 10^{-11}$

8  
photon number density increases. It is interesting to note that for a weakly-coupled system above threshold, matched-mode oscillation ( $n_1 = n_2$ ) shows for each of the modes a greater variance than for the single mode that oscillates and inhibits the other. This is even though, for the same pump level, the photon density is greater for the single mode than for either of the matched modes. However, this general phenomenon should be expected because of the relative influences of the second mode; in one case, it oscillates at equal intensity while in the other instance it exists barely above photon vacuum.

The correlation coefficient  $\rho_{12}$  indicates a significant linear relationship between the photon densities of the two modes only at threshold and above threshold with both modes lasing. In these cases a change in the photon density of one mode will have definite impact on the density of the other. At threshold, even though the standard deviations are still on the order of the mean densities, this indicates the onset of order within the system. Below threshold, and above threshold with only one mode oscillating,  $\rho_{12}$  is very small and the two modes are very nearly uncorrelated. Below threshold, both modes are dominated by spontaneous emission. Therefore, neglecting the small amount of stimulated emission that may occur, the photons in one mode will have no effect on the photon number in the other mode. Likewise, above threshold with one inhibiting the other, the inhibited mode is inhabited almost entirely by spontaneous photons and can do very little to affect the number density of the lasing mode.

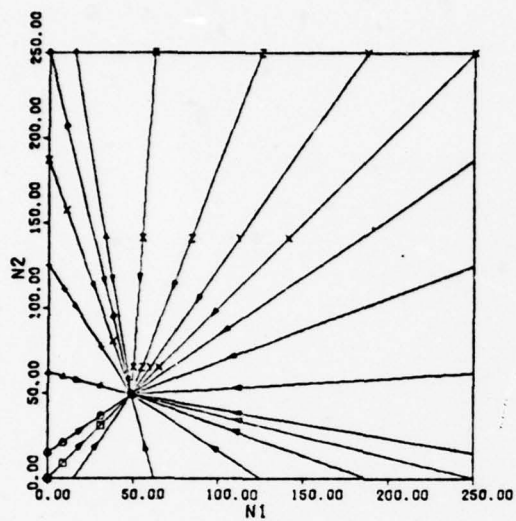
#### Dynamic Analysis

General. Representative plots showing the evolution of the mean photon number densities and of the standard deviations and correlation

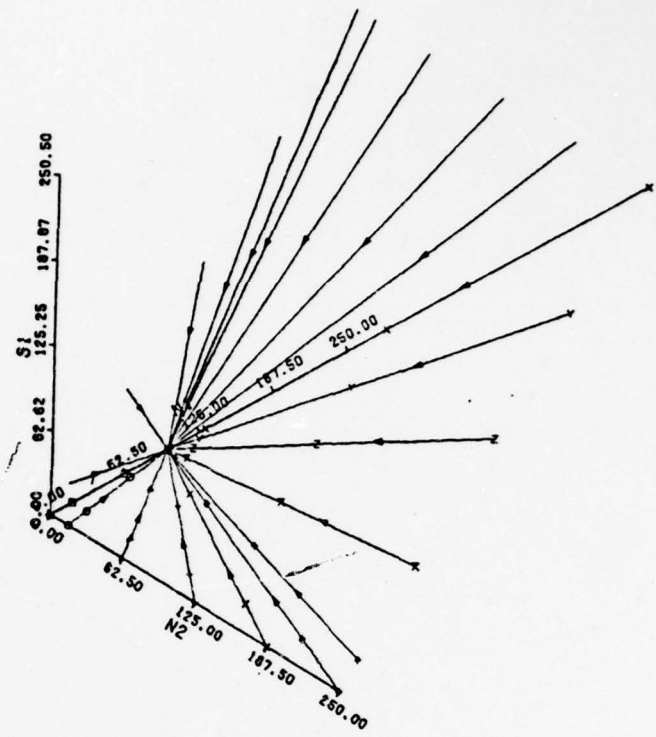
coefficient are shown in Figs. 6-13. Each figure comprises four plots:  $n_1$  vs.  $n_2$ ;  $n_1$  vs.  $n_2$  vs.  $s_1$ ;  $n_1$  vs.  $n_2$  vs.  $s_2$ ; and  $n_1$  vs.  $n_2$  vs.  $\rho_{12}$ . There were no significant differences in the behavior of the system between the two levels of above threshold pump considered in this study. Therefore, only one of these pump levels is considered in this section. The same was true for the two levels of pump below threshold. In addition, the degree of coupling had no real noticeable effect below threshold on the evolution of the variables and caused only minor differences at threshold. Therefore, only one threshold case and two below threshold cases (corresponding to matched and unmatched pumping) are considered. The remainder of the plots are included in Appendix C.

Below Threshold. Figs. 6 and 7 illustrate the evolution of the first and second moments for the two below threshold cases A41 and A42, respectively. As predicted, the mean photon densities follow deterministic paths. In both cases the modes are dominated by spontaneous emission. Therefore, they exhibit characteristics of white (incoherent) light. The standard deviations  $s_1$  and  $s_2$  are on the order of the mean densities throughout the transitions and, therefore, experience the same general behavior as the mean photon densities. Also, the correlation coefficient is very near zero throughout the regions of interest indicating that the modes have little on each other.

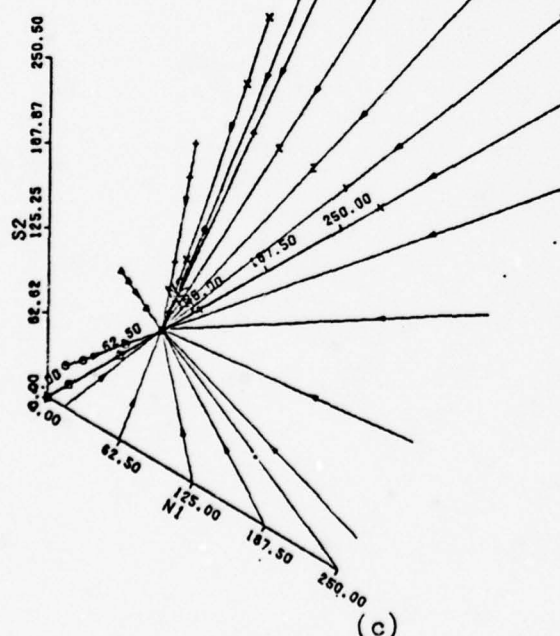
At Threshold. At threshold, only the weakly-coupled case A31 has real-valued saddle points. The strongly-coupled system A33 has two complex-valued singularities, while the neutrally-coupled system A35 has only two nodes, one stable and one unstable. Comparing these three cases, it is seen that there is little impact caused by the presence (or absence) of saddle points.



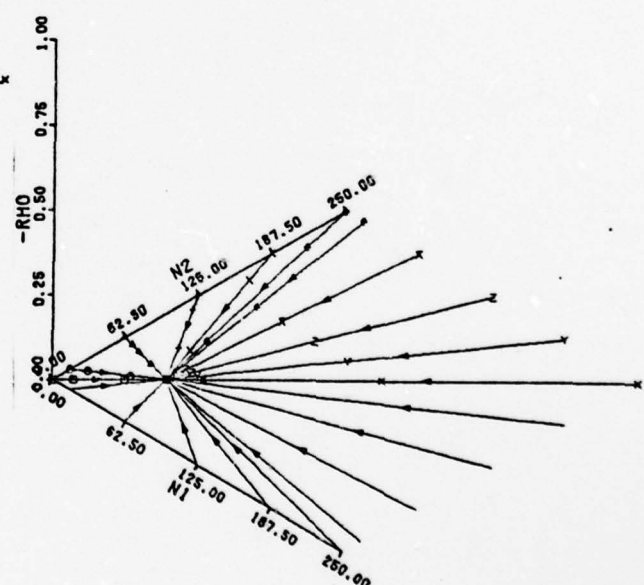
(a)



(b)



(c)



(d)

Figure 6. Evolution Curves for Case A41

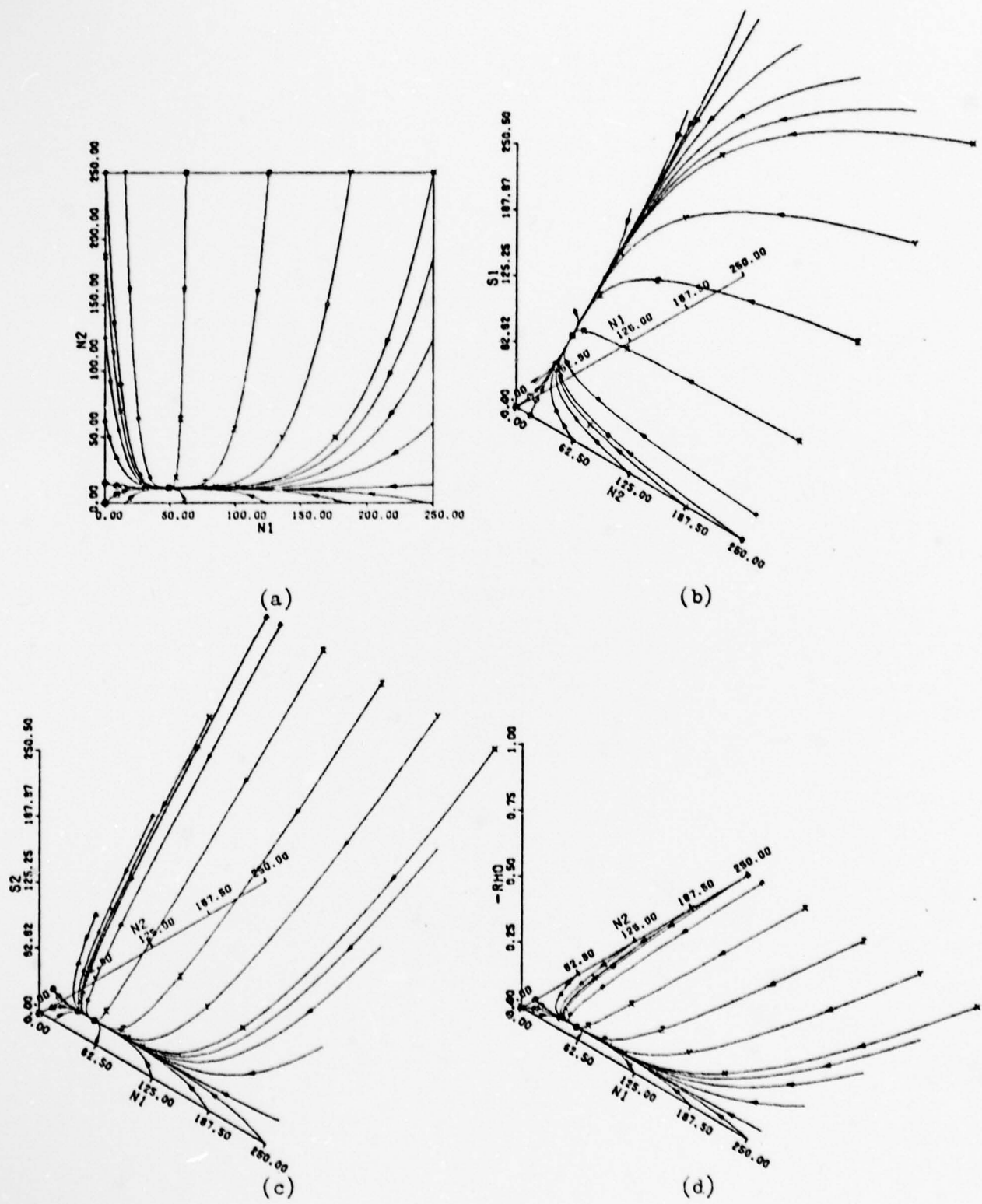
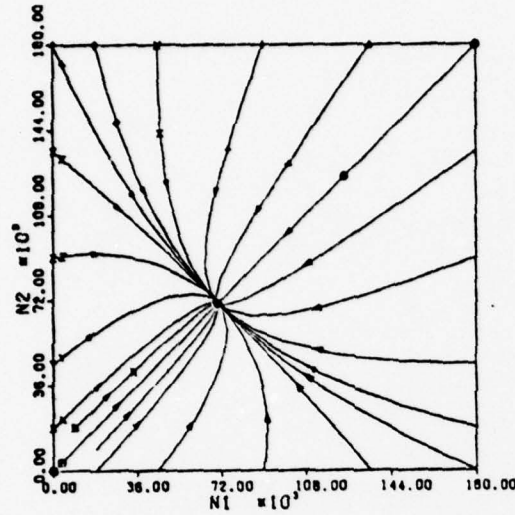


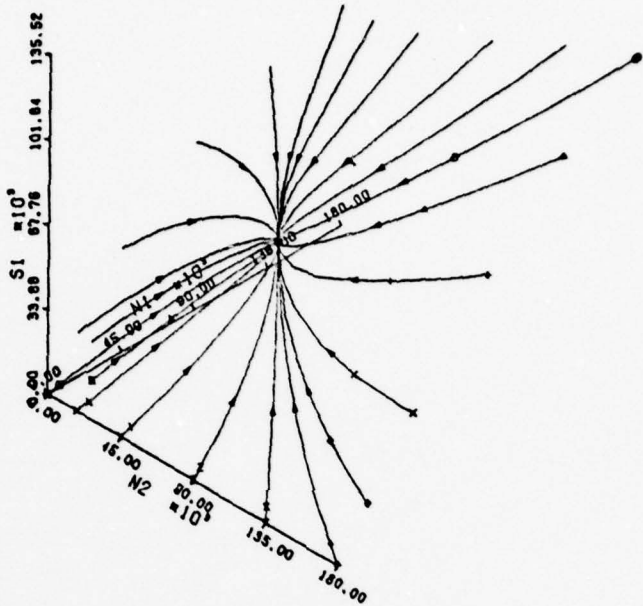
Figure 7. Evolution Curves for Case A42

Considering the case A35 (Fig. 8), the same general relationships exist between the mean photon densities and the standard deviations as exist below threshold. The modes are still dominated primarily by spontaneous emission and, therefore,  $s_1$  and  $s_2$  remain on the order of  $n_1$  and  $n_2$ . However, the correlation coefficient no longer is negligible. When either mode is operating well below equilibrium the correlation between modes is very small. As the mode(s) grow(s), the effects of saturation and coupling cause the modes to affect each other and thus they become correlated. Because of the simulated Q-switch used to determine the initial variances and covariances, the curves associated with large initial photon densities in both modes start out indicating significant correlation between modes which then decrease or increase monotonically towards the equilibrium value.

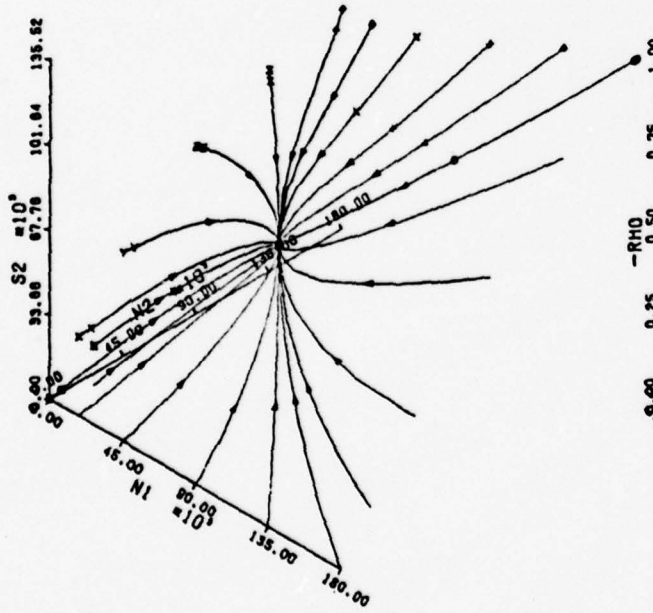
Above Threshold. Above threshold, the behavior of the system is strongly affected by the singular points (Table II). Consider first the weakly-coupled case A21 as shown in Fig. 9. Comparing Fig. 9a, the plot of  $n_1$  vs.  $n_2$ , to Fig 1, its equivalent plot resulting from Lamb's semiclassical treatment, favorable agreement is noted with an important addition. Fig. 9a includes phase curves from points with one or both modes in a photon vacuum. The curves between the saddle points at approximately  $(0, 4 \times 10^8)$  and  $(4 \times 10^8, 0)$  and the stable equilibrium act as "limit lines" of the system to which other phase curves are pulled by the saddle points. This is especially evident for those lines beginning with one of the modes in a photon vacuum (such as those with initial points identified on the  $n_2$  axis by several different characters). These curves move quickly towards the closest saddle point before the non-lasing mode can build significantly, as there are not enough excited



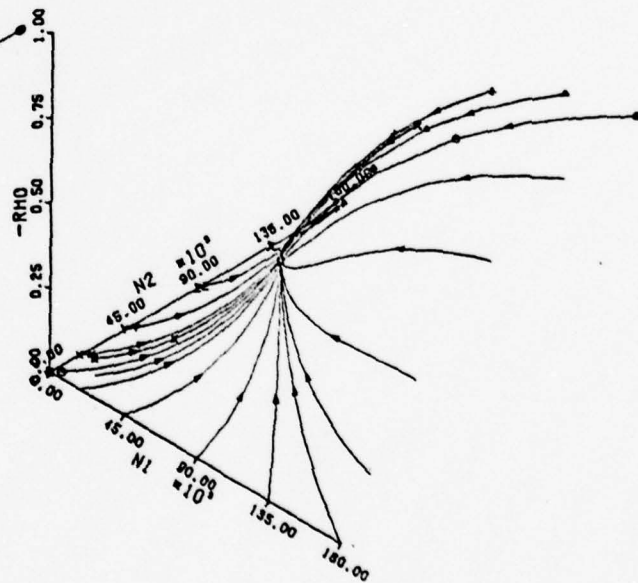
(a)



(b)

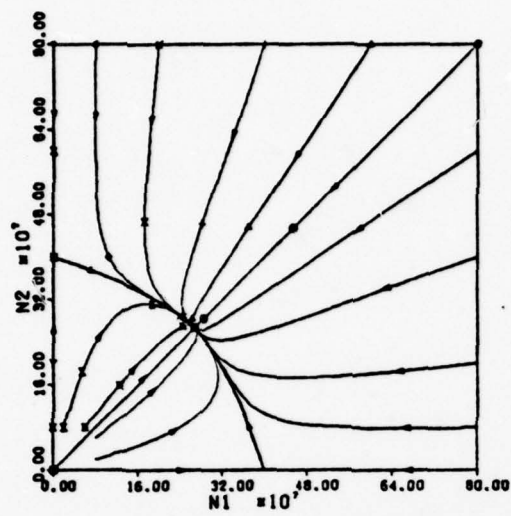


(c)

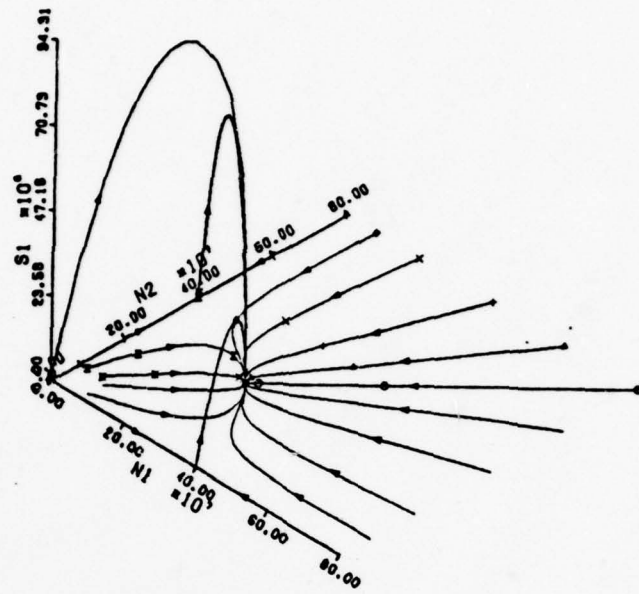


(d)

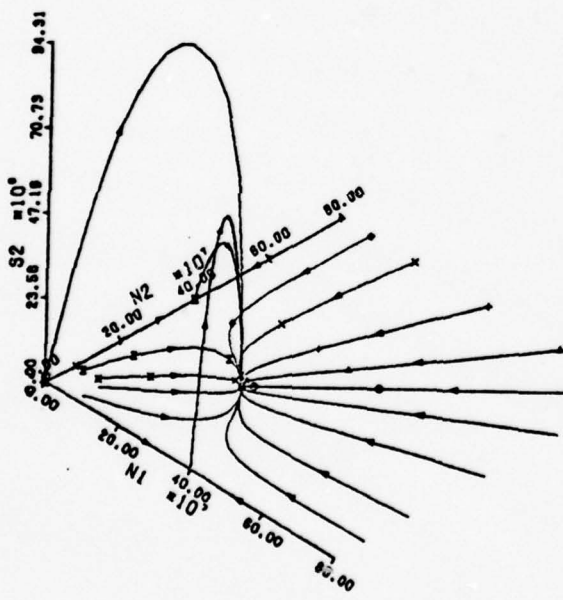
Figure 8. Evolution Curves for Case A35



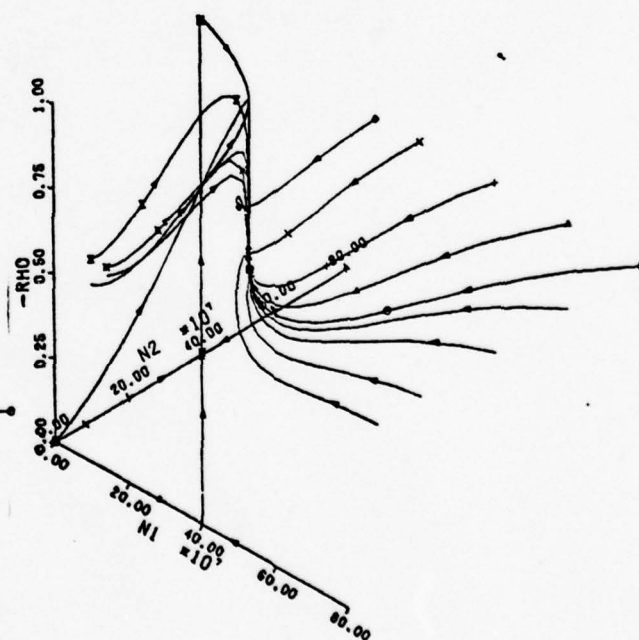
(a)



(b)



(c)

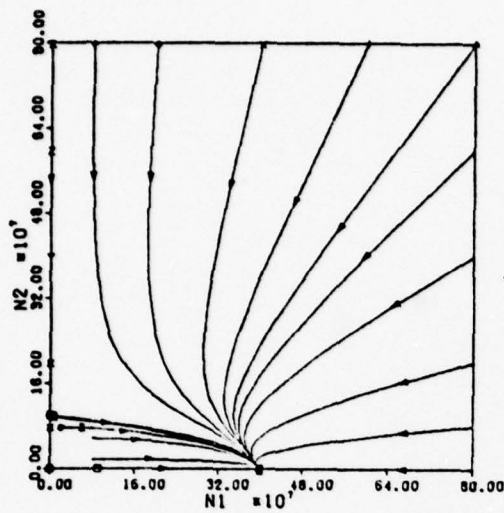


(d)

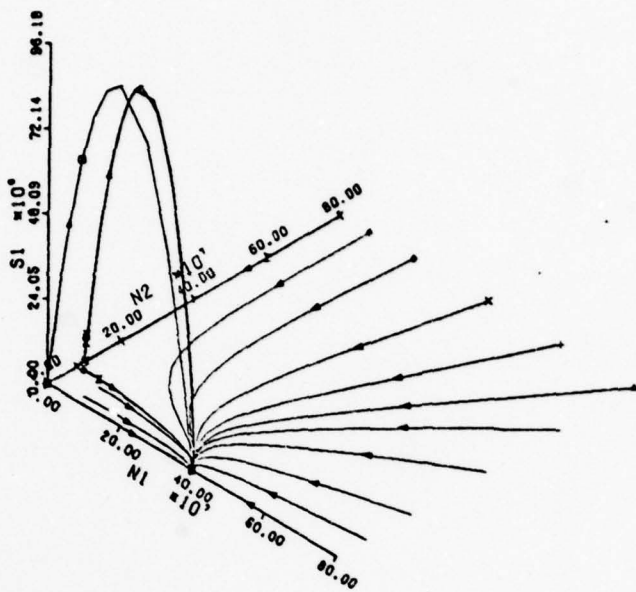
Figure 9. Evolution Curves for Case A21

atoms to maintain the system at its current level. They then follow very closely the "limit line" in the transition to stable equilibrium. Figs. 9b and 9c indicate that the occurrence of anomalous fluctuations is associated with buildup in one or both modes from a photon vacuum, and that the maximum fluctuation occurs approximately half-way along the curve between the stable and unstable equilibria. In buildup from  $(n_1, n_2) = (0, 0)$  both modes experience the same degree of fluctuation as both modes are expected to grow at the same rate. When only one mode is building from zero both modes again experience the anomalously large fluctuations, even though the other mode is already oscillating. However, the growing mode experiences a larger fluctuation. Comparing the curves for  $s_1$  and  $s_2$  to their associated curves for  $\rho_{12}$  in Fig. 9d, it is seen that movement along the "limit line" is associated with a high correlation between modes ( $\rho_{12} \approx -1.0$ ). Also, the phase curve associated with buildup from a photon vacuum in both modes moves towards  $\rho_{12} = -1.0$  before relaxing to the equilibrium value of -0.5.

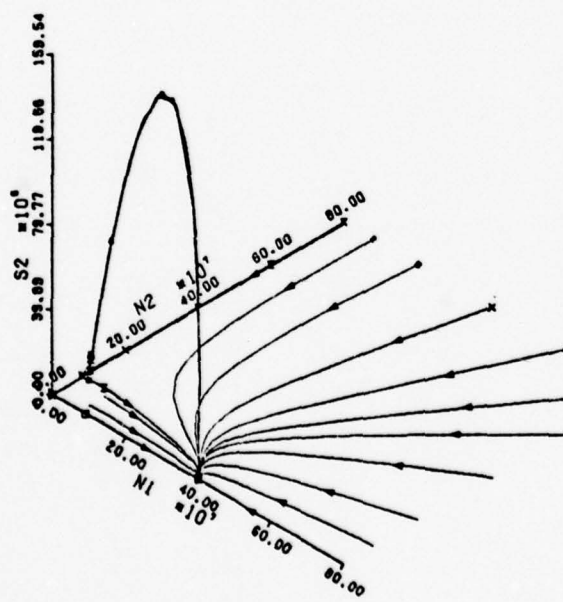
Case A22, representing weakly-coupled modes with mode 2 inhibited at equilibrium, is shown in Fig. 10. As with case A21, a comparison of Fig. 10a with its equivalent from Lamb's theory (Fig. 2) indicates favorable agreement in  $n_1$  and  $n_2$ . There is now only one saddle point, at  $(n_1, n_2) \approx (0, 10^8)$ , which affects the system and all phase curves move toward the one equilibrium where only mode 1 lases. The anomalously large fluctuations are again associated with buildup from a photon vacuum. The single-to-dual-mode transition of Fig. 9 is replaced by transition from unstable to stable mode oscillation, and again both modes experience the anomalous fluctuations, as seen in Figs. 10b and 10c. However, only mode 1 experiences anomalous fluctuations in build-



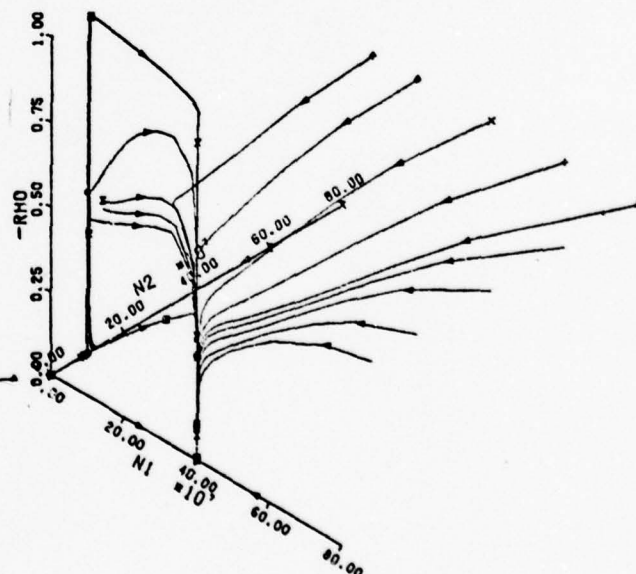
(a)



(b)



(c)

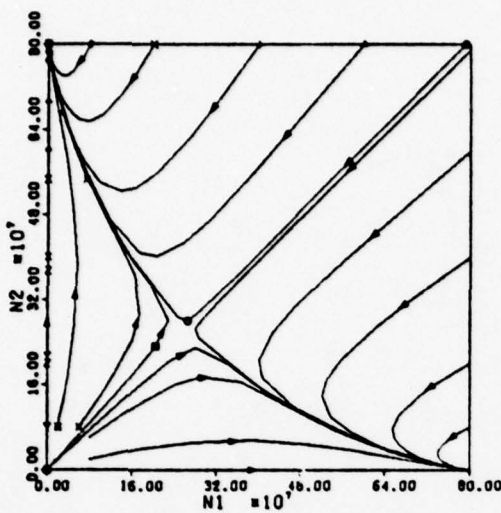


(d)

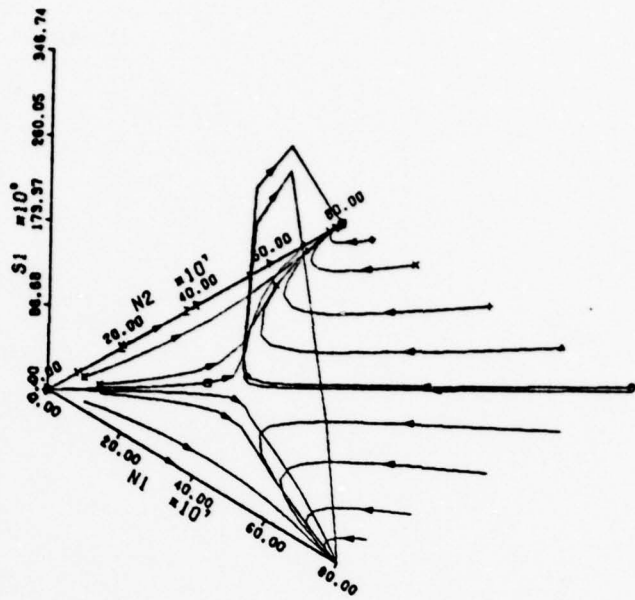
Figure 10. Evolution Curves for Case A22

up from (0,0) since it is the only mode which oscillates at equilibrium. Also, movement along or close to the "limit line" is again associated with strong correlation between the modes, as illustrated in Fig. 10d.

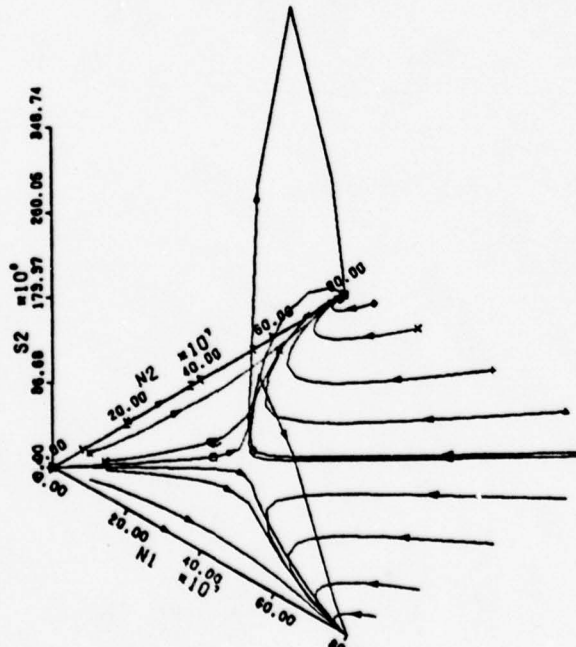
The case of strongly-coupled modes pumped equally, as shown in Fig. 11, is unique from the other cases studied because it has two different equilibria which are stable nodes and to which the system can relax. It also has an unstable equilibrium lying in the physical region of the  $(n_1, n_2)$  plane. This internal saddle point determines the stable point to which the system will move. As before, the evolution of the mean photon densities, Fig. 11a, compares favorably with Lamb's results as plotted in Fig. 3. Since both modes can be stable, depending on one's current position, the system does not have an unstable mode from which to transition, as in case A22. Similarly, it cannot move to two-mode oscillation. Therefore, one might expect that for this case the only anomalous fluctuations are associated with buildup in one of the modes from a photon vacuum while the other mode remains essentially empty. However, while photon buildup transitions do experience the anomalous fluctuations, the strongest influence is the internal saddle point. As is evident in Figs. 11b and 11c, the phase curves experiencing the largest fluctuations are those passing closest to this saddle point. Again, it is interesting to note that the maximum fluctuations occur not nearest the unstable equilibrium, but approximately half-way between the unstable point and the stable point. As in all the above-threshold cases studied, movement along the "limit lines" extending between the stable and unstable equilibria was associated with high correlation between the modes, or  $\rho_{12} = -1.0$ . However, for strongly-coupled modes, due to the stronger mode interaction, this same correlation exists



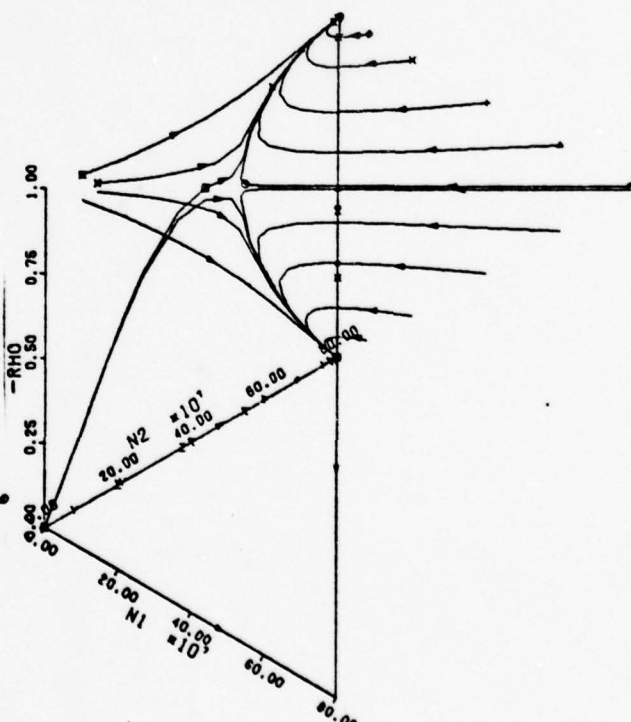
(a)



(b)



(c)



(d)

Figure 11. Evolution Curves for Case A23

whenever both modes are oscillating, as seen in Fig. 11d.

When the strongly-coupled modes are unequally pumped such that only one mode is inhibited, as in case A24, the evolution of the moments is as shown in Fig. 12. There is again only one stable point to which the system can relax and there is only one saddle point affecting the system. As in case A22, anomalous fluctuations occur during both transition from unstable to stable mode oscillation and buildup of mode 1 from a photon vacuum  $(0,0)$ . However, the largest fluctuations are associated with phase curves which begin with both modes oscillating and then pass near the saddle point. Both modes oscillating under strong coupling is a highly unstable configuration and, therefore, the curves associated with these points begin with large uncertainties on the order of the mean photon densities. As the system evolves toward the stable equilibrium,  $s_2$  maintains the same relative value throughout the transition (Fig. 12c). Likewise, for those curves which approach the "limit line" before the half-way point where the maximum fluctuations are expected to occur,  $s_1$  stays on the order of  $n_1$  and as  $n_1$  grows, so does  $s_1$  (Fig. 12b). Once the maximum point is reached,  $s_1$  decreases rapidly and approaches its relative low value characteristic of stable lasing modes.

Looking at Fig. 13, there are only minor differences between the evolution curves for neutrally-coupled modes and those for strongly-coupled modes under unequal pumping. For the neutrally-coupled modes (case A25) the effect of the saddle point is not as pronounced. The phase curves do not approach as close to the saddle point and, excepting those which begin on the  $n_2$  axis, do not approach the "limit line" as quickly. Therefore, even though the two-mode-oscillation initial points have associated uncertainties on the order of the photon densities,

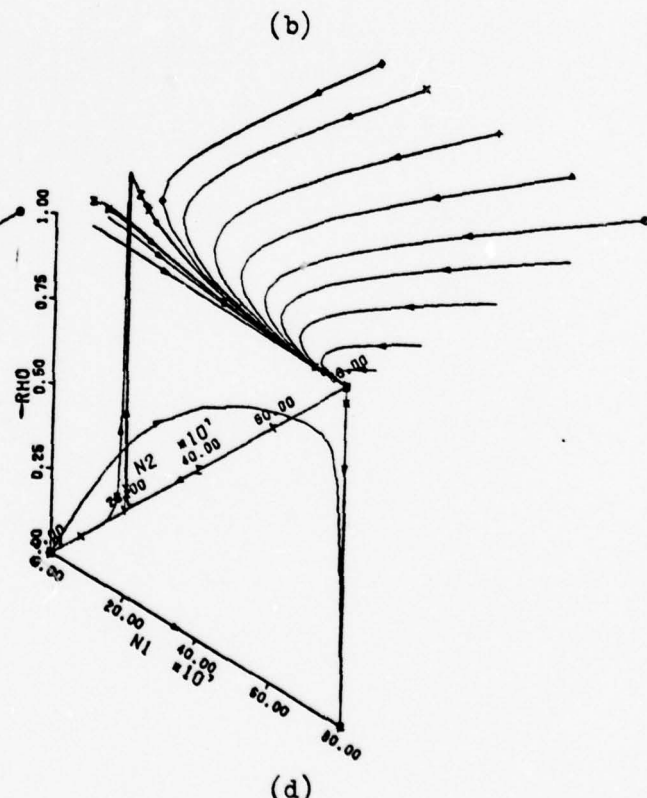
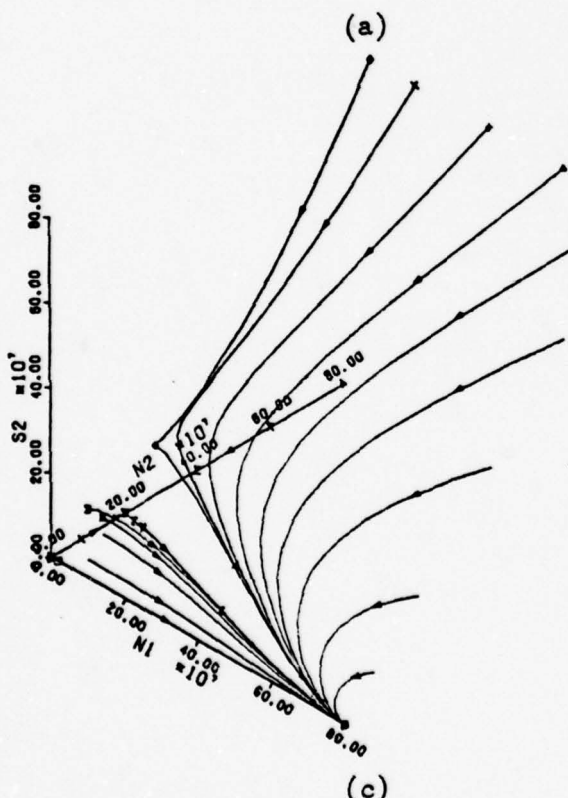
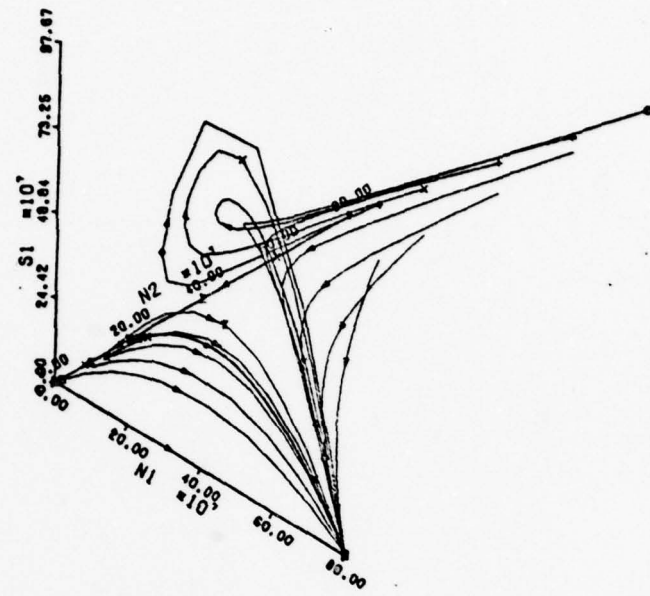
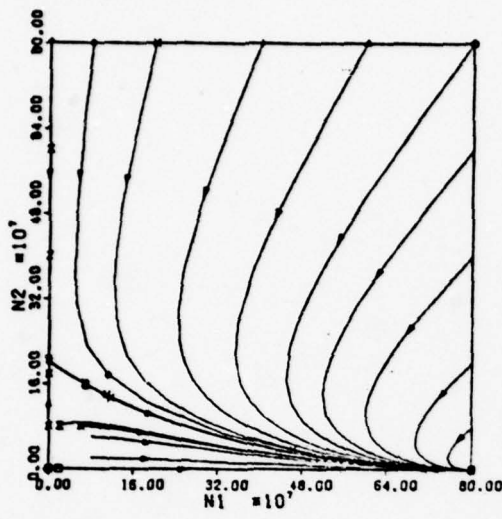
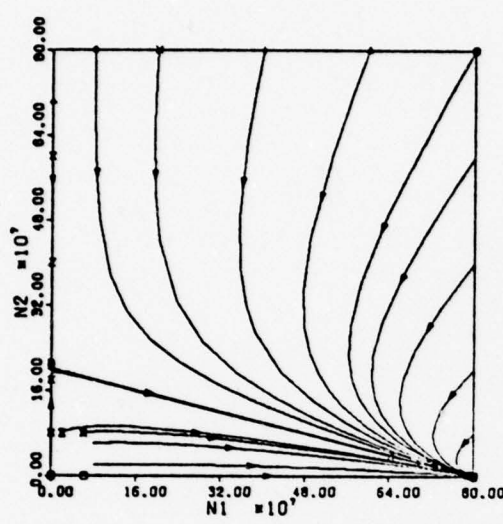
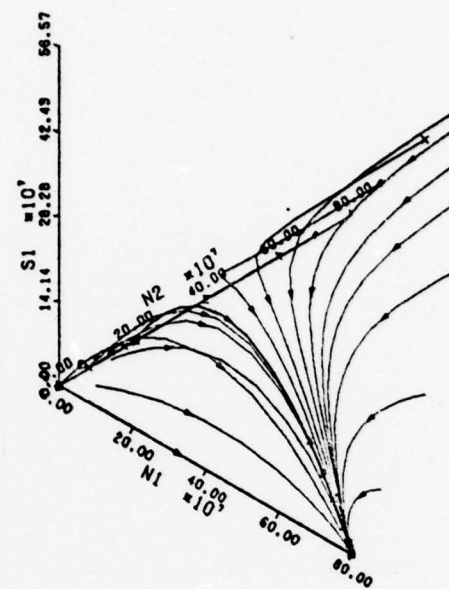


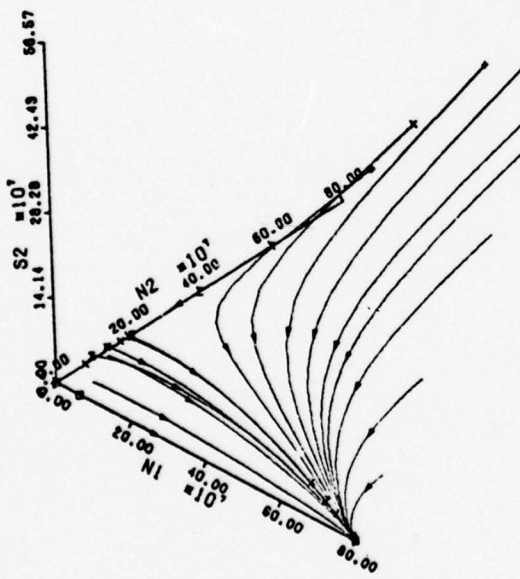
Figure 12. Evolution Curves for Case A24



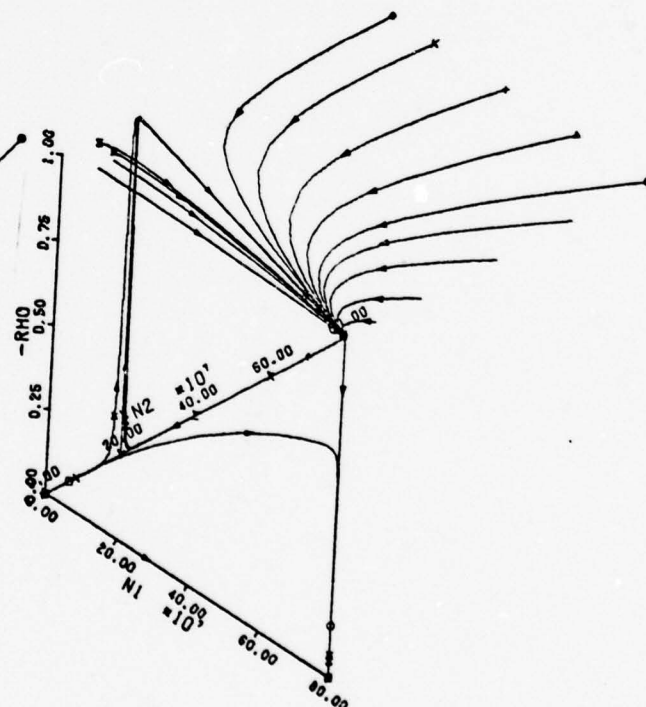
(a)



(b)



(c)



(d)

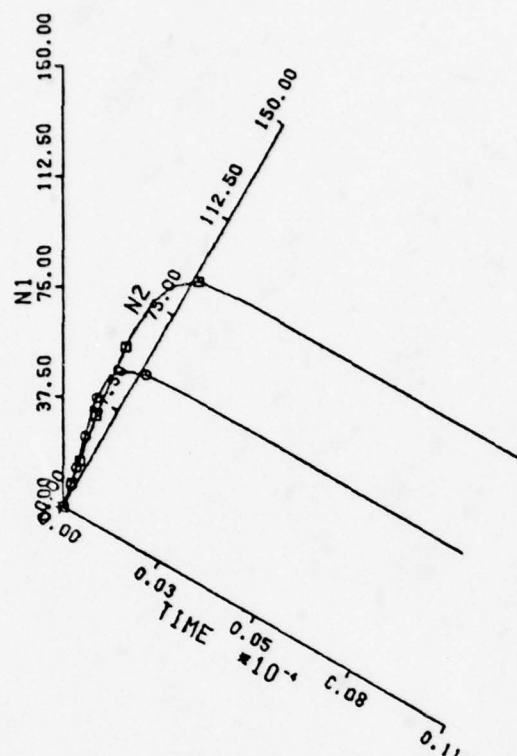
Figure 13. Evolution Curves for Case A25

the loops in the  $s_1$  curves of Fig. 12b do not occur in the  $s_1$  curves of Fig. 13b.

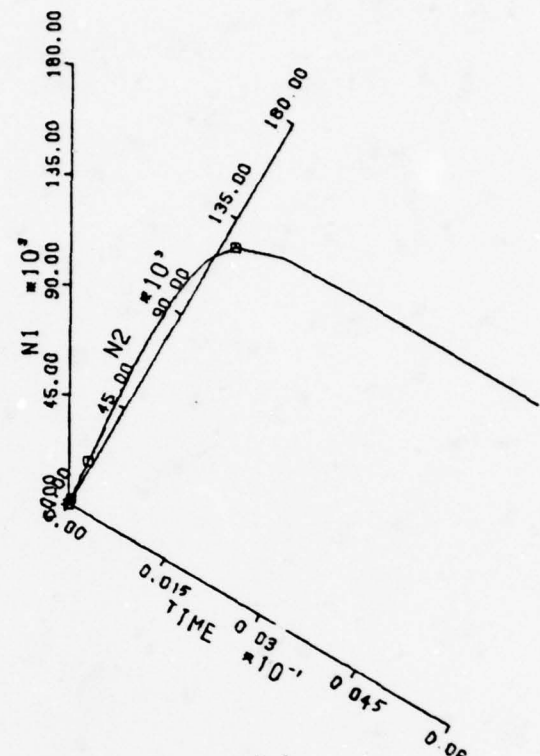
It is interesting to look at the general shape of the "limit lines" relative to the mode coupling. When the modes are weakly coupled and the system is in the vicinity of a saddle point, one of the mode densities will be near zero. As this mode grows, the other mode density will decrease as both modes pull towards their own respective equilibria. However, the decrease required will be less than the growth of the first mode. Therefore, the "limit lines" are concave downward or towards the origin. On the other hand, the "limit lines" are concave upward for strongly-coupled modes as the opposite relative responses between modes are encountered. When the system is neutrally-coupled, the "limit line" becomes a straight line showing no preferred concavity, just as the system shows no preferred method of saturation.

In comparing Figs. 9a, 10a, and 11a to the results of Lamb's theory (Figs. 1, 2, and 3) the one important difference noted was the inclusion of phase curves originating from a photon vacuum. There is one other significant difference between these two models. Lamb's model predicted that any point along lines  $l_1$  and  $l_2$  (Eqs (43) and (44)) would be stable with deviations away from either line decaying back towards that line. However, when the spontaneous emission is included, this stability is destroyed and, as seen in Fig. 13, the system moves to equilibrium at a single point.

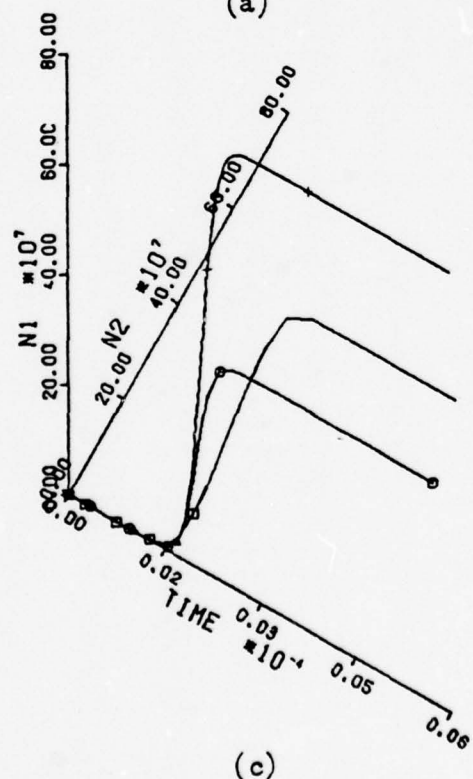
Mode Buildup from Vacuum. Of particular interest is the buildup of the mode densities from a photon vacuum. Figs. 14a, 14b, and 14c illustrate this buildup in time for several levels of pump and degrees of coupling. Fig. 14c shows the buildup in both modes from a photon



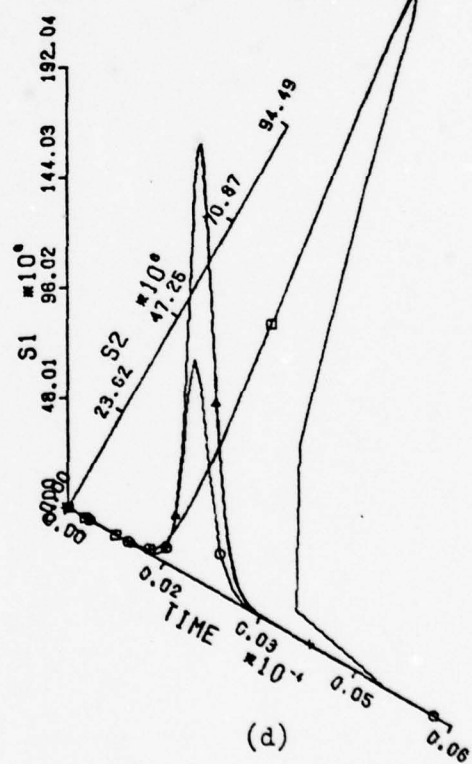
(a)



(b)



(c)



(d)

Figure 14. Time Evolution of Moments During Buildup of Photon Densities

vacuum for the five different above threshold cases shown in Figs. 9-13. Fig. 14b corresponds to Fig 8, and Fig. 14a does the same for the cases of Figs. 6 and 7. Below threshold, the modes grow independently with the time relationship

$$n_i = n_{i_{eq}} (1 - e^{-at}) \quad (74)$$

where  $n_{i_{eq}}$  is the equilibrium density for that mode and  $a_i$  is a decay constant. This decay constant is equal to the net losses of the mode, or the difference between the loss parameter  $h_i$  and the stimulated gain parameter  $g_{2i}$ . Coupling and saturation have negligible effects. At threshold, according to Eq (74) both modes should increase linearly with no damping or amplification effects, since the stimulated gains equal the losses. This does occur initially. However, as the mode densities continue to increase, saturation sets in and the rate of buildup declines as equilibrium is reached. Above threshold, both modes experience initial exponential rises with growth constants equal to the net gain of the system. As they approach and pass the threshold equilibria, saturation and coupling begin to modify this rise, gradually slowing the rate of increase and even causing a decrease for the mode which is inhibited from lasing at equilibrium.

The time to equilibrium is primarily determined by the size of the net gain or loss of the system. The closer the system is to threshold operation, the longer it will take for the system to buildup to equilibrium. Below threshold, the net loss (or the decay constant) is the only determining factor, whereas above threshold, and even at threshold, the effects of coupling and inhibition speed up or slow down the process.

For example, consider the times to equilibria as shown in Figs. 14a-14c. At threshold (Fig. 14b), this time was on the order of 1 msec. Below threshold (Fig 14a), it took about  $5\mu\text{sec}$  for the system to reach an equilibrium. In Fig. 14c the times to equilibrium were in the range of  $5-10\mu\text{sec}$ .

As with the photon densities, the buildup of the mode densities is used to illustrate the evolution of the standard deviations in time. See Fig. 14d. Since the standard deviations for systems at and below threshold are very close to the mean photon densities, only the above threshold cases represented in Fig 14c are considered. Also, the strongly-coupled equally-pumped system experienced fluctuations two orders of magnitude greater than the fluctuations for the other four cases involved. Therefore, the time behavior of its standard deviations is not included in Fig. 14d. Comparing the curves of Fig. 14d to Fig 14c, it is seen that the fluctuations do peak approximately half-way to equilibrium, as predicted and seen before, with the case of two-mode oscillation peaking farther towards the equilibrium than the cases of single-mode oscillation. The height of the peak is dependent primarily on the pumping, as different pump parameters produce different photon densities. There is also a dependence on the mode coupling for the same pump level. For each of the curves in Fig 14d, the peak represents approximately the same relative standard deviation ( $s_1 \approx n_1$ ). Therefore, since the peak occurs when the photon density is about half that of the equilibrium value, the heights of the peaks will have the same relative values as do the equilibrium photon densities.

## V Conclusions and Recommendations

### Conclusions

Based on the results of this study, several conclusions can be drawn. The most important of these, without which the rest would be meaningless, is that the method used in this study of photon statistics is valid. The lasing process can be described adequately by the Chapman-Kolmogorov master equation and the proposed transition rates used in solving the master equation are appropriate. Accepting this, the other conclusions are:

- 1). Any two-mode laser system has at most two stable equilibria, with all but some strongly-coupled systems having only one. This includes systems with neutrally-coupled modes, contrary to the predictions of the Lamb model.
- 2). The laser system experiences large, anomalous fluctuations in one or both modes in three specific types of transition. First, whenever the system builds up from a near photon vacuum such as at initial startup, the mode or modes which will be oscillating at equilibrium will experience the anomalous fluctuations. Second, whenever only one mode is oscillating and both modes oscillate at equilibrium, both modes will experience the anomalous fluctuations during the transition to equilibrium. Third, whenever an unstable mode is oscillating alone both modes will have anomalous fluctuations in the transition from the unstable to the stable mode.
- 3). Strongly-coupled laser systems operating with two modes oscillating experience large fluctuations, especially when there are two possible stable points to which the laser system can transition.

4). A mode experiences normal fluctuations when the system is below threshold, when the mode both begins and ends the transition below threshold, and when one mode ceases lasing while the other mode continues to lase (excepting the case where two physical stable points exist).

5). Inhibited modes above threshold experience the same type of fluctuation as if they were below threshold.

6). The anomalous fluctuations are accompanied by a strong linear relationship between the mode densities ( $\rho_{12} \approx -1$ ).

7). There is significant correlation at equilibrium between the modes only at threshold and above threshold with both modes oscillating.

#### Recommendations for Further Study

1). A better qualitative understanding of the effect of coupling could be gained by solving several different cases for various values of the coupling parameters.

2). Operation very close to threshold should be given a closer look, possibly resulting in a better definition of "near threshold".

3). This study was limited to constant pump parameters which turned on or changed instantaneously. Therefore, a similar analysis could be done allowing the pump parameters to be functions of time. This could then allow for analysis of pulsed operation as well as continuous wave.

4). This analysis could be repeated for other proposed expressions for the transition rates.

5). The equation development used in this study should be expanded to include multimode laser operation and the general results for two-mode operation extended as appropriate.

### Bibliography

1. Arecchi, F. T. and A. M. Ricca. "Statistical Properties of a Many-Mode Laser," Physical Review A, 15: 308-318 (January 1977).
2. Arecchi, F. T. et al. "Time-Dependent Statistical Properties of the Laser Radiation," Physical Review Letters, 19: 1168-1171 (13 November 1967).
3. Haken, H. "Cooperative Phenomena in Systems Far From Thermal Equilibrium and in Nonphysical Systems," Reviews of Modern Physics, 47: 67-121 (January 1975).
4. Kubo, R. "Non-linear Relaxation," Statistical Physics-StatPhys 13, Annals of the Israel Physical Society, Vol 2, Part 1, edited by D. Cahib, et al. New York: Adam Hilger, Bristol and the Israel Physical Society in association with the American Physical Society, 1978.
5. -----. "Relaxation and Fluctuation of Macrovariables," Synergetics - Cooperative Phenomena in Multi-component Systems, edited by H. Haken. Stuttgart: Teubner, 1973.
6. Kubo, R. et al. "Fluctuation and Relaxation of Macrovariables," Journal of Statistical Physics, 2: 51-96 (September 1973).
7. Lamb, W. E., Jr. "Theory of an Optical Maser," Physical Review, 134: A1429-A1450 (15 June 1964).
8. Mandel, P. "Quantum Multi-mode Laser Theory," Physica B & C, Netherlands, 82: 353-367 (April 1976).
9. Risken, H. "Statistical Properties of Laser Light," Progress in Optics, VIII: 241-296 (1970).
10. Sargent, M. III et al. "Buildup of Laser Oscillations from Quantum Noise," Applied Optics, 9: 2423-2427 (November 1970).
11. -----. Laser Physics. Reading, Massachusetts: Addison-Wesley Publishing Co., 1974.
12. Siegman, A. E. An Introduction to Lasers and Masers. New York: McGraw-Hill Book Co., 1971.
13. Skappel, J., Boeing Aircraft. "FORTRAN IV Subroutine BLCKDQ," Coordination Sheet No. PS-769, 22 March 1968.
14. Standard Math Tables (17th Edition), edited by Samuel M. Selby. Cleveland, Ohio: The Chemical Rubber Co., 1969.

15. Stoker, J. J. Nonlinear Vibrations in Mechanical and Electrical Systems. New York: Interscience Publishers, Inc., 1950.
16. van Kampen, N. G. "A Power Series Expansion of the Master Equation," Canadian Journal of Physics, 39: 551-567 (1961).

## Appendix A Derivation of the Evolution Equations

Let  $\underline{X} = (X_1, X_2)$  be a vector variable representing the photon numbers of a two-mode laser system. It is assumed that  $\underline{X}$  is a stochastic process as it evolves in time. Further,  $\underline{X}$  is assumed to be Markovian and, therefore, can be described by the Chapman-Kolmogorov equation in the form

$$\frac{\partial}{\partial t} P(\underline{X}, t) = - \int W(\underline{X}, \underline{r}) P(\underline{X}, t) d\underline{r} + \int W(\underline{X} - \underline{r}, \underline{r}) P(\underline{X} - \underline{r}, t) d\underline{r} \quad (75)$$

where  $P(\underline{X}, t)$  is the probability distribution of  $\underline{X}$  at time  $t$  and  $W(\underline{X}, \underline{r})$  is the transition rate for a jump from  $\underline{X}$  by an amount  $\underline{r}$ . Since the values of  $\underline{X}$  will be discrete, the integrations are understood as summations.

$\underline{X}$ , as defined above, represents the extensive macrovariables of the laser system, each of which is made up of contributions from many elementary units - in this case, photons. However, it is assumed that the transition rate  $W(\underline{X}, \underline{r})$  is determined by the internal state of the system, rather than by  $\underline{X}$ . Therefore, the transition rate takes the form

$$W(\underline{X}, \underline{r}) = \Omega \omega(\underline{x}, \underline{r}) \quad (76)$$

where  $\Omega$  is the size of the system and  $\underline{x}$  is the normalized intensive macrovariable vector corresponding to  $\underline{X}$  and defined by

$$\underline{x} = \underline{X}/\Omega \quad (77)$$

With this assumption, the master equation (75), rewritten for  $P(\underline{x}, t) = \Omega P(\underline{x}, t)$ , becomes

$$\frac{1}{\Omega} \frac{\partial}{\partial t} P(\underline{x}, t) = - \int \omega(\underline{x}, \underline{z}) P(\underline{x}, t) d\underline{z} + \int \omega(\underline{x} - \frac{\underline{z}}{\Omega}, \underline{z}) P(\underline{x} - \frac{\underline{z}}{\Omega}, t) d\underline{z} \quad (78)$$

By expanding the second integral on the right-hand side of Eq (78) in a power series about  $\underline{x}$ , Eq (78) can be written formally as

$$\frac{1}{\Omega} \frac{\partial}{\partial t} P(\underline{x}, t) = - \int \left[ 1 - \exp \left( - \frac{\tilde{\underline{r}}}{\Omega} \cdot \nabla \right) \right] \omega(\underline{x}, \underline{z}) P(\underline{x}, t) d\underline{z} \quad (79)$$

or, maintaining the expanded form

$$\frac{1}{\Omega} \frac{\partial}{\partial t} P(\underline{x}, t) = \sum_{n=1}^{\infty} \left( \frac{-1}{\Omega} \right)^n \frac{1}{n!} \int d\underline{z} (\tilde{\underline{r}} \cdot \nabla)^n \omega(\underline{x}, \underline{z}) P(\underline{x}, t) \quad (80)$$

where  $\tilde{\underline{r}}$  is the transpose of  $\underline{z}$ .

Following the work of Kubo (Ref 5:29), a solution of Eq (80) of the form

$$P(\underline{x}, t) = C \exp \left[ \Omega f(\underline{x}, t) \right] \quad (81)$$

is assumed. Then, the time derivative of  $P(\underline{x}, t)$  is

$$\frac{\partial}{\partial t} P(\underline{x}, t) = \frac{\partial}{\partial t} \left[ C \exp \left[ \Omega f(\underline{x}, t) \right] \right] = \Omega P(\underline{x}, t) \frac{\partial}{\partial t} f(\underline{x}, t) \quad (82)$$

and the integrand on the right-hand side of Eq (80) becomes

$$\begin{aligned}
 (\tilde{\underline{r}} \cdot \nabla)^n \omega(\underline{x}, \underline{z}) \rho(\underline{x}, t) &= (\tilde{\underline{r}} \cdot \nabla)^n \omega(\underline{x}, \underline{z}) \exp[-\Omega f(\underline{x}, t)] \\
 &= \Omega^n \omega(\underline{x}, \underline{z}) \rho(\underline{x}, t) (\tilde{\underline{r}} \cdot \nabla f)^n \\
 &\quad + O(\Omega^{n-1}) \quad (83)
 \end{aligned}$$

Therefore, to order  $\Omega^0$ , Eq (80) becomes

$$\frac{d}{dt} f(\underline{x}, t) = \sum_{n=1}^{\infty} (-1)^n \frac{1}{n!} \int d\underline{z} \omega(\underline{x}, \underline{z}) (\tilde{\underline{r}} \cdot \nabla f)^n \quad (84)$$

and (79) becomes

$$\frac{d}{dt} f(\underline{x}, t) = - \int d\underline{z} \omega(\underline{x}, \underline{z}) [1 - \exp(-\tilde{\underline{r}} \cdot \nabla f(\underline{x}, t))] \quad (85)$$

To solve this equation, a solution of the form

$$f(\underline{x}, t) = g(\underline{z}, t), \quad \underline{x} = \underline{y}(t) + \underline{z} \quad (86)$$

is assumed, where  $\underline{y}(t)$  is the expected value of  $\underline{x}$  and  $\underline{z}$  is the deviation of  $\underline{x}$  away from  $\underline{y}$ . This, then, transforms (85) into

$$\frac{d}{dt} g(\underline{z}, t) - \dot{\underline{y}}(t) \cdot \nabla_z g(\underline{z}, t) = - \int d\underline{z} \omega(\underline{y} + \underline{z}, \underline{z}) [1 - \exp(-\tilde{\underline{r}} \cdot \nabla g)] \quad (87)$$

Assuming  $|\underline{z}| \ll |\underline{y}(t)|$ , the transition rate  $w(\underline{y} + \underline{z}, \underline{z})$  can be written as

$$\omega(\underline{y} + \underline{z}, \underline{z}) = \omega(\underline{y}, \underline{z}) + \tilde{\underline{z}} \cdot \nabla_{\underline{y}} \omega(\underline{y}, \underline{z}) + \dots \quad (88)$$

which then transforms (87) into

$$\frac{\partial}{\partial t} g(\underline{z}, t) - \dot{\underline{y}} \cdot \nabla_{\underline{z}} g(\underline{z}, t) = - \int d\underline{\zeta} \omega(\underline{y}, \underline{\zeta}) [1 - \exp(-\tilde{\underline{\zeta}} \cdot \nabla_{\underline{z}} g)] \\ - \int d\underline{\zeta} \tilde{\underline{\zeta}} \cdot \nabla_{\underline{z}} \omega(\underline{y}, \underline{\zeta}) [1 - \exp(-\tilde{\underline{\zeta}} \cdot \nabla_{\underline{z}} g)] \quad (89)$$

Expanding the exponential terms, Eq (89) becomes

$$\frac{\partial}{\partial t} g(\underline{z}, t) - \dot{\underline{y}} \cdot \nabla_{\underline{z}} g(\underline{z}, t) = \sum_{n=1}^{\infty} \frac{(-1)^n}{n!} \int d\underline{\zeta} \omega(\underline{y}, \underline{\zeta}) (\tilde{\underline{\zeta}} \cdot \nabla_{\underline{z}} g)^n \\ + \tilde{\underline{z}} \cdot \nabla_{\underline{z}} \sum_{n=1}^{\infty} \frac{(-1)^n}{n!} \int d\underline{\zeta} \omega(\underline{y}, \underline{\zeta}) (\tilde{\underline{\zeta}} \cdot \nabla_{\underline{z}} g)^n \quad (90)$$

Noting that the first moment of the transition,  $\int d\underline{\zeta} \omega(\underline{y}, \underline{\zeta}) \underline{\zeta}$ , is just the average velocity of  $\underline{y}$  when the system is in the state  $\underline{y}$ , and that  $\underline{y}(t)$  is already an average or expected value, it is easily seen that  $\underline{y}(t)$  satisfies the condition

$$\dot{\underline{y}}(t) = \int d\underline{\zeta} \omega(\underline{y}, \underline{\zeta}) \underline{\zeta} \quad (91)$$

Therefore, the terms in Eq (90) linear in  $\nabla_{\underline{z}} g(\underline{z}, t)$  vanish and the resultant equation is

$$\frac{\partial}{\partial t} g(\underline{z}, t) = \sum_{n=2}^{\infty} \frac{(-1)^n}{n!} \int d\underline{\zeta} \omega(\underline{y}, \underline{\zeta}) (\tilde{\underline{\zeta}} \cdot \nabla_{\underline{z}} g)^n \\ + \tilde{\underline{z}} \cdot \nabla_{\underline{z}} \sum_{n=1}^{\infty} \frac{(-1)^n}{n!} \int d\underline{\zeta} \omega(\underline{y}, \underline{\zeta}) (\tilde{\underline{\zeta}} \cdot \nabla_{\underline{z}} g)^n \quad (92)$$

Assuming an approximate gaussian solution of

$$g(\underline{z}, t) = -\frac{1}{2} \underline{\underline{\Sigma}} \cdot \underline{\underline{\Delta}}(t) \cdot \underline{z} + O(|\underline{z}|^3) \quad (93)$$

where  $\underline{\underline{\Delta}}$  is the inverse of the covariance tensor, then

$$\begin{aligned} \underline{\underline{\Sigma}} \cdot \nabla_{\underline{z}} g(\underline{z}, t) &= -\frac{1}{2} \underline{\underline{\Sigma}} \cdot \nabla_{\underline{z}} (\underline{\underline{\Sigma}} \cdot \underline{\underline{\Delta}}(t) \cdot \underline{z}) + O(|\underline{z}|^3) \\ &= -\frac{1}{2} \underline{\underline{\Sigma}} \cdot \underline{\underline{\Delta}}(t) \cdot (\underline{z}_{\alpha} \Lambda_{\beta\gamma} \underline{z}_{\gamma}) + O(|\underline{z}|^3) \\ &= -\frac{1}{2} \underline{\underline{\Sigma}} \cdot \underline{\underline{\Delta}}_{\alpha\gamma} \underline{z}_{\gamma} - \frac{1}{2} \underline{\underline{\Sigma}}_{\alpha} \underline{z}_{\beta} \Lambda_{\beta\alpha} + O(|\underline{z}|^3) \quad (94) \end{aligned}$$

However

$$\Lambda_{\alpha\beta} = \Lambda_{\beta\alpha} \quad (95)$$

and, therefore

$$\begin{aligned} \underline{\underline{\Sigma}} \cdot \nabla_{\underline{z}} g(\underline{z}, t) &= -\underline{\underline{\Sigma}} \cdot \Lambda_{\alpha\beta} \underline{z}_{\beta} + O(|\underline{z}|^3) \\ &= -\underline{\underline{\Sigma}} \cdot \underline{\underline{\Delta}} \cdot \underline{z} + O(|\underline{z}|^3) \quad (96) \end{aligned}$$

Inserting (93) and (96) into Eq (92) and taking the leading terms to order  $|\underline{z}|^2$ , Eq (92) becomes

$$\begin{aligned} -\frac{1}{2} \underline{\underline{\Sigma}} \cdot \dot{\underline{\underline{\Delta}}} \cdot \underline{z} &= \frac{1}{2} \underline{\underline{\Sigma}} \cdot \underline{\underline{\Delta}} \cdot \int d\underline{r} \omega(\underline{y}, \underline{r}) \underline{\underline{\Sigma}} \cdot \underline{\underline{\Delta}} \cdot \underline{z} \\ &\quad + \underline{\underline{\Sigma}} \cdot \nabla_{\underline{y}} \int d\underline{r} \omega(\underline{y}, \underline{r}) \underline{\underline{\Sigma}} \cdot \underline{\underline{\Delta}} \cdot \underline{z} \quad (97) \end{aligned}$$

This leads directly to

$$\dot{\underline{\underline{\Delta}}} = -\underline{\underline{\Delta}} \cdot \int d\underline{r} \omega(\underline{y}, \underline{r}) \underline{\underline{r}} \cdot \underline{\underline{\Delta}} - 2 \nabla_y \int d\underline{r} \omega(\underline{y}, \underline{r}) \underline{\underline{r}} \cdot \underline{\underline{\Delta}} \quad (98)$$

which can then be made symmetric (recovering the symmetry lost by using (95) to combine the terms of Eq (94) by noting again the equivalence of Eq (95)). Therefore

$$\nabla_y \int d\underline{r} \omega(\underline{y}, \underline{r}) \underline{\underline{r}} \cdot \underline{\underline{\Delta}} = \underline{\underline{\Delta}} \cdot \left( \nabla_y \int d\underline{r} \omega(\underline{y}, \underline{r}) \underline{\underline{r}} \right) \quad (99)$$

and Eq (98) becomes

$$\begin{aligned} \dot{\underline{\underline{\Delta}}} = & -\underline{\underline{\Delta}} \cdot \int d\underline{r} \omega(\underline{y}, \underline{r}) \underline{\underline{r}} \cdot \underline{\underline{\Delta}} - \nabla_y \int d\underline{r} \omega(\underline{y}, \underline{r}) \underline{\underline{r}} \cdot \underline{\underline{\Delta}} \\ & - \underline{\underline{\Delta}} \cdot \left( \nabla_y \int d\underline{r} \omega(\underline{y}, \underline{r}) \underline{\underline{r}} \right) \end{aligned} \quad (100)$$

An equivalent expression for the covariance tensor  $\underline{\underline{B}}(t)$  is obtained by first noting several tensor identities. By definition

$$\underline{\underline{B}} = \underline{\underline{\Delta}}^{-1} \quad (101)$$

and, therefore

$$\underline{\underline{B}} \underline{\underline{\Delta}} = \underline{\underline{E}} \quad (102)$$

where  $\underline{\underline{E}}$  is the identity tensor. Taking the time derivative of Eq (102)

$$(\dot{\underline{\underline{B}} \underline{\underline{\Delta}}}) = \underline{\underline{\Delta}} \dot{\underline{\underline{B}}} + \underline{\underline{B}} \dot{\underline{\underline{\Delta}}} = 0 \quad (103)$$

which leads to

$$\dot{\underline{\underline{B}}} = - \underline{\underline{B}} \dot{\wedge} \underline{\underline{B}} \quad (104)$$

Defining  $\underline{c}_1(\underline{y})$  and  $\underline{c}_2(\underline{y})$  as the first and second moments of the transition rate  $w(\underline{y}, \underline{z})$

$$\tilde{\underline{c}}_1(\underline{y}) = \int d\underline{z} \, \omega(\underline{y}, \underline{z}) \tilde{\underline{z}} \quad (105)$$

$$\underline{c}_2(\underline{y}) = \int d\underline{z} \, \omega(\underline{y}, \underline{z}) \underline{\underline{z}} \quad (106)$$

and inserting (100) into Eq (104), the equation for the covariance tensor is

$$\dot{\underline{\underline{B}}}(t) = \underline{c}_2(\underline{y}) + \underline{\underline{B}} \nabla_{\underline{y}} \tilde{\underline{c}}_1(\underline{y}) + \widetilde{(\nabla_{\underline{y}} \tilde{\underline{c}}_1(\underline{y}))} \underline{\underline{B}} \quad (107)$$

or

$$\dot{B}_{\alpha\beta}(t) = c_{2\alpha\beta}(\underline{y}) + B_{\alpha\gamma} \frac{\partial}{\partial y^\gamma} c_{1\beta}(\underline{y}) + \frac{\partial}{\partial y^\gamma} c_{1\alpha}(\underline{y}) B_{\gamma\beta} \quad (108)$$

To obtain the covariance tensor for  $\underline{x}$ , (107) must be divided by  $\underline{\underline{z}} \cdot \underline{\underline{z}}$ . This is seen by first inserting (93) into (87) to get (keeping only the leading term in  $|\underline{z}|^2$ )

$$\begin{aligned} P(\underline{x}, t) &= C \exp \left[ -\frac{1}{2} \underline{\underline{z}} \cdot \underline{\underline{\Delta}} \cdot \underline{\underline{z}} \right] \\ &= C \exp \left[ -\frac{1}{2} \underline{\underline{z}} \cdot (\underline{\underline{\Delta}} \underline{\underline{z}}) \right] \quad (109) \end{aligned}$$

Letting

$$\underline{\underline{\sigma}}^{-1}(t) = \underline{\Omega} \underline{\underline{\Delta}} \quad (110)$$

be the inverse covariance tensor for  $\underline{x}$ , the covariance tensor becomes

$$\underline{\underline{\sigma}}(t) = \frac{1}{\underline{\Omega}} \underline{\underline{B}} \quad (111)$$

Similarly

$$\underline{\underline{\lambda}}(t) = \underline{\Omega} \underline{\underline{B}} \quad (112)$$

where  $\underline{\underline{\lambda}}(t)$  is the covariance tensor for  $\underline{X}$ . Therefore, by substituting (111) back into Eq (107) the equation for the covariance tensor for  $\underline{x}$  results :

$$\dot{\underline{\underline{\sigma}}}(t) = \frac{1}{\underline{\Omega}} \underline{\underline{C}}_2(\underline{y}) + \underline{\underline{\sigma}} \nabla_{\underline{y}} \tilde{\underline{\underline{C}}}_1(\underline{y}) + \widetilde{(\nabla_{\underline{y}} \tilde{\underline{\underline{C}}}_1(\underline{y}))} \underline{\underline{\sigma}} \quad (113)$$

where  $\underline{\underline{C}}_1$  and  $\underline{\underline{C}}_2$  are as defined in Eqs (105) and (106).

Thus, Eq (113) and Eq (97), which can be rewritten as

$$\dot{\underline{y}}(t) = \underline{\underline{C}}_1(\underline{y}) \quad (114)$$

are the general equations governing the evolution of the first and second moments of the normalized intensive macrovariable  $\underline{x}$ . Equation (114) defines the most probable path  $\underline{y}(t)$  which the variable  $\underline{x}$  will follow, while Eq (113) determines a measure of the fluctuations of the variable around this average path.

## Appendix B Linearization of the Photon Rate Equations

To linearize the photon rate equations (36) and (37), consider a small disturbance around an equilibrium point. Let

$$n_1 = n_1^0 + n_1' \quad (115)$$

and

$$n_2 = n_2^0 + n_2' \quad (116)$$

where  $n_1^0$  and  $n_2^0$  are the equilibrium point values. Substituting these into Eq (36), the rate equation becomes

$$\dot{n}_1 = \dot{n}_1^0 + \dot{n}_1' = \frac{g_{11} + g_{21}(n_1^0 + n_1')}{1 + \alpha_{11}(n_1^0 + n_1') + \alpha_{12}(n_2^0 + n_2')} - h_1(n_1^0 + n_1') \quad (117)$$

$$= \frac{g_{11} + g_{21}n_1^0 + g_{21}n_1'}{1 + \alpha_{11}n_1^0 + \alpha_{11}n_1' + \alpha_{12}n_2^0 + \alpha_{12}n_2'} - h_1n_1^0 - h_1n_1' \quad (118)$$

Now

$$\frac{1}{x + \Delta x} \approx \frac{x - \Delta x}{x^2} \quad (119)$$

Therefore, letting

$$x = 1 + \alpha_{11}n_1^0 + \alpha_{12}n_2^0 \quad (120)$$

and

$$\Delta x = \alpha_{11}n_1' + \alpha_{12}n_2' \quad (121)$$

Eq (118) becomes

$$\dot{n}_1' = \frac{(g_{11} + g_{21}n_1^0 + g_{21}n_1')(1 + \alpha_{11}n_1^0 + \alpha_{12}n_2^0 - \alpha_{11}n_1' - \alpha_{12}n_2')}{(1 + \alpha_{11}n_1^0 + \alpha_{12}n_2^0)^2} - h_1n_1^0 - h_1n_1' \quad (122)$$

Separating out zero order terms

$$\dot{n}_1' = \frac{(g_{11} + g_{21}n_1^0)(1 + \alpha_{11}n_1^0 + \alpha_{12}n_2^0 - \alpha_{11}n_1' - \alpha_{12}n_2')}{(1 + \alpha_{11}n_1^0 + \alpha_{12}n_2^0)^2} - h_1n_1^0 \quad (123)$$

$$+ \frac{g_{21}n_1' (1 + \alpha_{11}n_1^0 + \alpha_{12}n_2^0 - \alpha_{11}n_1' - \alpha_{12}n_2')}{(1 + \alpha_{11}n_1^0 + \alpha_{12}n_2^0)^2} - h_1n_1' \quad (123)$$

$$= \left( \frac{g_{11} + g_{21}n_1^0}{1 + \alpha_{11}n_1^0 + \alpha_{12}n_2^0} - h_1n_1^0 \right) \left( \frac{1 + \alpha_{11}n_1^0 + \alpha_{12}n_2^0 - \alpha_{11}n_1' - \alpha_{12}n_2'}{1 + \alpha_{11}n_1^0 + \alpha_{12}n_2^0} \right)$$

$$+ \frac{g_{21}n_1' (1 + \alpha_{11}n_1^0 + \alpha_{12}n_2^0 - \alpha_{11}n_1' - \alpha_{12}n_2')}{(1 + \alpha_{11}n_1^0 + \alpha_{12}n_2^0)^2} - \frac{h_1n_1^0 (\alpha_{11}n_1' + \alpha_{12}n_2')}{1 + \alpha_{11}n_1^0 + \alpha_{12}n_2^0} - h_1n_1' \quad (124)$$

Now, the first bracketed factor of the first term in Eq (124) is just  $\dot{n}_1^0$  which is equal to zero. Therefore, the entire first term vanishes and the rate equation becomes

$$\dot{n}_1' = \frac{g_{21}n_1' (1 + \alpha_{11}n_1^0 + \alpha_{12}n_2^0 - \alpha_{11}n_1' - \alpha_{12}n_2')}{(1 + \alpha_{11}n_1^0 + \alpha_{12}n_2^0)^2} - \frac{h_1n_1^0 (\alpha_{11}n_1' + \alpha_{12}n_2')}{1 + \alpha_{11}n_1^0 + \alpha_{12}n_2^0} - h_1n_1' \quad (125)$$

Since the disturbance was originally assumed to be small, only the first order terms are of significance; therefore, separating out all higher order terms, Eq (125) becomes

$$\dot{n}_1' = \frac{g_{21}n_1' (1 + \alpha_{11}n_1^0 + \alpha_{12}n_2^0)}{(1 + \alpha_{11}n_1^0 + \alpha_{12}n_2^0)^2} - \frac{g_{21}n_1' (\alpha_{11}n_1' + \alpha_{12}n_2')}{(1 + \alpha_{11}n_1^0 + \alpha_{12}n_2^0)^2} \xrightarrow{\text{H.O.T.} \approx 0}$$

$$- \frac{h_1n_1^0 (\alpha_{11}n_1' + \alpha_{12}n_2')}{1 + \alpha_{11}n_1^0 + \alpha_{12}n_2^0} - h_1n_1' \quad (126)$$

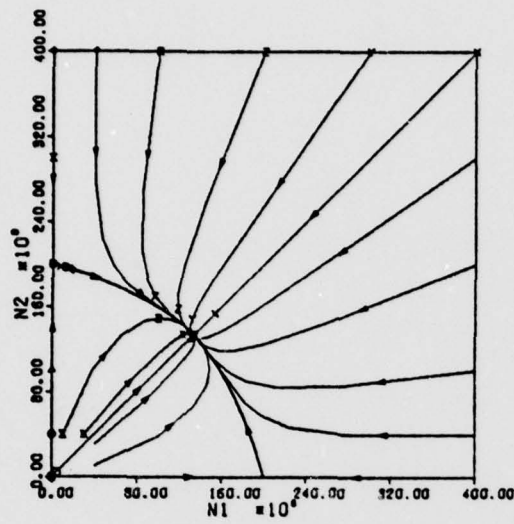
Thus, the linearized photon rate equations are written as

$$\dot{n}'_1 = \frac{g_{11}n'_1 - h_1 n_i^0 (\alpha_{11}n'_1 + \alpha_{12}n'_2)}{1 + \alpha_{11}n_i^0 + \alpha_{12}n_2^0} - h_1 n'_1 \quad (127)$$

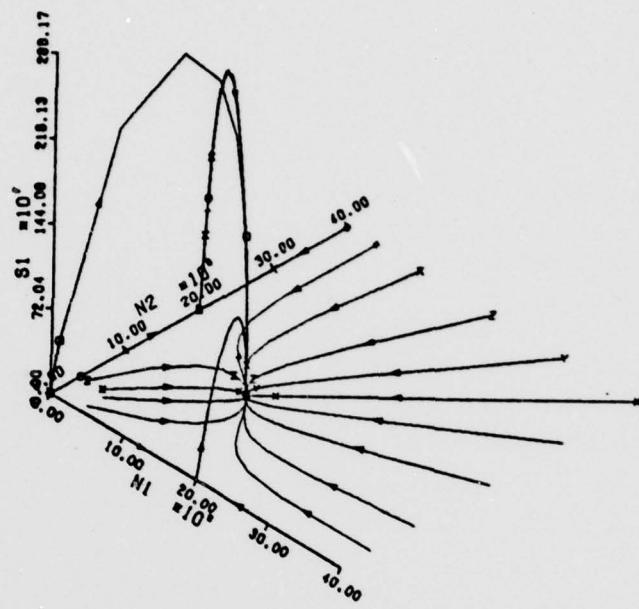
and

$$\dot{n}'_2 = \frac{g_{22}n'_2 - h_2 n_i^0 (\alpha_{22}n'_2 + \alpha_{21}n'_1)}{1 + \alpha_{21}n_i^0 + \alpha_{22}n_2^0} - h_2 n'_2 \quad (128)$$

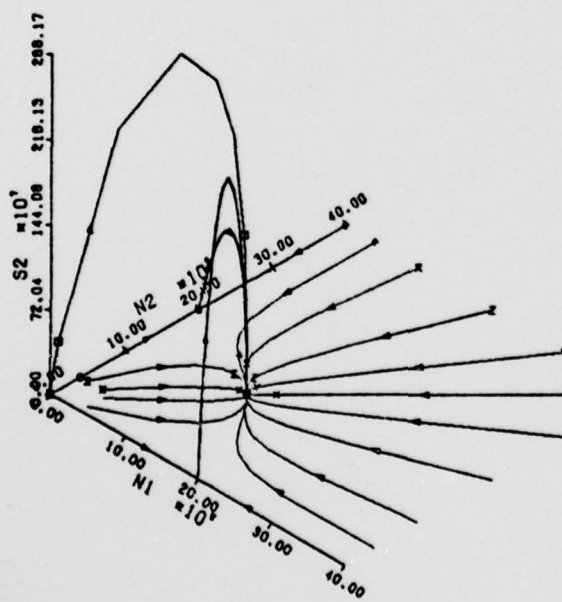
Appendix C Additional Evolution Curves



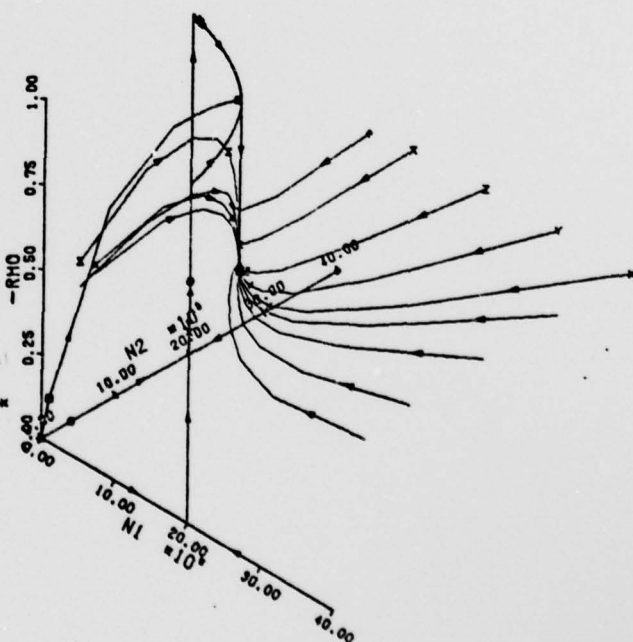
(a)



(b)

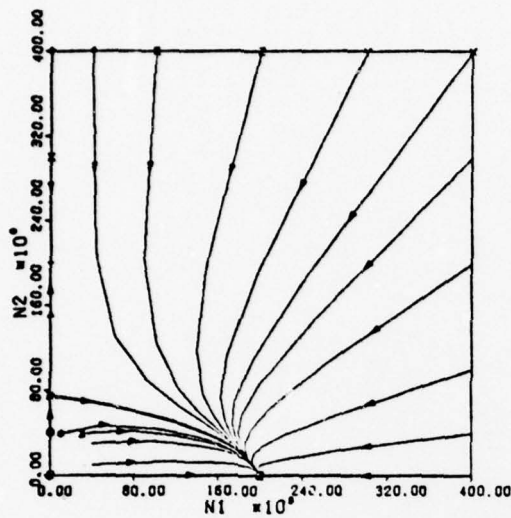


(c)

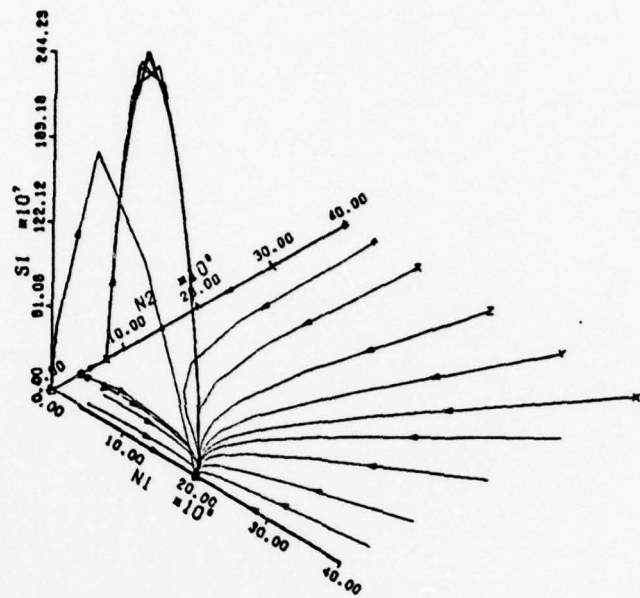


(d)

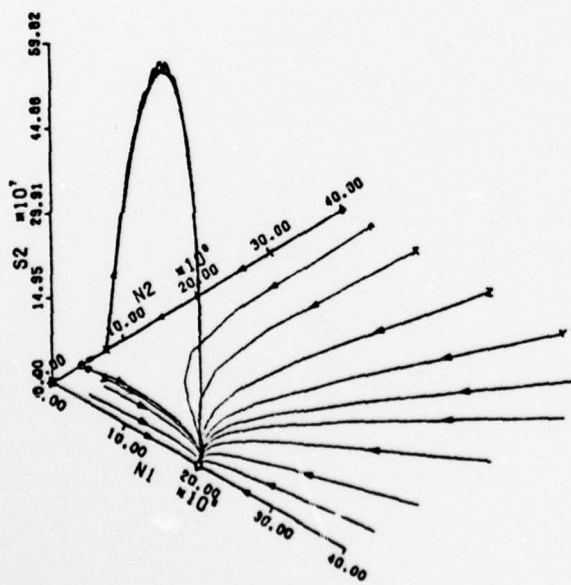
Figure 15. Evolution Curves for A11



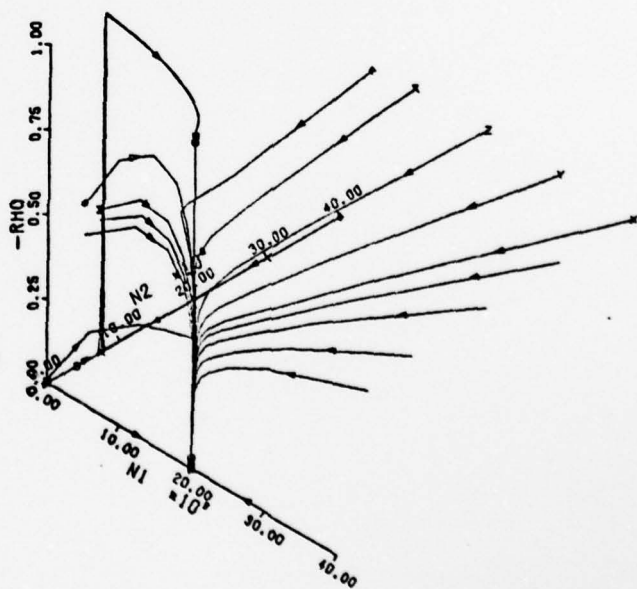
(a)



(b)

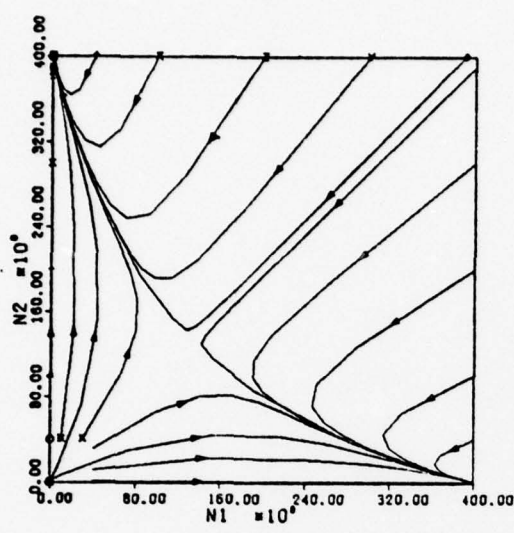


(c)

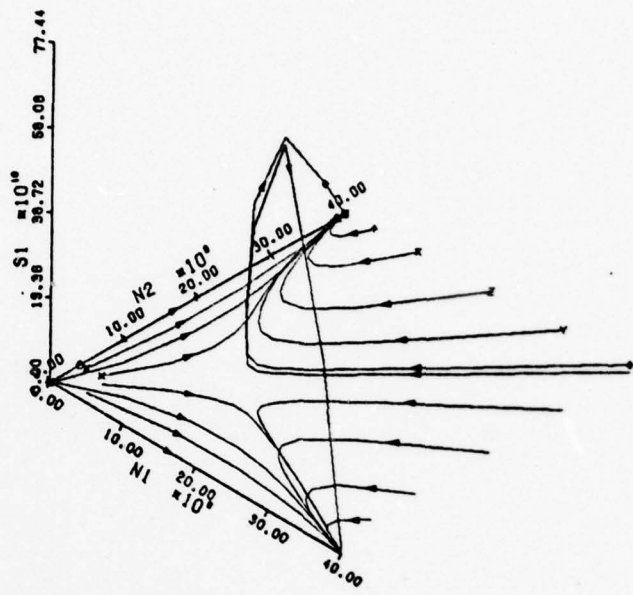


(d)

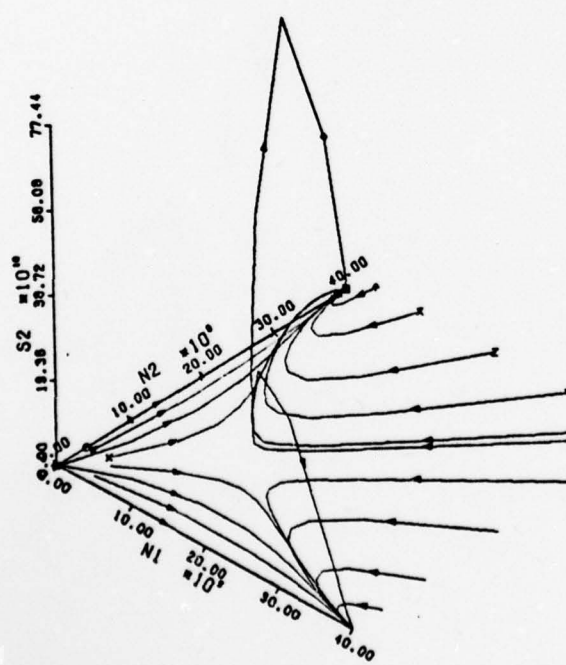
Figure 16. Evolution Curves for Case A12



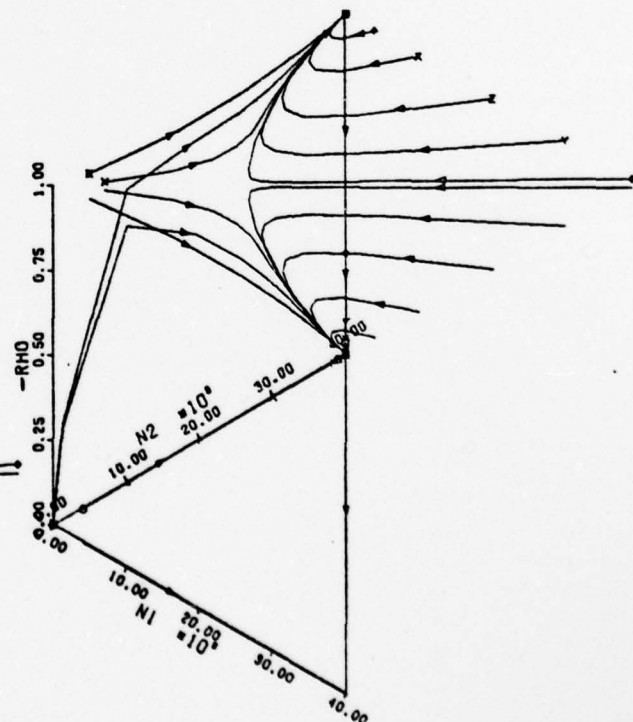
(a)



(b)

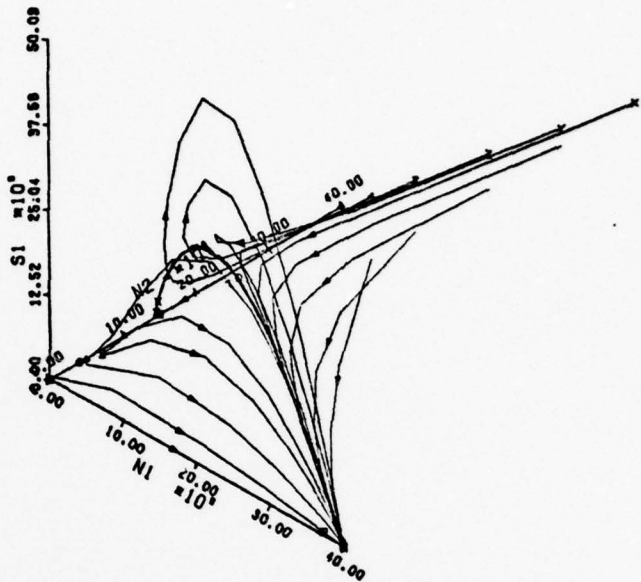
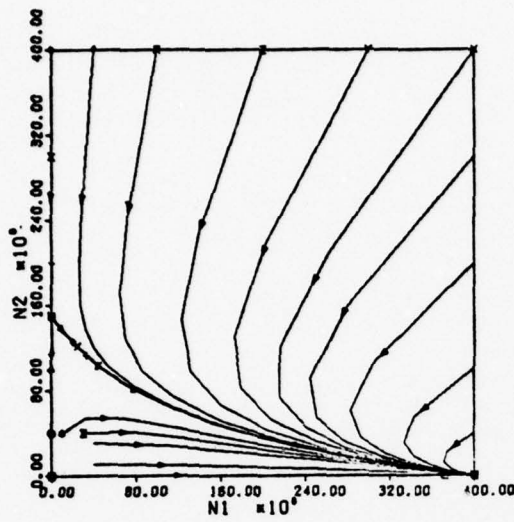


(c)



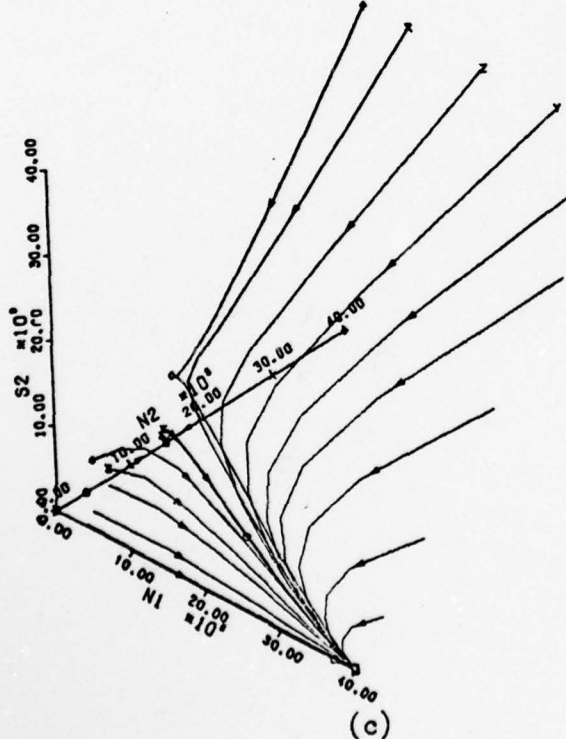
(d)

Figure 17. Evolution Curves for Case A13

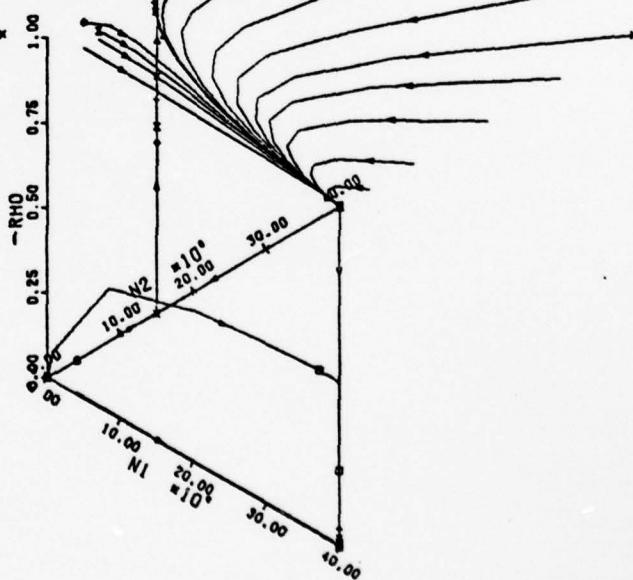


(a)

(b)

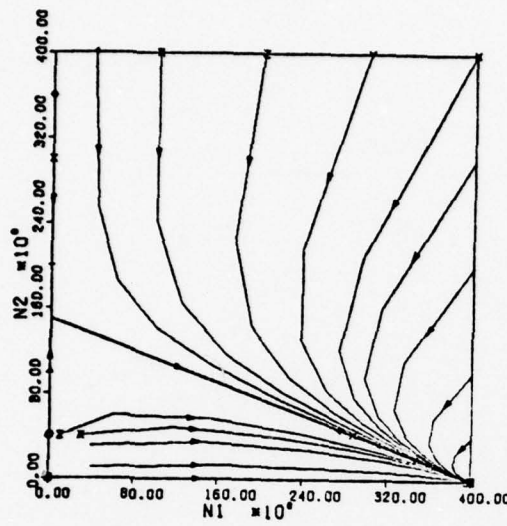


(c)

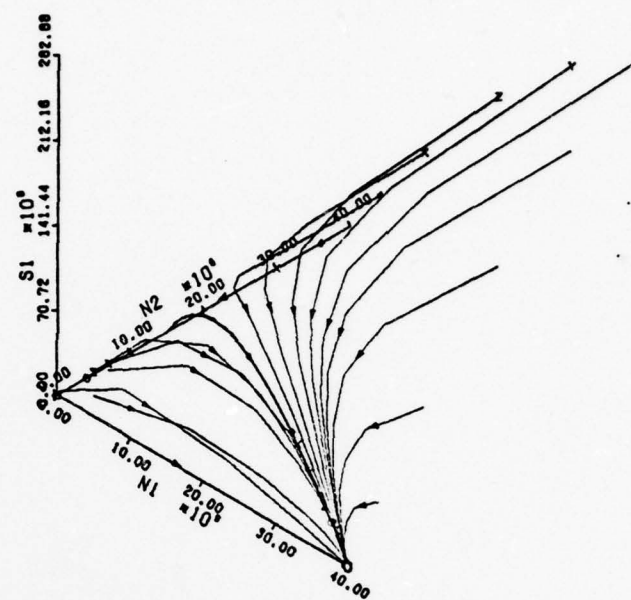


(d)

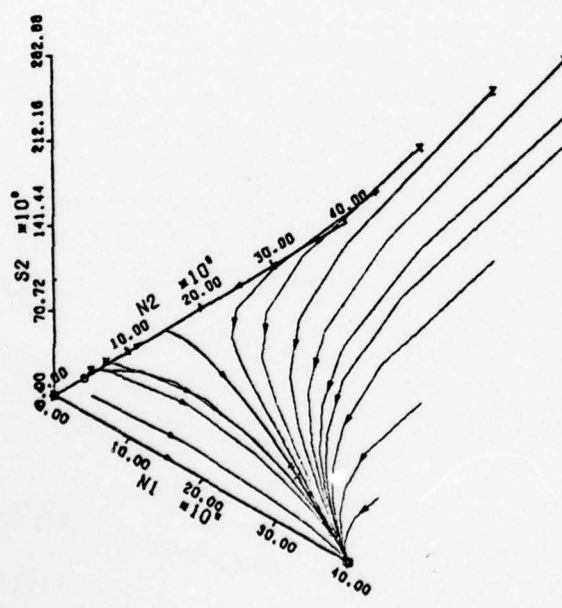
Figure 18. Evolution Curves for Case A14



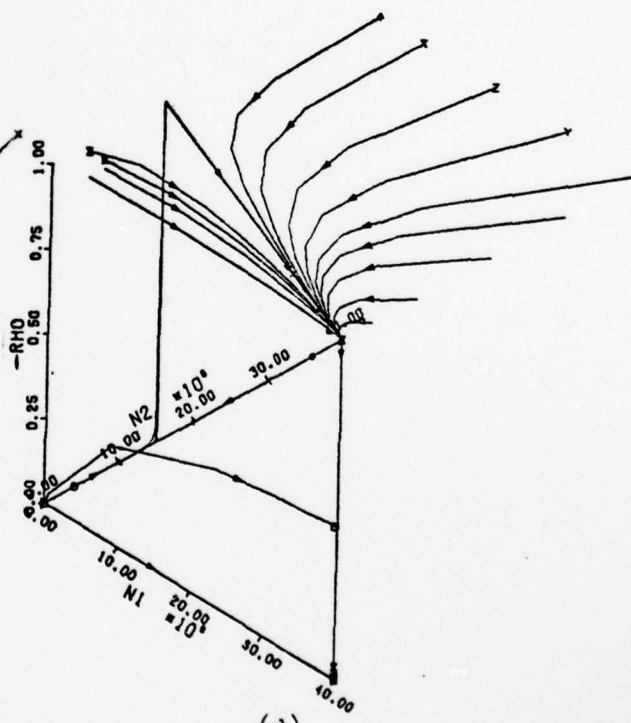
(a)



(b)

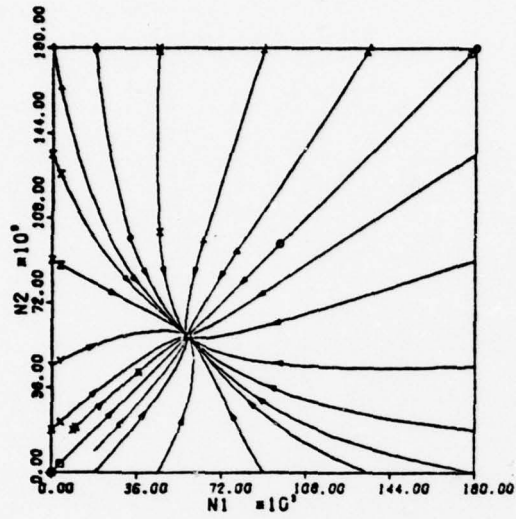


(c)

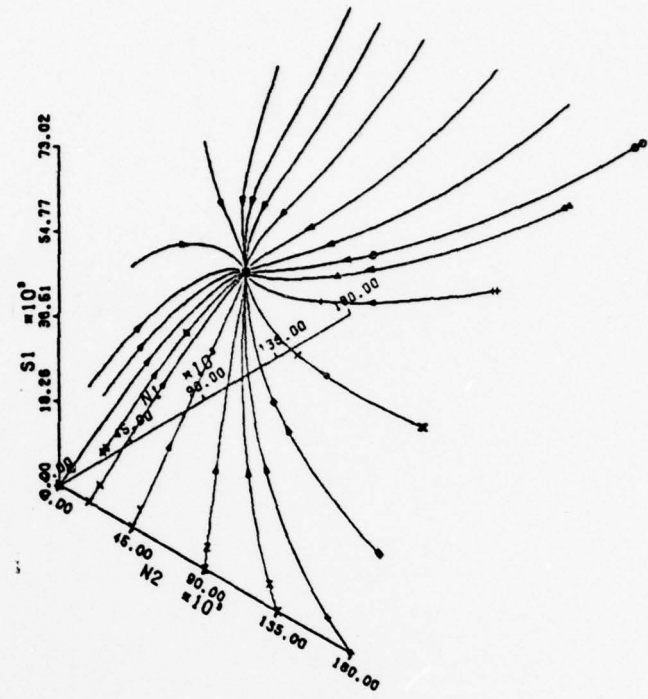


(d)

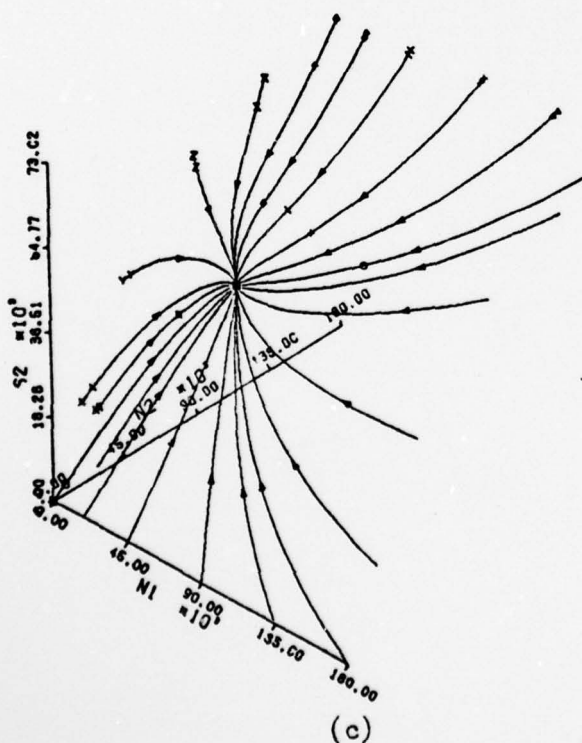
Figure 19. Evolution Curves for Case A15



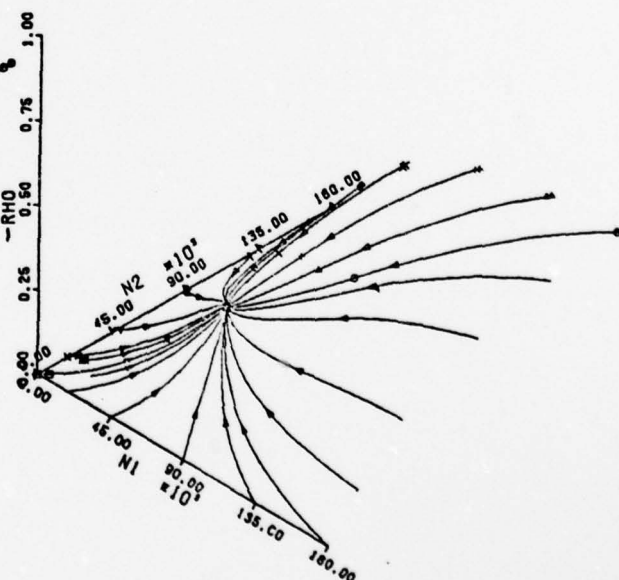
(a)



(b)

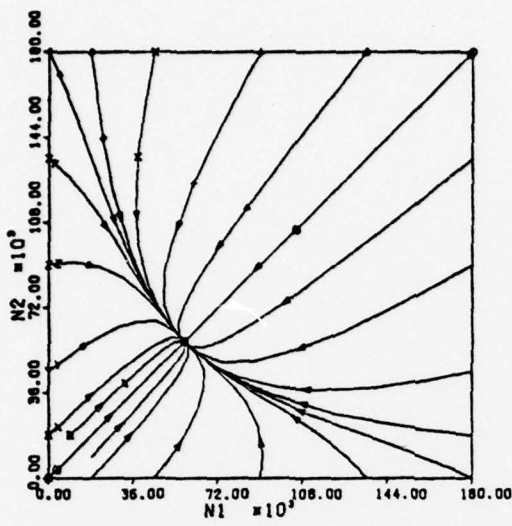


(c)

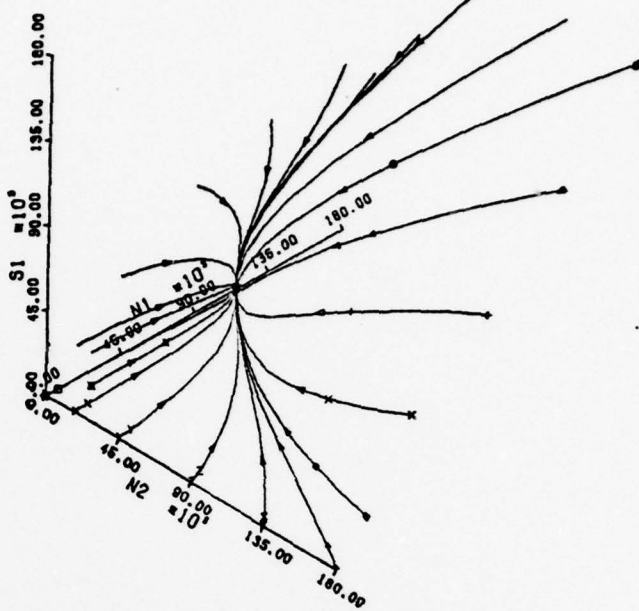


(d)

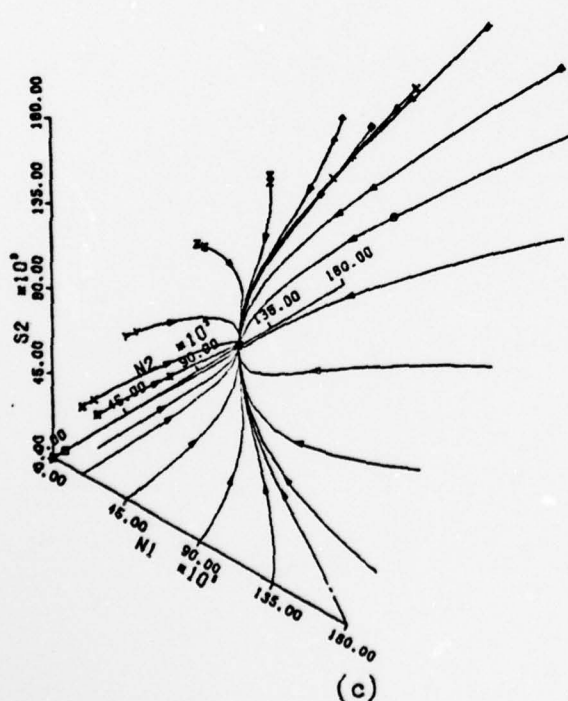
Figure 20. Evolution Curves for Case A31



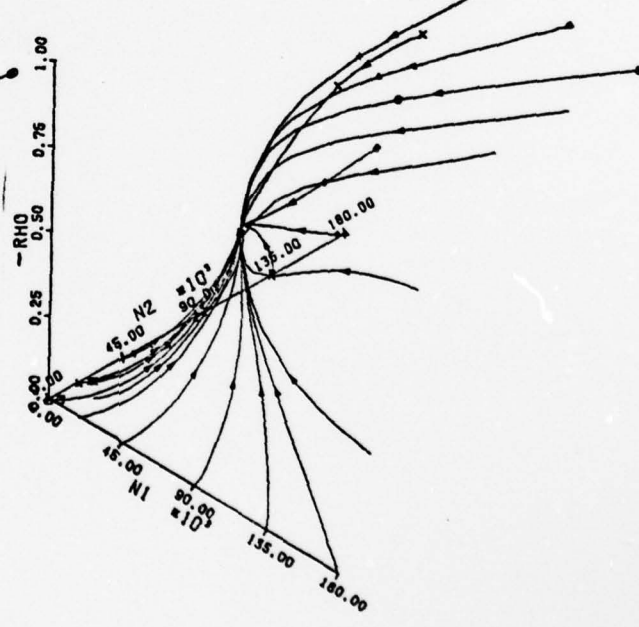
(a)



(b)



(c)



(d)

Figure 21. Evolution Curves for Case A33

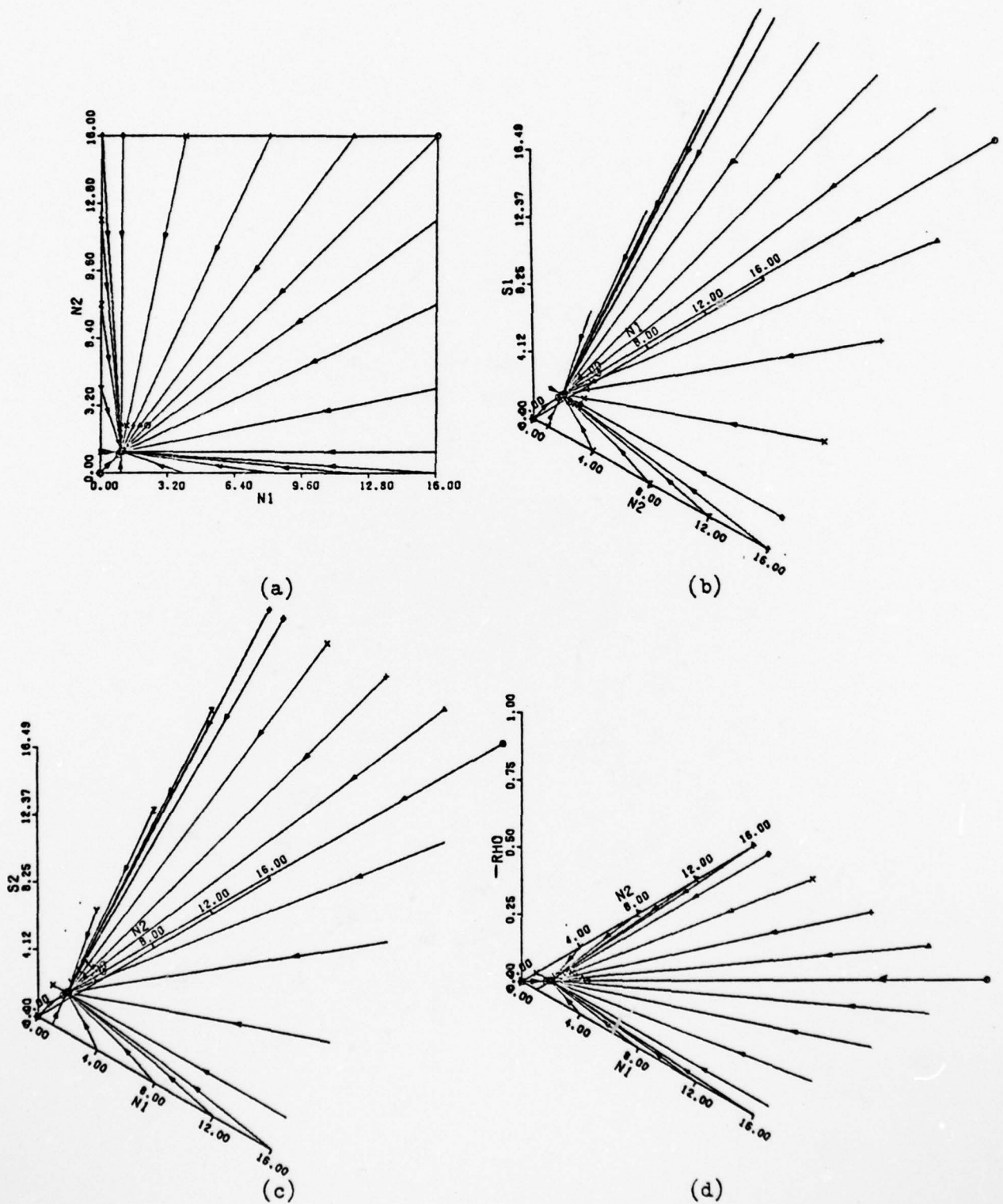
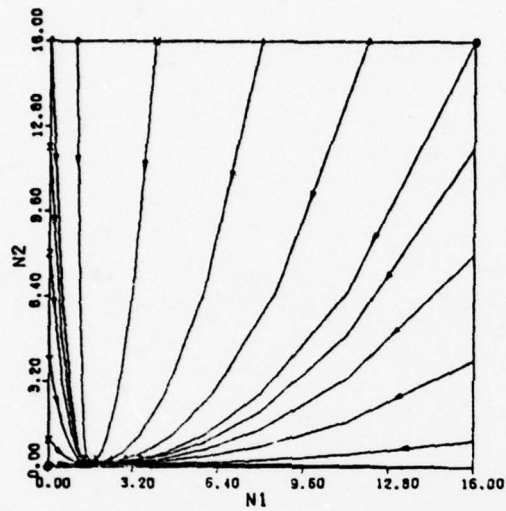
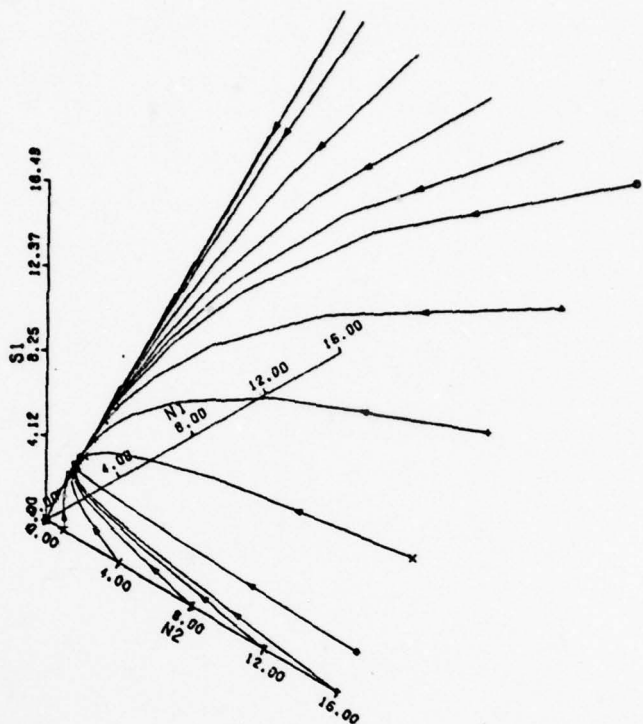


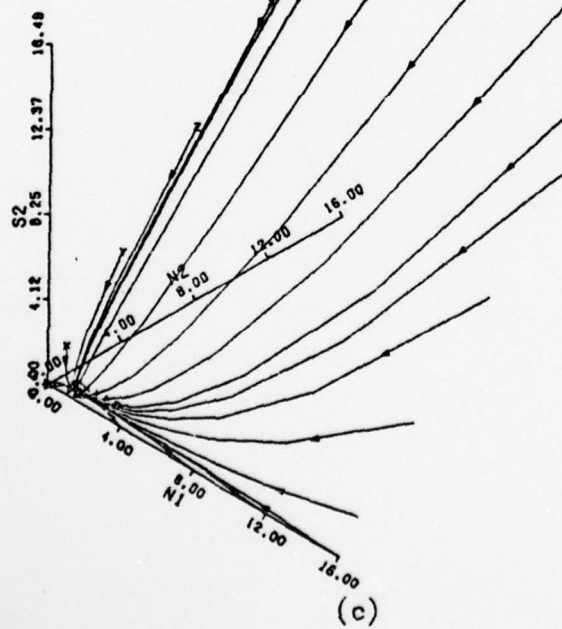
Figure 22. Evolution Curves for Case A51



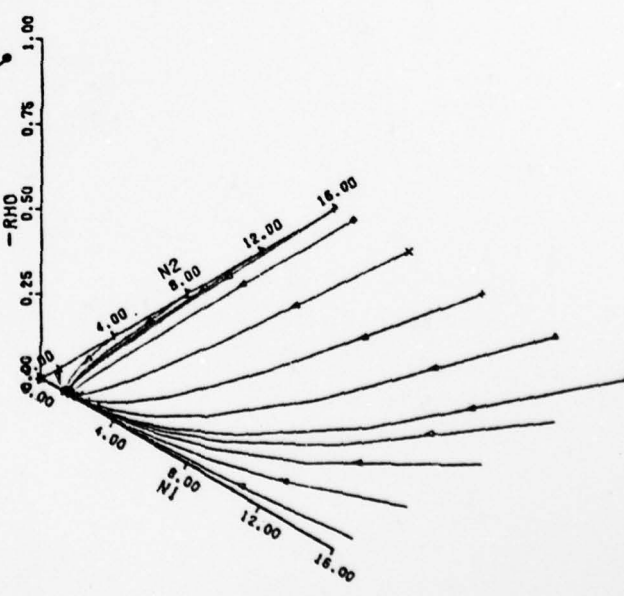
(a)



(b)



(c)



(d)

Figure 23. Evolution Curves for Case A52

VITA

Bruce Robert Anderson was born 16 October 1952 in Salt Lake City, Utah. He graduated from high school in Tustin, California in 1970 and attended the United States Air Force Academy where he majored in physics and mathematics. Upon graduation with distinction he received a Bachelor of Science degree and a commission in the United States Air Force. His initial assignment took him to San Antonio, Texas where he worked as a research physicist for the Laser Effects Branch, School of Aerospace Medicine, Brooks AFB until entering the School of Engineering, Air Force Institute of Technology, in June 1977.

Permanent address: 14128 Cameron Lane

Santa Ana, California 92705

## UNCLASSIFIED

SECURITY CLASSIFICATION OF THIS PAGE (When Data Entered)

REPORT DOCUMENTATION PAGE		READ INSTRUCTIONS BEFORE COMPLETING FORM
1. REPORT NUMBER AFIT/CEP/PH/78-1	2. GOVT ACCESSION NO.	3. RECIPIENT'S CATALOG NUMBER
4. TITLE (and Subtitle) PHOTON STATISTICS IN TWO-MODE LASERS	5. TYPE OF REPORT & PERIOD COVERED MS Thesis	
7. AUTHOR(s) Bruce R. Anderson Capt USAF	6. PERFORMING ORG. REPORT NUMBER	
9. PERFORMING ORGANIZATION NAME AND ADDRESS Air Force Institute of Technology (AFIT-EN) Wright-Patterson AFB, Ohio 45433	10. PROGRAM ELEMENT, PROJECT, TASK AREA & WORK UNIT NUMBERS	
11. CONTROLLING OFFICE NAME AND ADDRESS	12. REPORT DATE December 1978	
14. MONITORING AGENCY NAME & ADDRESS (if different from Controlling Office)	13. NUMBER OF PAGES 96	
16. DISTRIBUTION STATEMENT (of this Report)  Approved for public release; distribution unlimited	15. SECURITY CLASS. (of this report) Unclassified	
17. DISTRIBUTION STATEMENT (of the abstract entered in Block 20, if different from Report)	15a. DECLASSIFICATION/DOWNGRADING SCHEDULE 1-23-79	
18. SUPPLEMENTARY NOTES  Approved for public release; IAW AFR 190-17  JOSEPH P. HIPPS, MAJOR, USAF Director of Information		
19. KEY WORDS (Continue on reverse side if necessary and identify by block number) Lasers Photons Photon Statistics Statistics		
20. ABSTRACT (Continue on reverse side if necessary and identify by block number)  The evolution of the first and second moments of the photon density distribution for a two-mode laser system was studied by proposing appropriate transition rate expressions and using the Kubo equations developed for a Chapman-Kolmogorov system. A numerical analysis technique was used in solving the rate equations and computer plots were generated for various combinations of laser parameter values. Anomalously large fluctuations, similar to those occurring in single-mode lasers, were observed during		

AD-A064 394 AIR FORCE INST OF TECH WRIGHT-PATTERSON AFB OHIO SCH--ETC F/G 20/5  
PHOTON STATISTICS IN TWO-MODE LASERS.(U)  
DEC 78 B R ANDERSON  
UNCLASSIFIED AFIT/GEP/PH/78-1 NL

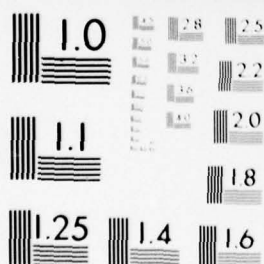
2 OF 2  
AD  
A064394



END  
DATE  
FILED  
4-79  
DDC

OF 2

064394



MICROSCOPY RESOLUTION TEST CHART

UNCLASSIFIED  
SECURITY CLASSIFICATION C

photon buildup o  
buildup in the n  
lasing mode. In  
linear relations

UNCLASSIFIED

SECURITY CLASSIFICATION OF THIS PAGE(*When Data Entered*)

photon buildup of the modes. When only one mode was oscillating, a photon buildup in the non-lasing mode was seen to cause similar fluctuations in the lasing mode. In all cases, these fluctuations were accompanied by a strong linear relationship between the modes.

UNCLASSIFIED

SECURITY CLASSIFICATION OF THIS PAGE(*When Data Entered*)